Progress in Materials Science 140 (2023) 101170

Contents lists available at ScienceDirect

Progress in Materials Science

journal homepage: www.elsevier.com/locate/pmatsci

Smart and bioinspired systems for overcoming biological barriers and enhancing disease theranostics

Xin Li [a,b,1], Yue Gao [c,1], Helin Li [d], Jean-Pierre Majoral [e], Xiangyang Shi [c,*], Andrij Pich [a,b,f,*]

[a] DWI-Leibniz-Institute for Interactive Materials e.V., 52056 Aachen, Germany
[b] Institute for Technical and Macromolecular Chemistry, RWTH Aachen University, 52074 Aachen, Germany
[c] College of Biological Science and Medical Engineering, Donghua University, Shanghai 201620, China
[d] Collaborative Innovation Center of Yangtze River Delta Region Green Pharmaceuticals, Zhejiang University of Technology, Hangzhou 310014, China
[e] Laboratoire de Chimie de Coordination du CNRS, Université de Toulouse, 31077 Toulouse Cedex 4, France
[f] Aachen Maastricht Institute for Biobased Materials, Maastricht University, 6167 RD Geleen, The Netherlands

ARTICLE INFO

Keywords:
Nanotheranostics
Biological barriers
Tumor delivery mechanism
Smart nanocarriers
Bioinspired systems

ABSTRACT

Nanomedicine has emerged as a promising mean to improve theranostic efficacy and reduce side effects. Currently, only very small percentage of injected dose reaches the solid tumors after intravenous administration due to the systemic biological barriers, including blood circulation, reticuloendothelial system capture, vasculature extravasation, tissue accumulation, deep penetration, cellular internalization, lysosome escape, intracellular efflux, and cell nuclear targeting. To optimize clinical translation and exploitation of nanomedicine, we here propose three safe and effective strategies to systematically overcome all barriers by the novel design of smart and bioinspired systems for highly efficient theranostics of various diseases, such as cancers, neurodegenerations, myocardial infarctions, inflammations, and infections. (1) Surface charge conversion, (2) size transformation, (3) bioinspired systems display unprecedented potential to achieve higher requirement of precise and personalized medicine. Alone or specially together, these strategies can address different barriers with intrinsically conflicting and promote the development of successful disease theranostics, that is impossible for almost of conventional delivery systems. Moreover, the challenges and perspectives of next-generation smart nanomedicine are featured for accurate theranostics and clinical practice in various diseases.

1. Introduction

Over the past few decades, nanomedicine has been under intensive development for applications in precise diagnosis and efficient treatment of various diseases [1–4]. The main goal of nanomedicine is to deliver theranostic agents to targeted region *in vivo*. However, according to current reports, only less than 1 % of intravenously injected agents by nanomedicine can reach the intended target, and most of them are accumulated in healthy tissues or metabolized rapidly out of body [5–8]. This is due to the fact that these agents by systemic administration encounter a series of biological barriers in 1) blood circulation [9,10], 2) vasculature extravasation [11,12], 3)

* Corresponding authors.
E-mail addresses: xshi@dhu.edu.cn (X. Shi), pich@dwi.rwth-aachen.de (A. Pich).
[1] X. Li and Y. Gao contributed equally to this work.

https://doi.org/10.1016/j.pmatsci.2023.101170
Received 23 January 2022; Received in revised form 30 June 2023; Accepted 22 July 2023
Available online 19 August 2023

tissue accumulation [13,14], 4) deep penetration [15,16], 5) cellular internalization [17,18], 6) lysosome escape [19,20], 7) intracellular efflux [21,22], and 8) nuclear targeting (BVTDCLIN) [23,24]. Likewise, for therapeutic applications, the controllable drug release after internalization in the targeted region also needs to be considered [25–27].

To overcome these biological barriers, all kinds of appropriate nanoplatforms were developed with different properties, involving size, shape, morphology, surface charge, amphipathy, and functional modification to alter their interactions with physiological components for improving diagnostic sensitivity and enhancing treatment efficacy [28–32]. Generally, size and surface charge of nanoplatforms greatly influence their blood circulation half-lives, vasculature extravasation, cellular internalization (e.g. macrophage phagocytosis), so as lead to different biodistributions throughout organs and tissues and specific sites of interest [33,34]. Shape, morphology, and amphipathy, as another three important features, also affect the blood circulation and cellular uptake behaviors of nanoplatforms and often result in distinct *in vivo* fates [34,35]. Moreover, the combined modulation of surface modification chemistry and density can significantly improve the efficiency of vascular active transcytosis and cellular internalization [36–38]. Meanwhile, functional modification and assembly render the nanoplatforms with targeting or responsive specificity to certain endogenous components or exogenous factors, and thereby controlling the nano-bio interactions to considerably influence the penetration as well as uptake efficacy and pathways [39]. Despite this, most of nanoplatforms are still suboptimal in biomedical applications because their specific optimized performances display often intrinsically conflicting features for the sequential biological barriers. For instance, the nanoplatforms with positive charge [40,41], small size [42,43], or targeting molecules [44,45] are able to promote tissue deep penetration, cellular internalization, and lysosome escape attributing to the strong interactions with cell membranes, which also lead to their accelerated clearance by the kidney or reticuloendothelial system (RES) [46–49]. As a contrast, the nanoplatforms having negative charge [50,51], large size [52,53], or hydrophilic "stealth coating" (e.g., polyethylene glycol (PEG) or zwitterions) [54,55] may accumulate and retain effectively into targeted region through prolonged blood circulation time and enhanced permeability and retention (EPR) effect, while their deep penetration, cellular uptake, and unclear targeting are restricted [56,57].

Recently, some innovative strategies, remodeling disease microenvironment, designing convertible or bioinspired systems, were developed to address aforementioned the predicaments for further augmenting cargo delivery and theranostic effects. Comparing

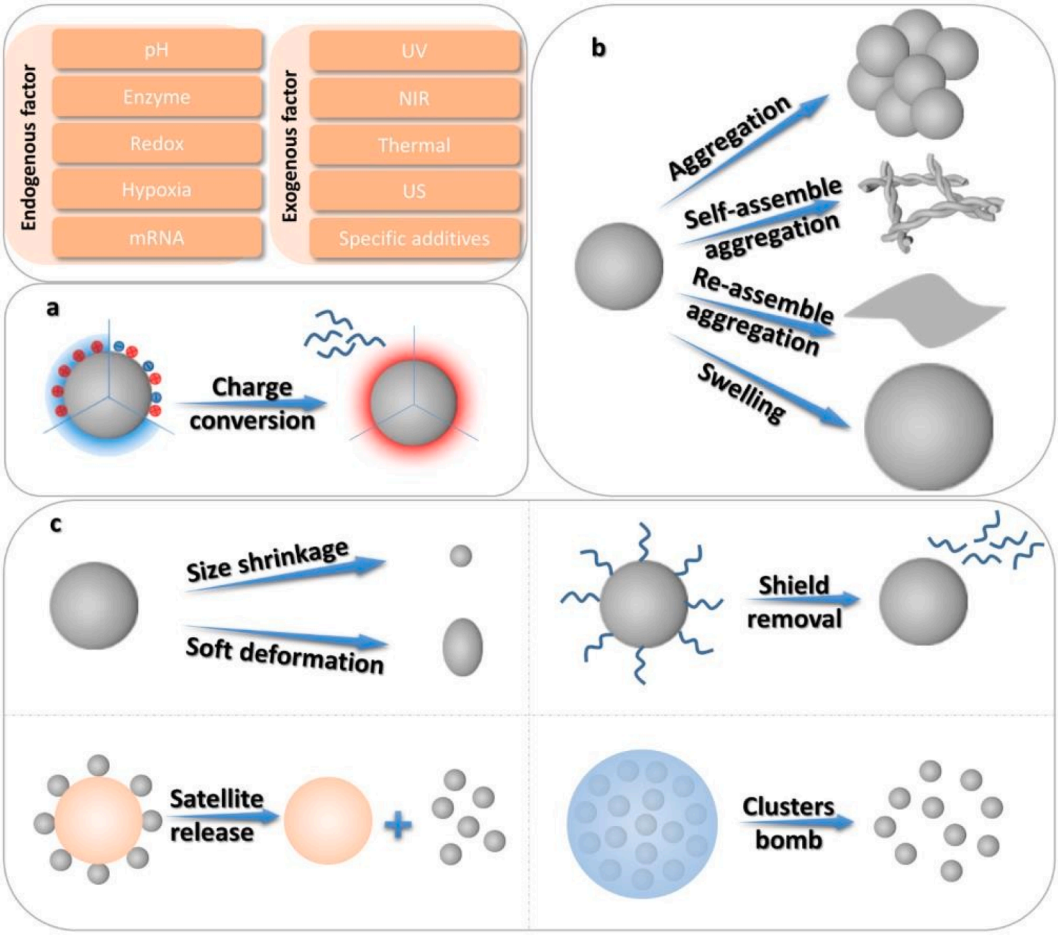

Scheme 1. Schematic illustration of smart NPs with endogenous- or exogenous-triggered (a) charge conversion, (b) size increase, (c) size decrease and soft deformation.

Table 1
The design of smart and bioinspired systems to overcome biological barriers in "BVTDCLIN" and enhance disease Theranostics

Strategies	Overcoming barriers *in vivo*	Stimuli factors	Functional structures	Applications	Ref.
Charge conversion (Neutral/negative/ zwitterionic to positive)	1) Blood circulation 3) Tissue accumulation 4) Deep penetration 5) Cellular internalization 6) Lysosome escape	Extracellular pH (6.0–6.8)	DMMA	1. MR imaging-guided PTT/gene therapy of melanoma 2. Chemotherapy of breast tumor	[90,113]
			Benzoic-imine bonds	Drug delivery *in vitro*	[130]
			Glycol chitosan	MR imaging-guided PDT of tumor	[146]
			Pyrrole ring	Chemotherapy of ovarian carcinoma	[147]
			Azepane ring	Cisplatin delivery for chemotherapy *in vitro*	[145]
			Zwitterions bearing APAS	SPECT/CT images *in vitro*	[150]
		Intracellular pH (5.0–5.5)	Hydrazone bonds	Chemotherapy of drug-resistant cancer stem cells	[120]
			Acetal bonds	PDT/gas therapy of biofilm infection	[131]
		MMP	PLGLAG	1. Chemotherapy of fibrosarcoma 2. Fluorescence and MR images of fibrosarcoma 3. Chemotherapy of glioma	[161–163]
		MMP/pH	ACPP with isoelectric point	1. Gene therapy of hepatocellular carcinoma 2. Gene-chemotherapy of glioma	[164,165]
		HAase	HA	Chemotherapy of hepatocellular carcinoma	[169]
		H_2S	Azides	Fluorescence imaging-guided chemotherapy of breast cancer	[184]
		ROS	Boronic acid	Neuroprotection	[192]
		Hypoxia	4-nitrobenzyl chloroformate	Chemotherapy of breast cancer	[208]
			Azobenzenes	Gene therapy of melanoma	[209]
		UV	*o*-nitrobenzyl carbamate	Controlled release	[218]
			DMNB	Transmembrane delivery *in vivo*	[219]
		NIR	DMNB-protected phenolic hydroxyl	Gene therapy of breast cancer	[232]
		Thermal	Amino-modified thermal sensitive MGs	Drug delivery *in vitro*	[235]
			Poly(allylamine) hydrochloride	Anti-cell adhesion	[212]
		Specific additives	Cationic cages and Pyr	Drug delivery *in vitro*	[213, 244]
(Negative to positive)	1) Blood circulation 2) Vascular extravasation 4) Deep penetration 5) Cellular internalization	GGT	γ-glutamylamides	Chemotherapy of pancreatic or/and hepatocellular and breast tumors	[88, 252, 253]
Extracellular size increase (From small to large)	1) Blood circulation 3) Tissue accumulation	pH	Carboxylic and amine groups	PTT *in vitro* and *in vivo*	[278, 279]
			Citraconic amide	PET imaging of hepatocellular carcinoma	[280]
			Carboxylate anion	PDT of tumor and apoptosis imaging	[281]
			DMMA or WP5 modified DOX	Chemotherapy of breast or hepatocellular cancer	[282, 283]
			Cytosine-rich DNA	PTT and chemotherapy of breast cancer	[322]
		Gelatinase	PLGVRG peptide	PA imaging-guided PTT of glioma	[298]
		FAP-α	GPA peptide	NIR fluorescence imaging of pancreatic tumor	[299]
		MMP	L-amino acids	1. Fluorescence imaging of tumors 2. Prolonged retention in heart after MI	[306–308]
		ALP	Tyrosine phosphorus ester	1. Fluorescence and PA imaging guided PTT of tumor 2. PTT of prostate cancer	[311, 312]
		Caspase	DEVD	Fluorescence imaging-guided drug delivery and surgery	[313]

(*continued on next page*)

Table 1 (*continued*)

Strategies	Overcoming barriers *in vivo*	Stimuli factors	Functional structures	Applications	Ref.
		Legumain	Thiolamino and cyano groups	PA imaging-guided chemotherapy of glioma	[327]
		Light	Diazirine	1. PA imaging and PTT of breast cancer 2. Dynamic T_2/T_1 MR imaging of arthritis	[329, 343]
Intracellular size increase (From small to large)	4) Deep penetration	MMP	PLGL peptide	Intracellular assembly-induced selective cancer apoptosis	[352]
	5) Cellular internalization	GSH	β-cyclodextrin and ferrocene	Intracellular aggregation-induced apoptosis of hepatocellular cancer	[355]
	6) Lysosome escape	Intracellular pH	Acetal bond	Nanovaccine for cancer immunotherapy	[360]
	7) Intracellular efflux		NLSC	Chemotherapy of hepatocellular carcinoma	[371]
			DMMA modified PEI	Chemotherapy of breast tumor	[372]
		mRNA	DNA	1. PTT *in vitro* 2. PTT and gene therapy *in vitro*	[366, 367]
		ROS	thiol-modified oligo(*p*-phenylene vinylene)	Chemotherapy for combating drug resistance	[368]
		Intracellular pH/ ATP	Ternary DNA	Chemotherapy/PTT of tumor	[370]
Size decrease (From large to small)	4) Deep penetration 5) Cellular internalization 8) Nuclear targeting	Extracellular pH	AEMA	1. Chemotherapy and PDT of breast cancer 2. Fluorescence imaging of tumors 3. Cisplatin delivery of pancreatic cancer 4. Chemoimmunotherapy of breast cancer 5. Radiotherapy of breast cancer	[375, 429, 431–433]
			Tertiary amine	PDT-mediated pyroptosis of tumors	[430]
			Polyglutamate acid	Chemotherapy of hepatocellular carcinoma	[387]
			Benzoic-imine bonds	1. Chemotherapy and PTT of breast cancer 2. T1 MR imaging of hepatocellular carcinoma	[388, 415]
			PDA	PA/NIR imaging-guided PTT/ chemotherapy of breast cancer	[403]
			CDM	1. Cisplatin delivery for chemotherapy of pancreatic/lung/breast tumors 2. Lymph nodes delivery and tumor metastasis inhibition	[405, 406]
			i-motif DNA	1. Gene-chemotherapy of tumors 2. Inverse MR imaging of small hepatocellular carcinoma	[424, 425]
		Extracellular pH/ telomerase	Triplex /hairpin DNA	Chemotherapy of breast cancer	[423]
		Single oxygen	Thioketal bonds	PDT/PTT of breast cancer	[407]
		HAase	HA	PTT/chemo-gas therapy of breast tumor	[398]
			Gelatin	1. Fluorescence imaging of fibrosarcoma 2. Fluorescence imaging-guided chemotherapy of glioma 3. Chemotherapy of breast cancer 4. Chemotherapy of melanoma and breast cancers	[408–411]
		GSH	Disulfide bonds	Dynamic T2/T1 MR imaging of breast cancer	[414]
		UV	SP	1. Drug delivery of cornea 2. Chemotherapy of fibrosarcoma	[379, 380]
		NIR	aza-BODIPY	PA imaging-guided PTT of breast cancer	[382–384]
			ICG-based lipid	Cisplatin delivery of breast tumor	[435]
		PA shockwave	PFH	Cisplatin delivery and PA therapy of breast cancer	[436]

(*continued on next page*)

Table 1 (*continued*)

Strategies	Overcoming barriers *in vivo*	Stimuli factors	Functional structures	Applications	Ref.
Soft deformation	1) Blood circulation 3) Tissue accumulation 4) Deep penetration 5) Cellular internalization	Mechanical pressure of ECM	HMONs	Chemotherapy or PDT of breast cancer	[441, 442]
			CCM-camouflaged MSNs	Chemotherapy of breast cancer	[445]
			MGs or NGs	N.A.	[443]
			Liposome or Lipid-entrapped PLGA	Chemotherapy of pancreatic cancer	[446, 460]
Biomimetic systems	1) Blood circulation	Biomimetic block	Poly(L-lysine) dendrimers	Gene or drug delivery *in vitro*	[476, 477]
	3) Tissue accumulation		Poly(arginine) dendrimers	Gene delivery *in vitro*	[475, 478]
	5) Cellular internalization	Biomimetic coating	Artificial phospholipid	1. Chemotherapy of breast cancer 2. Drug delivery	[491, 498–500]
	6) Lysosome escape 8) Nuclear targeting		CCM	1. Chemotherapy and lung metastasis inhibition of breast cancer 2. Fluorescence imaging-guided PDT of tumor 3. Starvation-immunotherapy of melanoma 4. Dynamic MR imaging-guided chemotherapy of tumor	[514–517]
			BM	1. Drug delivery 2. Antibacterial vaccine	[522, 527]
Cell-based systems	1) Blood circulation 2) Vascular extravasation 3) Tissue accumulation 4) Deep penetration 5) Cellular internalization 6) Lysosome escape		RBCs	1. Dynamic X-ray imaging of blood pool 2. PDT of hypoxia tumor	[531, 533]
			MAs	1. Combined PTT/chemotherapy of breast cancer 2. Combined PTT/immunotherapy of lymphoma 3. CT imaging-guided chemotherapy/cell therapy of osteosarcoma	[538, 539, 541]
			NEs	1. Chemotherapy of glioma and other tumors 2. Immunotherapy of melanoma 3. Detection and treatment of ALI	[542–545]
			T cells	1. Drug delivery 2. CT imaging of tumors 3. Immunotherapy of lymphoma	[546,549,550]
			Stem cells	1. MR imaging of tumors 2. Drug delivery 3. MR Imaging-guided chemotherapy of tumor	[553–555]
			Bioengineered cells	Anti-inflammatory for acute inflammation and pancreatitis	[528]
Bacterial-based systems	3) Tissue accumulation 4) Deep penetration 5) Cellular internalization		*E. coli*	PTT and immunotherapy of breast cancer	[563]
			Salmonella	Protein drug delivery in breast cancer	[568]
Phage-based systems	3) Tissue accumulation 4) Deep penetration 5) Cellular internalization		Phage	1. Ameliorating acute lung infections 2. Enhanced chemotherapy of colorectal cancer by microbiota modulation	[572,577]

normal tissues, some specific tissues (e.g., solid tumors or corneas) exhibit the denser extracellular matrix (ECM) or/and elevated interstitial fluid pressure (IFP), which hinder transport and penetration of nanoplatforms [58,59]. For the strategy of remodeling disease microenvironment, the degradation of the collagen matric to reduce transport hindrance or the normalization of vessels to restore the pressured gradients have been promising choices for improving the theranostic efficacy [60,61]. However, the strategy also shows some limitations that the normalization of vessels needs delicate balance in order not to dramatically compromise the EPR effect, and the uncontrollable disintegration of ECM may lead to various unexpected risks (e.g., musculoskeletal pain, secondary tissue injury, promoting tumor progression or even metastasis) [62].

Differently from the first strategy, other strategies do not exhibit potential risks and harms in the disease treatment. The strategy of designing convertible nanoplatforms is provided by regulating rationally the physiochemical properties of nanoparticles (NPs), such as the changeable performances of surface charge, particle size or amphiphilicity, to better overcome the barriers [63–65]. These smart NPs were properly designed to achieve stimuli-responsive charge-reversible, size-switchable, soft deformation, or coating-shedding behaviour under endogenous microenvironment (e.g., pH, enzyme, redox, hypoxia, mRNA) or exogenous factors (e.g., light, thermal, ultrasound (US), specific additives) (Scheme 1). The intelligent behaviours of the NPs render them with the improved stability, prolonged blood circulation, promoted transvascular extravasation, enhanced tissue accumulation, augment deep penetration, elevated cellular internalization, efficient lysosome escape, limited intracellular efflux, and ideal nuclear targeting [60,66–71]. Moreover, in recent years, the biomimetic strategies, such as biomimetic block-based or cancer cell membrane-coated NPs, have been

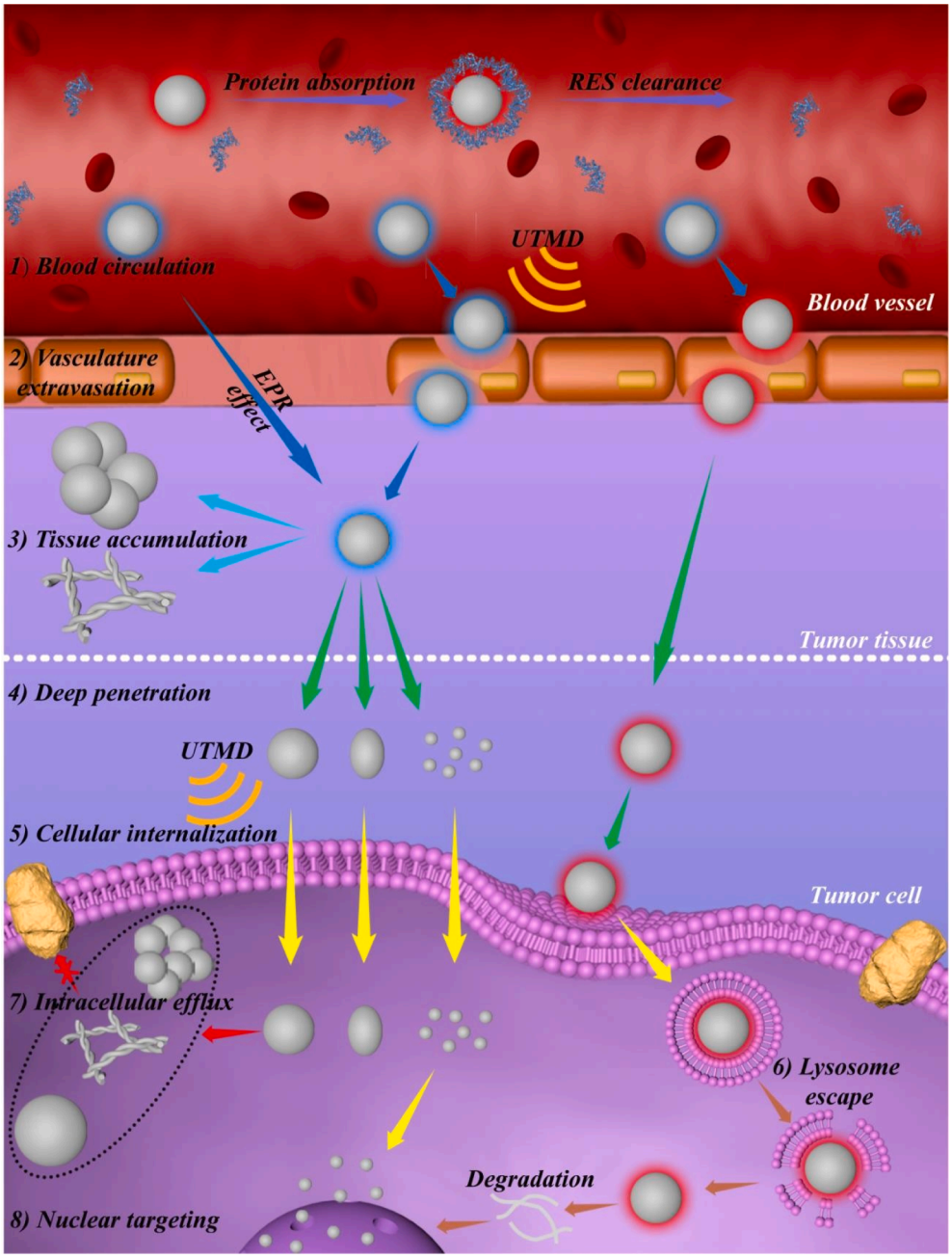

Scheme 2. Schematic illustration of the delivery procedure of smart NPs by overcoming biological barriers in BVTDCLIN for enhanced disease theranostics: 1) blood circulation, 2) vasculature extravasation, 3) tissue accumulation, 4) deep penetration, 5) cellular internalization, 6) lysosome escape, 7) intracellular efflux, and 8) nuclear targeting.

widely developed to render them with biomimetic functions for the reduced immunogenicity, improved pharmacokinetics and enhanced accumulation by the low RES capture, immune evasion as well as homologous targeting specificity [72–74]. Finally, living systems including cells, bacteria and phages were recently developed to achieve highly efficient delivery through the inherent tumor and inflammation migration/homing or cell/bacteria invasion/colonization ability [75–78].

Before that, some reviews regarding the development of smart NPs to overcome biological barriers by acidic tumor microenvironment targeting or hierarchical targeting strategy for improved imaging or enhanced therapy of tumors have been published [79–82]. Unfortunately, these strategies have mainly focused only on overcoming few barriers, and were limited to the cancer theranostics and hardly involve other diseases. Likewise, the mechanism for transvascular extravasation is based on the EPR effect that the NPs pass through the inter-endothelial gaps in tumor angiogenesis to passively enter and accumulate within tumor tissue [83–86]. Encouragingly, in 2020, the latest work evidenced that 97 % of NPs were transvascularized into solid tumors by active process of trancytosis rather than by vascular gaps of EPR effect [87], and the enzyme-activatable cationization of nanoplatforms enabled efficient transvascular and transcellular transport based on active process *in vivo* [88]. These important discoveries, which subvert traditional dogma, require us to re-think and re-summary the strategies for addressing biological barriers and enhancing disease diagnosis along with treatment. Therefore, in this review, we attempted to summarize the latest achievements and propose new opportunities as well as future challenges to design smart and bioinspired systems for precise diagnosis and efficient therapy of many diseases by overcoming all of biological barriers (BVTDCLIN) *in vivo* using the innovative strategies (Table 1 and Scheme 2).

2. Charge conversion

The surface charge of NPs is a critical factor for blood circulation, vasculature extravasation, deep penetration, cellular internalization, and endosome escape [89]. Various previous literatures [90–93] revealed that positively charged NPs exhibited insufficient

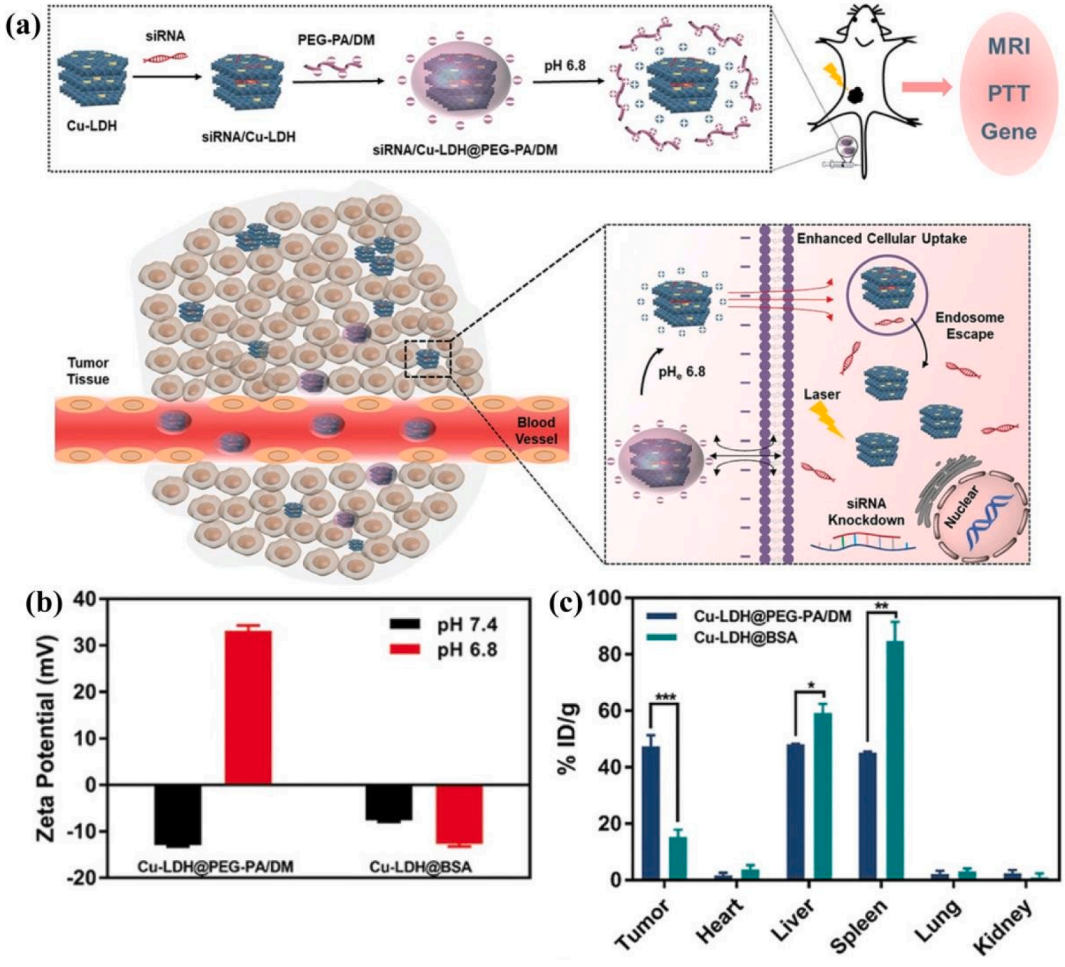

Fig. 1. (a) Schematic illustration of the preparation of siRNA/Cu-LDH@PEG-PA/DM NPs with pH-triggered charge reversal behavior for enhanced MR imaging-guided combined gene-PTT. (b) Zeta potential change at pH 7.4 and 6.8, and (c) biodistribution *in vivo* of pH-responsive Cu-LDH@PEG-PA/DM and non-responsive Cu-LDH@BSA. Reprinted with permission from 109. Copyright 2020, John Wiley and Sons.

blood circulation time attributing to strong nonspecific interaction with proteins, accelerating RES clearance and renal filtration. As expected, the NPs with initial neutral or negative charge, or zwitterionic groups are preferred to have a prolonged blood circulation [94]. Once they reach blood vessels wall or accumulate in targeted tissue, their surface charge converts to be positive to facilitate 2) vascular extravasation [95,96], 3) tissue accumulation [97], 4) deep penetration [53], 5) cellular internalization [98,99], and 6) endosome escape [100]. Therefore, the preparation of endogenous- or exogenous-triggered charge reversal NPs is an important way to overcome various barriers *in vivo* simultaneously.

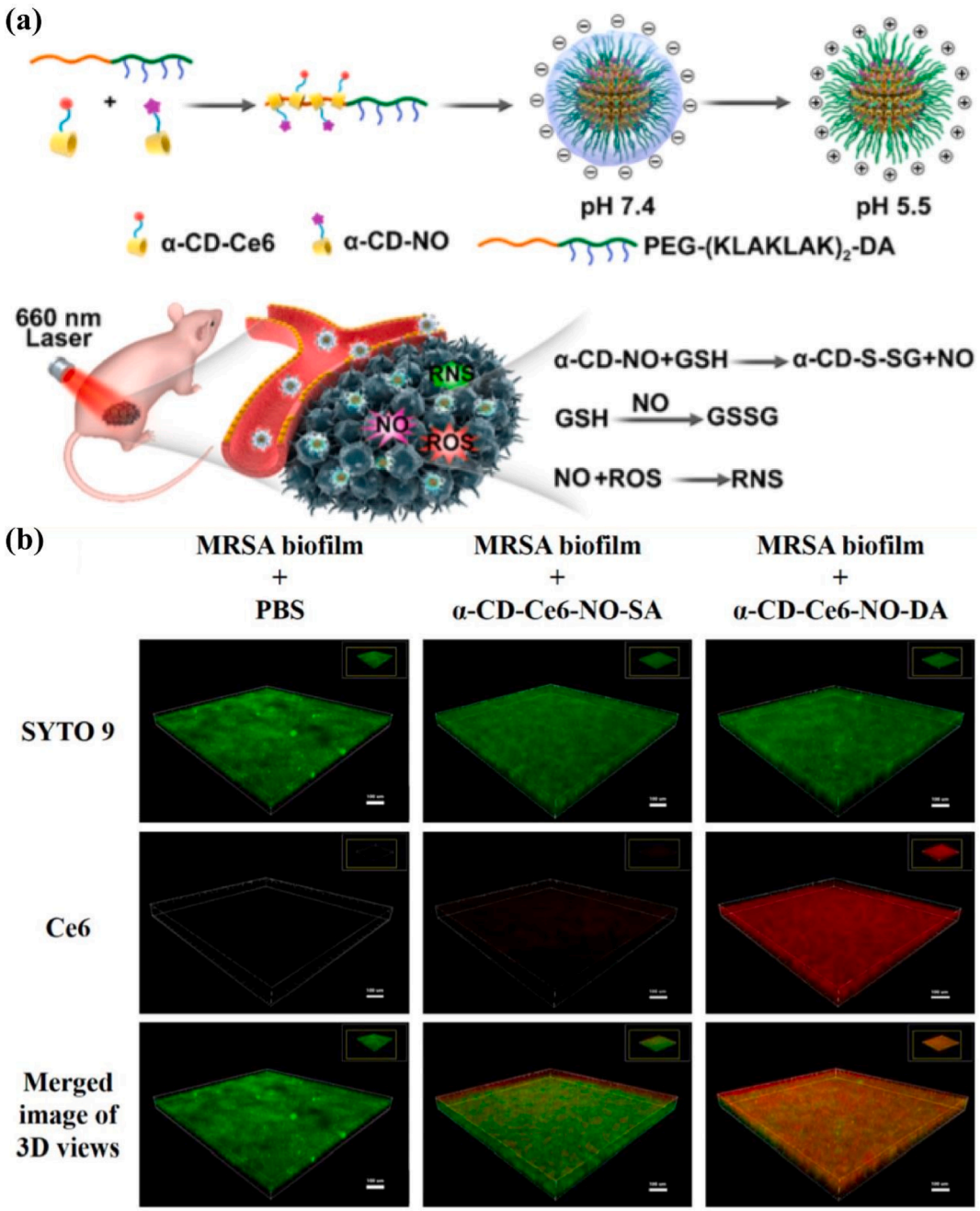

Fig. 2. (a) Schematic illustration of the preparation of pH-responsive charge reversal α-CD-Ce6-NO-DA for combined NO gas and PDT of biofilm infection. (b) Confocal laser scanning microscope (CLSM) images of MRSA biofilm after incubation with PBS, non-responsive α-CD-Ce6-NO-SA, and pH-responsive α-CD-Ce6-NO-DA. Scale bar: 100 μm. Reprinted with permission from 132. Copyright 2020, American Chemical Society.

2.1. Endogenous signals

In virtue of the unique lesion microenvironment of weak acidity [101], specific enzyme [102], redox [103], and hypoxia [104], the endogenous-responsive NPs have been designed to achieve the surface charge conversion from neutral, negative or zwitterion to positive by bond cleavage or group protonation [105].

2.1.1. pH

2.1.1.1. Bond cleavage. Differently from normal tissue environment of pH 7.4, the weak acidic tumor microenvironment (TME, pH 6.0–6.8) is a ubiquitous feature for almost all types of solid tumors [106]. In this regard, some acid-sensitive linkers (e.g., amide and benzoic-imine bonds) [107] have been employed to design pH-triggered charge reversal nanoTheranostics Among them, 2,3-dimethylmaleic amide (DMMA), a commonly used amino group protector, was adopted to form pH-sensitive bond which could be reversibly cleaved at weak acidic TME (pH∼6.8) [108]. For instance, Xu *et al.* [90] fabricated pH-triggered charge-reversible polymer-coated layered double hydroxide (Cu-LDH) nanoplatforms with siRNA compression for effective magnetic resonance (MR) imaging-guided combinational gene and photothermal therapy (PTT) of melanoma (Fig. 1a). The positively charged Cu-LDH was shielded by the DMMA modified polymer layer (PEG-PA/DM) to obtain the final Cu-LDH@PEG-PA/DM NPs with negative potential (−12.9 mV) at pH 7.4 (Fig. 1b), thus achieving the prolonged blood circulation, enhanced tumor accumulation and reduced non-specific cellular uptake. Once accumulated in tumor region, the PEG-PA/DM reversed to positively charged one by amide cleavage and further detached from Cu-LDH surface by electrostatic repulsion, re-exposing the positively charged Cu-LDH (33.1 mV) for facilitating cancer cell uptake *via* an endosomal escape pathway. Remarkably, the experiment *in vivo* demonstrated that about 6.0 % of injected Cu-LDH@PEG-PA/DM NPs was accumulated in tumor (Fig. 1c), far higher than the accumulation (around 3 %) of non-responsive Cu-LDH@BSA and the average accumulation (less than 1 %) of other NPs reported elsewhere [109,110].

Compared to the surface only exhibiting neutral or negative charges, the NPs containing zwitterionic groups or mixed anionic/cationic groups show higher protein resistance property [111,112]. Therefore, the novel pH-triggered charge switchable NPs based on DMMA modified zwitterionic polymers were synthesized for enhanced drug delivery to breast tumor [113]. Notably, the quick cleavage kinetics and unsatisfactory stability of the amide in DMMA at pH 7.4 limit its further applications [114]. Fortunately, 2-propionic-3-methylmaleic anhydride (CDM), a derivative of DMMA, has been synthesized and utilized to provide an acidic-sensitive structure and achieve a slower degradation rate in physiological environment [115,116].

Besides, due to the tremendous environment difference in pH values between cancer extracellular (pH 6.0–6.8) and intracellular (pH 5.0–6.0) [117,118], the nanocarriers are responsive to the single pH value, targeting either the cancer extracellular and intracellular condition, impairing the transport efficacy. For example, the extracellular pH-responsive nanocarriers release drugs prematurely, resulting in the inefficient antitumor activity, while the nanocarriers responding to intracellular pH is not capable of enhancing the cellular uptake. Differently from these aforementioned acid-sensitive linkers in response to extracellular pH (∼6.8), some acid-liable chemical bonds (e.g., acetal, hydrazone, *cis*-acony, and orthoester) [119] can only be cleaved within lower pH (5.0–6.0) and have been explored to design intracellular pH-responsive NPs. Motivated by this interesting property, the dual pH-responsive nanocarriers were prepared for efficient drug delivery [120]. The dual pH-responsive nanocarriers could reverse surface charge (negative to positive) by amide cleavage at tumor extracellular pH (∼6.8) for enhanced cellular uptake. After internalization, the lower pH (∼5.0) in intracellular of endosome further facilitated drug release by hydrazone bond cleavage, causing a significantly enhanced anticancer efficacy in drug-resistant cancer stem cells.

Comparison with the utilization of covalent linking method to construct these nanoplatforms, the non-covalent supramolecular interactions (e.g., host–guest [121,122] or hydrophobic interaction [123,124], hydrogen bonding [125,126], and metal–ligand coordination [127–129]) with convenient synthesis procedure also can be used to fabricate the smart NPs [130]. For instance, Ji *et al.* [131] developed pH/redox dual-responsive supramolecular nanocarriers (α-CD-Ce6-NO-DA) *via* host–guest interaction of α-CD prodrugs (α-CD-Ce6 and α-CD-NO) and acid-sensitive copolymer (PEG-$(KLAKLAK)_2$-DA) for improved biofilm infection treatment (Fig. 2a). Different from non-responsive α-CD-Ce6-NO-SA, the pH-responsive α-CD-Ce6-NO-DA could completely reverse their surface charge from negative to positive when reached the acidic methicillin-resistant *Staphylococcus aureus* (MRSA) biofilm (pH 5.5) for promoting effective penetration into the biofilm (Fig. 2b). Once infiltrated into the biofilm, α-CD-Ce6-NO-DA exhibited glutathione (GSH)-triggered nitric oxide (NO) release, which not only produced abundant NO for killing bacteria but also reduced the biofilm GSH level to improve photodynamic therapy (PDT) efficiency.

2.1.1.2. Protonation. Although the pH-triggered charge reversible NPs by bond cleavage have made great progress for enhanced disease theranostics, the charge reversible process often takes hours and the NPs may have been cleared before the bond cleavage occurs [132], resulting in low delivery efficacy [133]. To address these challenges, the pH-responsive switchable protonation/deprotonation systems, such as amino [134,135], tertiary amine [136–138], pyrrole [139–141], imidazole [142–144]. and azepane groups [145], provide an alternative strategy to design smart NPs to more efficiently realize disease Theranostics In very recent work, our group synthesized pH-responsive charge switchable glycol chitosan-based nanoclusters (neutral to positive) for elevated tumor penetration, cell internalization, and theranostic efficiency, thereby achieving MR imaging-guided PDT of tumors [146]. Moreover, we also developed ultrafast charge reversible chitosan-polypyrrole nanogels (CH-PPy NGs) for augment chemotherapy of ovarian carcinoma with low side effects (Fig. 3a) [147]. By fine treatment with alkaline solution (Fig. 3b), the formed charge reversible NGs (R-NGs) with initial negative charge (−11.3 mV) displayed excellent antifouling property and prolonged blood circulation. Once the R-

NGs accumulated in the tumor tissue, their surface charge converted to be positive through rapid protonation of pyrrole ring within 10 s to elevate deep penetration and cell uptake by the positive charge-enabled transcytosis (Fig. 3c). Notably, due to the ingenious design, a significantly high tumor accumulation of R-NGs/DOX (4.7 %) was achieved. Furthermore, the polyampholyte microgels (MGs) with defined chemical structure (controlled amounts of cationic imidazole and anionic carboxyl groups) and morphology (controlled distribution with random or core/shell) were synthesized in our group [148]. The MGs displayed pH-dependent charge conversion from negative (pH 7.4) to positive (pH 5.0–6.0). To further improve the antifouling performance of nanoplatforms, our group designed the pH-responsive zwitterionic alkoxyphenyl acylsulfonamide (APAS) [149] that emerged a sensitive charge conversion from zwitterionic to positive by the protonation at pH 6.0–6.5 [150]. Therefore, the APAS conjugated nanocarriers displayed the strong protein resistance and extended circulation time in blood, and high cellular uptake in cancer cells by the charge conversion of APAS moieties.

2.1.2. Enzyme

2.1.2.1. MMP. Apart from the acidic TME, the overexpressing of specific enzymes, such as matrix metalloproteinase (MMP) [151,152], hyaluronidase (HAase) [153], gelatinase [154] or phosphatase [155], is another hallmark in the TME [156,157]. Some literatures illustrated the peptide sequence of PLGLAG, a substrate of MMP, could be cleaved responding to high expression level of MMP [158–160]. According to these interesting features, Chen *et al.* [161] designed the MMP-activated low molecular weight protamine (ALWMP) for safe and effective tumor-targeting drug delivery. The positively charged ALWMP was initially masked by a

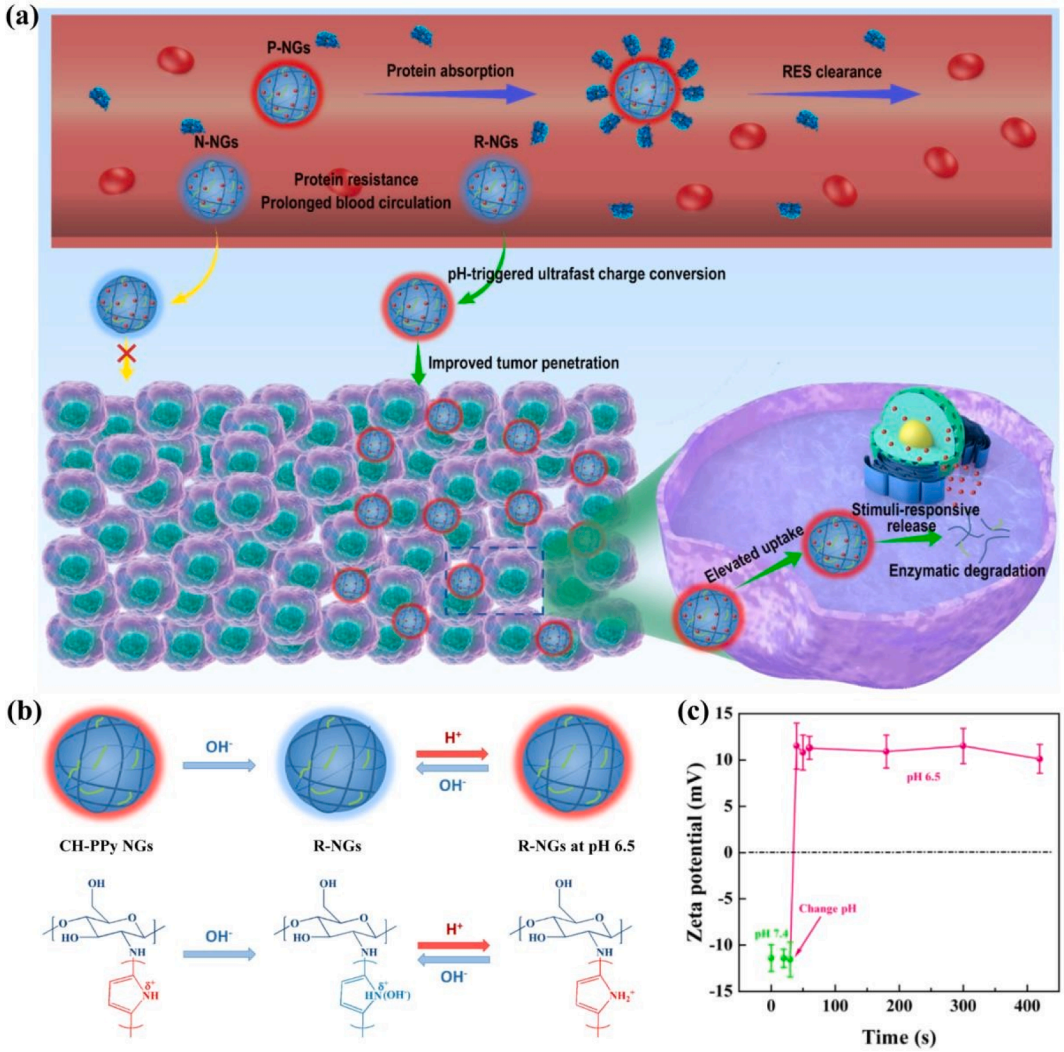

Fig. 3. (a) Schematic illustration of drug delivery procedure of positive, negative, and charge reversible NGs. (b) Schematic illustration of alkaline treated CH-PPy NGs and pH-dependent ultrafast charge conversion of R-NGs at pH 6.5. (c) Zeta potential change of R-NGs at pH 7.4 and 6.5. Reprinted with permission from 148. Copyright 2021, Elsevier.

polyanionic peptide (E10) sequence using the MMP-responsive linker of PLGLAG. The smart system showed three superior advantages: 1) the ALWMP sequence as activated cell penetrating peptides (ACPPs) is able to specifically target neuropilin-1 protein on cancer cells for enhanced internalization; 2) the neutrally charged ALWMP obviously reduces the recognition by the macrophage system and prolongs blood circulation; 3) after reaching the tumor tissue, the PLGLAG linker will be cleaved by the enzyme of MMP-2/9, enabling the exposure of positive charge for elevated deep penetration and cellular internalization. As a result, the tumor accumulation of enzyme-responsive nanoplatform was 4- to 15-fold higher than that without ACPPs conjugation [162].

Moreover, Jiang *et al.* [163] proposed the novel strategy that combined the benefit of dual-targeting delivery and ACPPs to effectively circumvent blood–brain and blood-tumor barriers (BBB and BTB) for improved glioma treatment (Fig. 4a). The dual-targeted ligands, angiopep-2 and ACPPs (E8-6-aminohexanoyl-PLGLAG-R8), modified NPs (AnACNPs) were able to penetrate through the BBB, and actively target glioma *via* the angiopep-2 mediated targeting (Fig. 4b). Subsequently, at the glioma site, E8 could be detached from cationic R8 by MMP-responsive PLGLAG cleavage to achieve surface charge conversion, leading to the enhanced penetration ability for BTB. Although these ACPPs can be cleaved by MMP, the polyanionic inhibitory peptides after cleavage are difficult to separate from the ACPPs because of the electrostatic interaction. To solve this predicament, the inhibitory peptides with an isoelectric point of around 6.4 was chosen to design MMP/pH dual-triggered novel ACPPs [164,165]. At acidic TME, the pre-existing electrostatic attraction in ACPPs was eliminated due to the isoelectric point. Accompanying the linker cleavage by MMP2, ACPPs would be activated to expose the positive surface charge to improve cellular uptake in tumor.

2.1.2.2. Haase. The hyaluronic acid (HA) as a kind of natural acidic polysaccharide macromolecules can be employed to coat the surface of cationic NPs and then hydrolyzed by the overexpressed HAase in TME to re-expose the positive charge of NPs [166–168]. Through combining the advantage of ACPPs, the HA-coated and ACPP-modified liposomes (HA-ACPP-L) were designed for enhanced drug delivery of hepatocellular carcinoma [169]. The HA was utilized to shield positive charge of ACPPs-modified liposomes (ACPP-L) for improved blood persistence. At the tumor region, the HA-ACPP-L disassembled to ACPP-L by HAase-responsive degradation, and induced the charge conversion due to the re-exposure of cationic ACPP-L. The HAase-responsive C6/HA-R6H4-L showed efficient intracellular trafficking including endosomal/lysosomal escape and cytoplasmic liberation because of the proton sponge effect of imidazole group of ACPPs.

2.1.3. Redox

Besides that, cancer cells also produce high amounts of reduced substances (e.g., GSH and hydrogen sulfide (H_2S)) [170–172] and reactive oxygen species (ROS, e.g., hydroxyl radicals, superoxide, and hydrogen peroxide (H_2O_2)) [173–177] to generate redox TME. Several work have been reported that, by H_2S-mediated reduction, the azides were introduced as the most common agents for endogenous H_2S detection [178–180]. After the reduction of azides, the formed amine nitrogen showed positive charge [181–183]. On the basis of mechanism, Lin *et al.* [184] designed H_2S-triggered charge reversal micelles using the self-assembly of azide-based H_2S probes ended amphiphilic block copolymers for fluorescence imaging and targeted drug delivery of breast cancer (Fig. 5a). The smart micelles showed high sensitivity and selectivity for H_2S in tumor cells. After monitoring H_2S, the surface charge of the micelles reversed from negative to positive, leading to the enhanced tumor uptake, efficient lysosome escape and imaging-guided therapy.

In addition to the tumor region, most of neurodegenerative diseases, such as ischemic stroke and amyotrophic lateral sclerosis, are

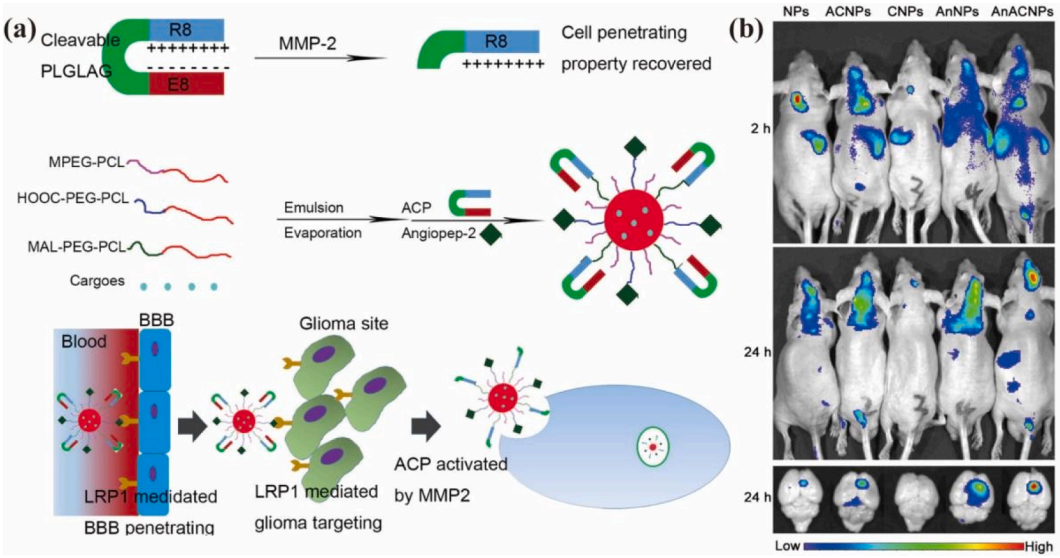

Fig. 4. (a) Schematic illustration of the preparation of MMP-responsive AnACNPs for enhanced glioma treatment by circumvent BBB and BTB. (b) Fluorescence imaging of glioma-bearing mice treated with different samples. Reprinted with permission from 164. Copyright 2014, American Chemical Society.

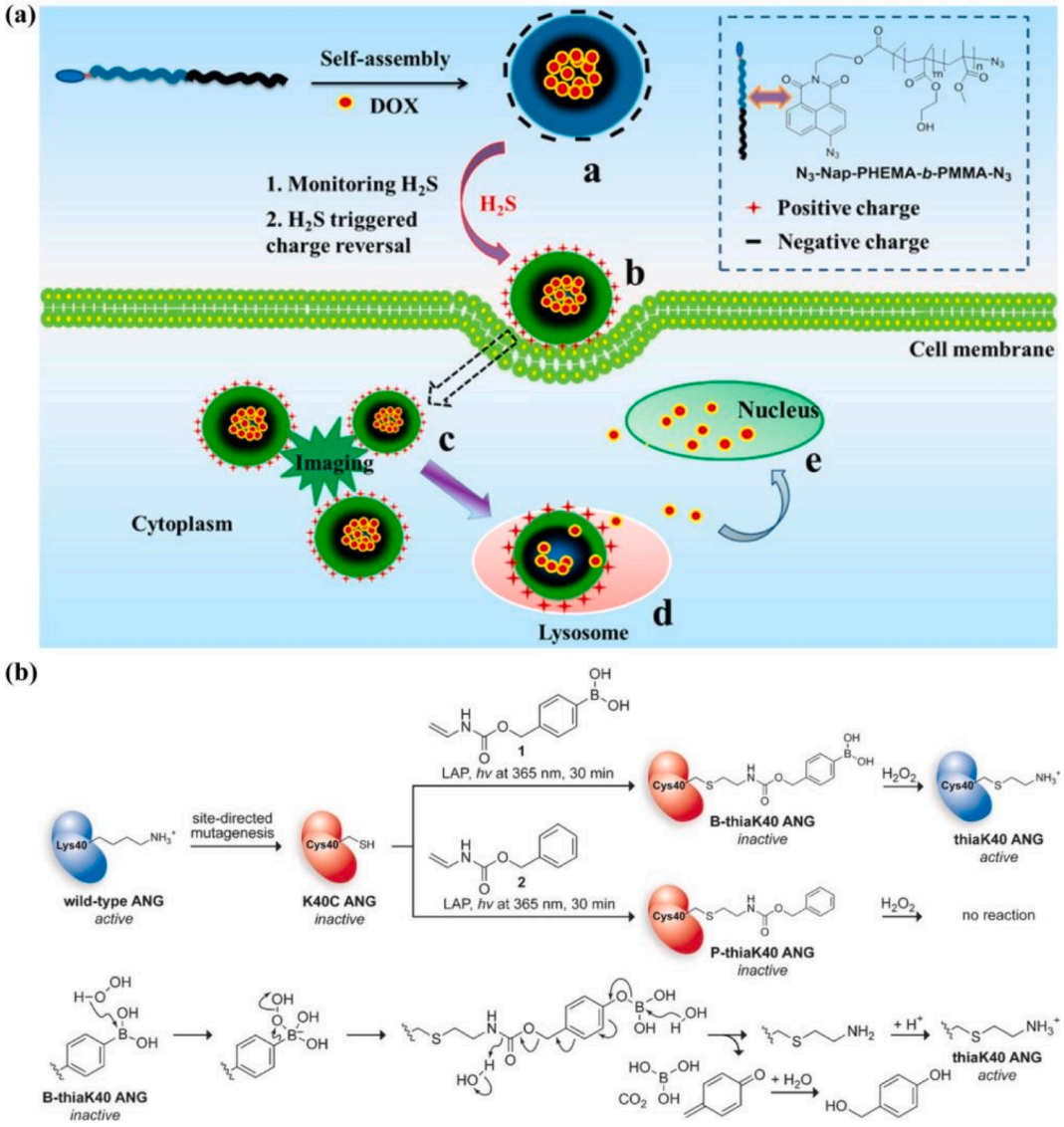

Fig. 5. (a) Schematic illustration of DOX loaded micelles for enhanced fluorescence imaging and targeted drug delivery of breast cancer. Reprinted with permission from 185. Copyright 2016, American Chemical Society. (b) Mechanism of ROS-triggered activated ANG. Reprinted with permission from 193. Copyright 2017, John Wiley and Sons.

associated with an abundance of ROS which is cytotoxic [185–188]. H_2O_2, a common form of ROS, is able to effectively destroy the boron–carbon bond of phenylboronic acid *via* the oxidative cleavage [114,189], and then various boronic acid conjugated nanocarriers with ROS-responsiveness have been employed for drug delivery and controllable release [190,191]. In view of these characteristics, the boronic acid modified angiogenin (ANG) with ROS-responsive activity was prepared for efficient neuroprotection (Fig. 5b) [192]. With the stimulation of H_2O_2, the modified boronic acid in B-thiaK40 ANG was cleaved to form thiaK40 ANG with positive charge due to the amino groups, enabling the activated neuroprotection.

2.1.4. Hypoxia-responsiveness

Hypoxia is a feature in TME of solid tumors attributing to the region distance from blood vessels and oxygen diffusion limitation, which is implicated in resistance to various therapy [193–195]. The insufficient delivery of nanotheranostics to hypoxic tumor is recognized as one of the causes of resistance to therapy [196,197]. As everyone knows, the oxygen concentration decreases with the depth of tumor tissue [198]. Therefore, gradually increasing the driving force, which could be achieved by a response to the tumor hypoxia gradient, may address the resistance to achieve deep penetration in tumors. Currently, some hypoxia-sensitive moieties of nitroimidazole [199–201], nitrobenzyl alcohols [202–204] or azobenzene groups [205–207] can be reduced to generate the cationic aminoimidazole, amino or aniline groups under hypoxia, respectively. For instance, Shi *et al.* [208] developed a novel hypoxia-

responsive micelle (RM) for effective tumor penetration (Fig. 6a). The RM was composed of poly(caprolactone) core and a hypoxia responsive mixed shell of 4-nitrobenzyl chloroformate (NBCF)-modified polylysine (PLL) and PEG. During the blood circulation, the NBCF-modified PLL was shielded by the PEG, which gave it the ability to inhibit its rapid removal by the immune system. Once reaching the tumor, the hypoxia-triggered partial NBCF degradation recovered the amine groups and reversed surface charge of PLL,

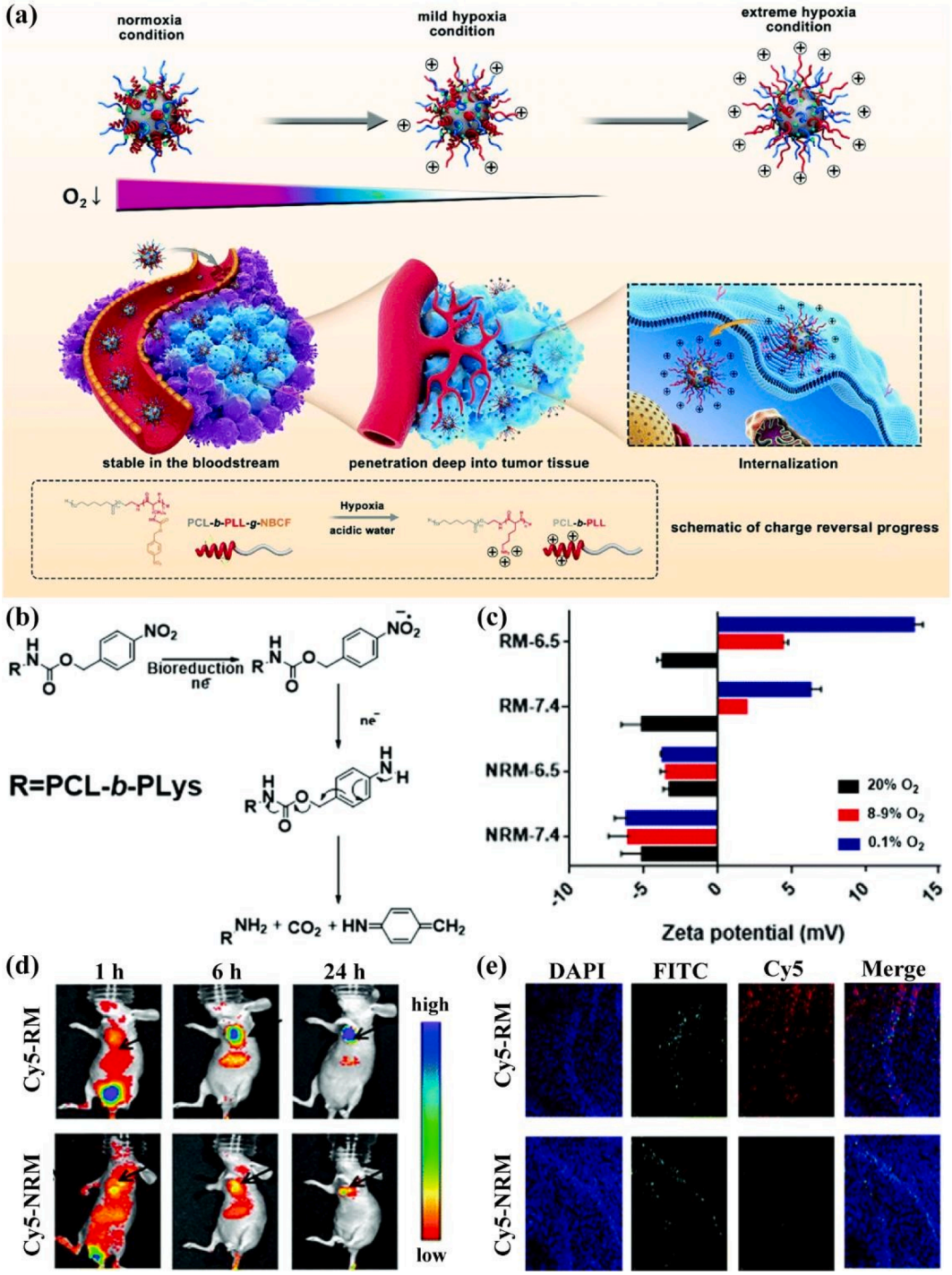

Fig. 6. (a) Schematic illustration of the hypoxia responsive nanocarrier for prolonged blood circulation and enhanced deep penetration. (b) Mechanism of hypoxia-triggered NBCF degradation of RM for charge conversion. (c) Zeta potential of RM and non-responsive micelle (NRM) under different O_2 gradients and pHs. (d) *In vivo* fluorescence imaging of the tumor bearing mice, and (e) CLSM images of the corresponding tumor sections after injection of Cy5-RM and Cy5-NRM. Reprinted with permission from 209. Copyright 2019, Royal Society of Chemistry.

leading to tumor deep penetration (Fig. 6b,c). With the decrease of oxygen within the interior of tumor, the surface positive charge of Cy5-labeled RM (Cy5-RM) further increased to improve tumor accumulation and penetration (Fig. 6d,e). Additionally, the azobenzene as other hypoxia-responsive bioreductive linker was used to prepare hypoxia-induced charge reversible nanocarrier for hypoxia-targeted siRNA delivery of ovarian cancer [209]. Overall, the hypoxia gradient response strategy showed great potential for enhancing theranostic efficiency.

2.2. Exogenous factors

In comparison with aforementioned endogenous TME-responsive nanotheranostics, other charge reversal NPs in responding to the exogenous factors, such as light [210], US [211], thermal [212], and specific additives [213], are designed for other diseases without the significantly difference microenvironment [214]. More importantly, these exogenous triggers can be spatiotemporally addressed according to diverse requirements.

2.2.1. Light

2.2.1.1. UV light. Several intelligent nanoplatforms with precise spatiotemporal controllability have been developed for efficient cargo delivery by light-triggered charge switching [215–217]. For instance, Shea *et al.* [218] designed the ultraviolet (UV) light-activated charge reversal NPs using the *o*-nitrobenzyl carbamate (a photoresponsive molecules)-protected amine-bridged polysilsesquioxane. Upon UV irradiation (254 nm), amine groups emerged by the deprotection to reverse the colloidal charge from negative to positive. What's more, 4,5-dimethoxy-2-nitrobenzyl (DMNB) as other UV-induced removal of protective molecule on the amine group was used to fabricate the UV-activated liposomes (DOPC:4) for membrane impermeable payloads delivery *in vivo* (Fig. 7a) [219]. Upon UV irradiation (370 nm), the complete photolysis of DOPC:4 was achieved by the deprotection of amine groups in less

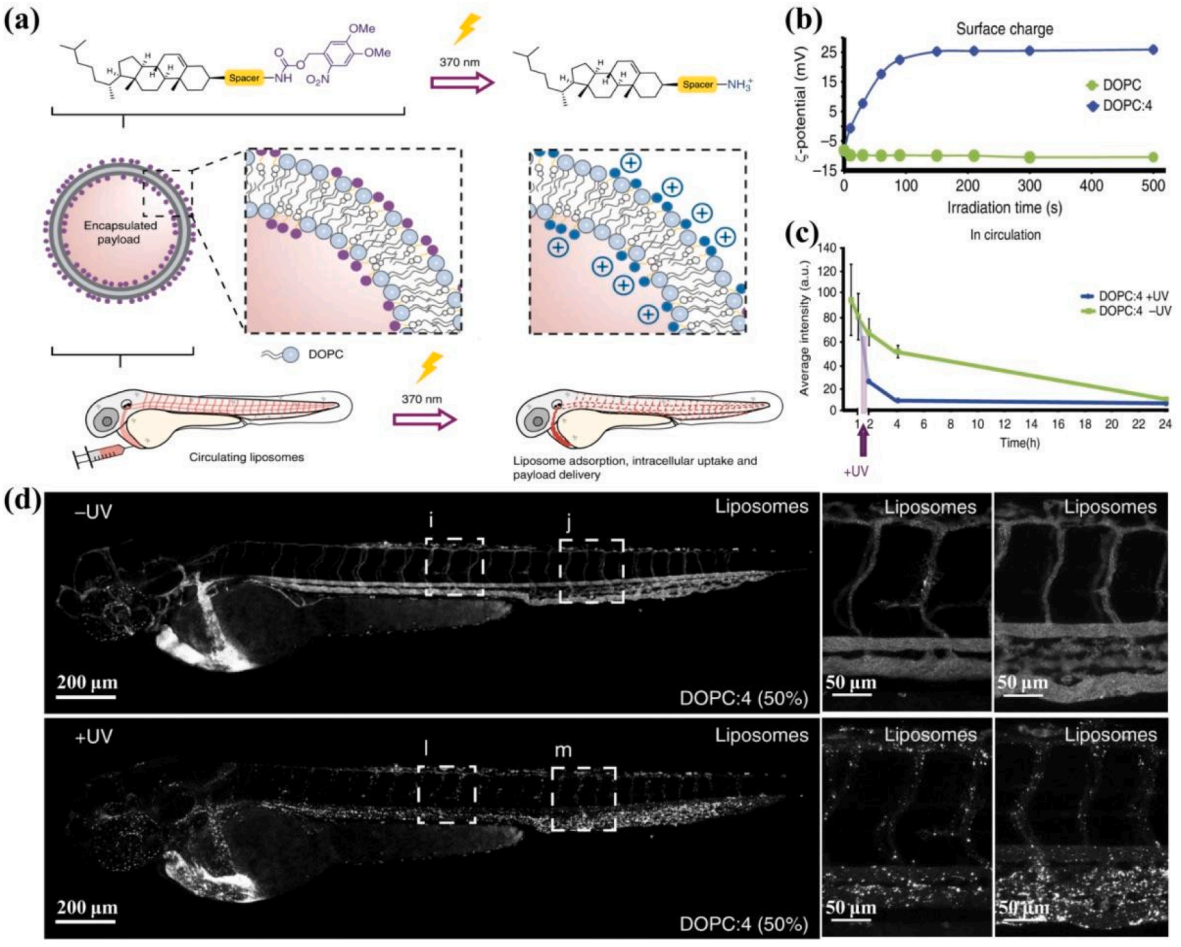

Fig. 7. (a) Schematic illustration of UV-activated charge reversal (DOPC:4) liposomes for membrane impermeable payloads delivery. (b) Zeta potential of DOPC:4 after UV irradiation for different times. (c) Fluorescence intensity of blood circulation, and (d) fluorescence imaging of whole embryo from DOPC:4 biodistribution before and after *in situ* UV irradiation. Reprinted with permission from 220. Copyright 2020, Springer Nature.

than 120 s, leading to the surface charge reversal from −8 mV to 26 mV (Fig. 7b). After intravenous (IV) injection of DOPC:4 into the embryonic zebrafish, DOPC:4 before UV irradiation was freely circulating and did not significantly interact with RES cell types of the embryonic fish, involving blood resident macrophages and scavenging endothelial cells. However, upon *in situ* irradiation, a dramatic change in DOPC:4 fate was observed, whereby the liposomes were visible as immobile punctae associated with all blood vessel walls and largely removed from the blood circulation (Fig. 7c,d). This result indicated that upon *in situ* irradiation and surface charge switching, the DOPC:4 rapidly adsorbed to, and was taken up by, endothelial cells and/or was phagocytosed by blood resident macrophages.

2.2.1.2. NIR light. To avoid unnecessary UV irradiation damage and achieve deeper tissue penetration, the near-infrared (NIR, more than 700 nm) light have been applied as a favorite triggering stimulus to activate charge conversion of nanoplatforms [220–223]. The NIR light exhibit various advantages of good spatial resolution, excellent controllability, negligible injury, and irreplaceable deep permeability (up to a depth of 2 cm) [224–227]. Recently, the DMNB-protected phenolic hydroxyl compound as photocleavable molecular response to NIR irradiation was explored for controllable cargo release [228–231]. Based on this sensitive group, the NIR/pH dual-responsive polypeptide-modified NPs (PPP-NPs) were synthesized by modifying the synthesized functional material (DSPE-PEG_{2000}-PPP) for enhanced and targeted gene therapy (Fig. 8a) [232]. In this system, the PPP consisted of three parts: cell-penetrating peptide (CPP), photocleavable linker, and acid-sensitive inhibitory peptide. After IV injection, PPP-NPs could be efficiently accumulated in the tumor region by cell-penetrating peptide-mediated targeting. At the acidic TME, the acid-sensitive inhibitory peptide was eliminated the electrostatic interaction, meanwhile the photocleavable linker was cleaved upon NIR (740 nm) irradiation for 30 min to release the inhibitory peptide to expose the CPPs (Fig. 8b) and expose the positively charged cell-penetrating peptide for enhanced cellular uptake (Fig. 8c).

2.2.2. Thermal

In our previous work, the thermal-responsive MGs were synthesized using amino-modified thermal-sensitive N-vinylcaprolactam (VCL) monomer [233–235]. The PVCL-based MGs exhibit an adjustable volume phase transition temperature (VPTT) from 30 to 40 °C that is close to body temperature [236,237]. Under high temperature more than VPTT, the surface positive charge of amino-modified PVCL MGs is further increased attributing to the concentration of charges by the shrinkage of MG out layer. The thermal-responsive property of MGs is able to improve the cell membrane affinity, resulting in the enhanced cellular internalization. Additionally, using thermal-sensitive cationic polymer of poly(allylamine) hydrochloride (PAH), the charge reversal behavior allowed for single-polymer

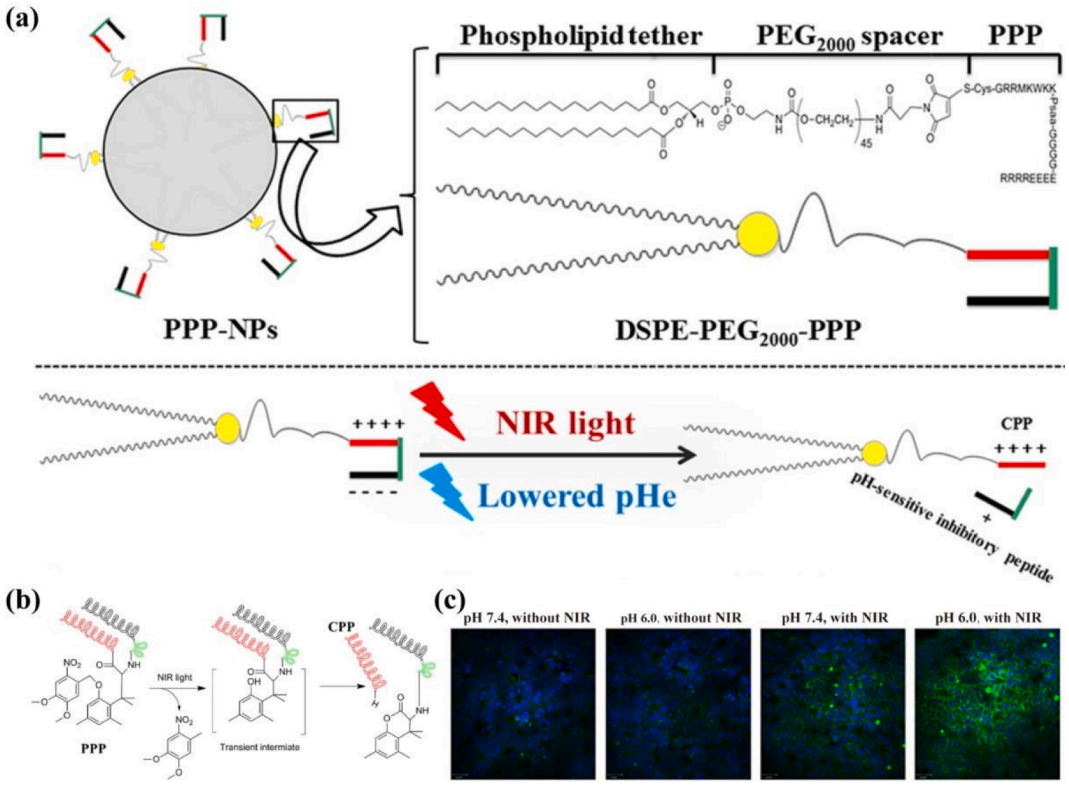

Fig. 8. (a) Schematic illustration of the preparation of polypeptides modified NPs (PPP NPs) with NIR/pH dual-responsive behavior. (b) Mechanism of NIR-triggered cleavage of PPP. (c) CLSM images of MCF-7 cells treated by PPP-NPs with or without NIR irradiation at pH 7.4 and 6.0. Reprinted with permission from 233. Copyright 2016, American Chemical Society.

layer-by-layer (LbL) assembly of PAH to prepare LbL films, capsules and replica particles [212]. After heating, the surface charge conversion from positive to negative of PAH could reduce protein fouling and cell adhesion (Fig. 9).

2.2.3. Specific additives

Although abovementioned strategies have raised expectations due to their efficient theranostics *in vivo*, relying on the linker cleavage limits the efficiency of the charge conversion, the selectivity of the process, and the reversibility of the switch [238–240]. In this context, the development of stimuli-responsive cell internalization strategies that do not rely on covalent linker-cleavage represents an appealing goal [241,242]. The host–guest interaction as one of high selectively and reversibility specific recognition is an ideal candidate to form stimuli-responsive noncovalent interactions [243]. Remarkably, Mascareñas *et al.* [244] proposed a novel approach to enhance cell uptake based on the formation of host–guest supramolecular complex involving an anion recognition process. Through *in situ* addition of cationic cages (host), the negatively charged pyranine (Pyr)-peptide (guest) was encapsulated by host using specific anion recognition to trigger the cell internalization based on the surface charge conversion. Interestingly, none of the components, neither the host or guest, were able to cross cell membranes as separate units, but their association promoted an efficient cellular uptake.

Furthermore, based on the similar strategy, they developed the charge reversal Pyr modified Au NPs for the spatio/temporal control of cellular uptake by cationic cages (**A**)-triggered anion specific recognition (Fig. 10a) [213]. Using the fluorescence microscopy images, a higher cell fluorescence value increased up to 15-fold was observed in Au NPs with **A** host when compared to that in Au NPs without **A** host (Fig. 10b,c), suggesting that the cell uptake of Au NPs was activated by the host–guest recognition-triggered charge conversion. Even in protein-rich biological media, an effective cell internalization also was achieved. More importantly, by the rational addition of either cationic **A** or anion Pyr, the cell uptake of NPs was highly controllable (Fig. 10d). Therefore, a supramolecular strategy was developed for enhanced cellular internalization using external additives as triggers.

2.3. GGT on cell membrane

The aforementioned strategies regarding surface charge conversion by the endogenous TME or exogenous stimulations have been developed to overcome four biological barriers in 1) blood circulation, 4) deep penetration, 5) cellular internalization, and 6) lysosome escape simultaneously. For the barrier in 2) vasculature extravasation, the transport of these smart NPs from blood to tumor still

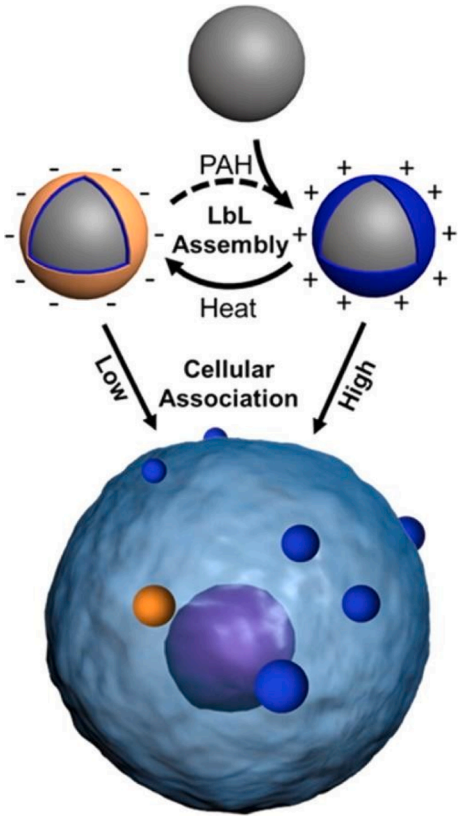

Fig. 9. Schematic illustration of the preparation of thermal-responsive LbL films, capsules and replica particles by LbL assembly of PAH for controlled cellular association. Reprinted with permission from 213. Copyright 2016, American Chemical Society.

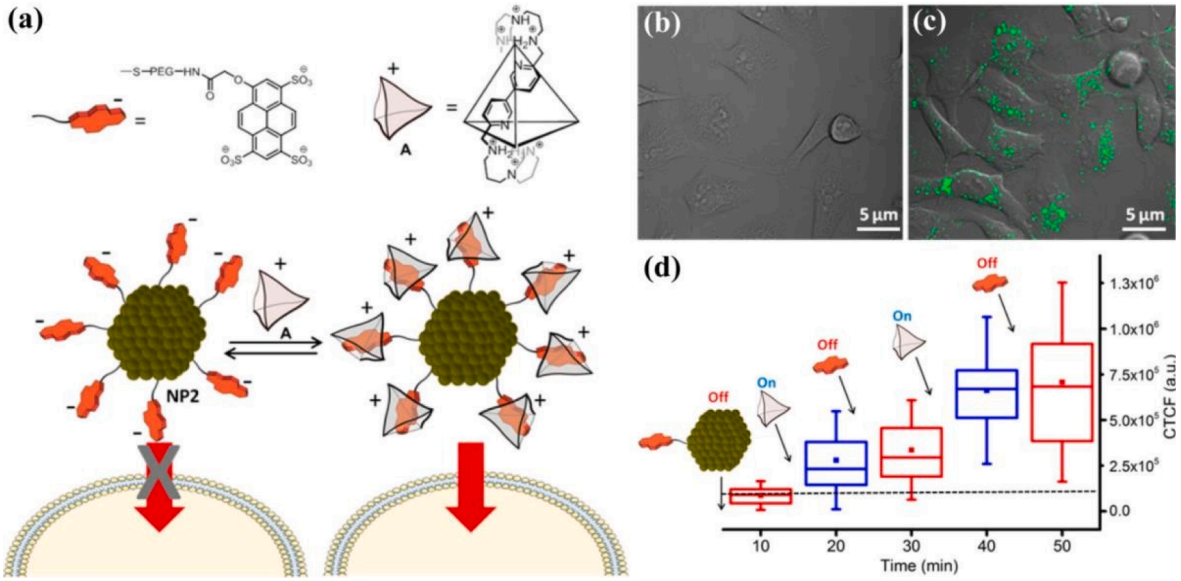

Fig. 10. (a) Schematic illustration of charge reversal Pyr modified Au NPs for the spatio/temporal control of cellular uptake by cationic A-triggered anion specific recognition. Fluorescence microscopy images of HeLa cells incubated with Au NPs (b) in the absence or (c) in the presence of A host. (d) The corrected total cell fluorescence (CTCF) change upon addition of cationic A or anion Pyr. Reprinted with permission from 214. Copyright 2018, American Chemical Society.

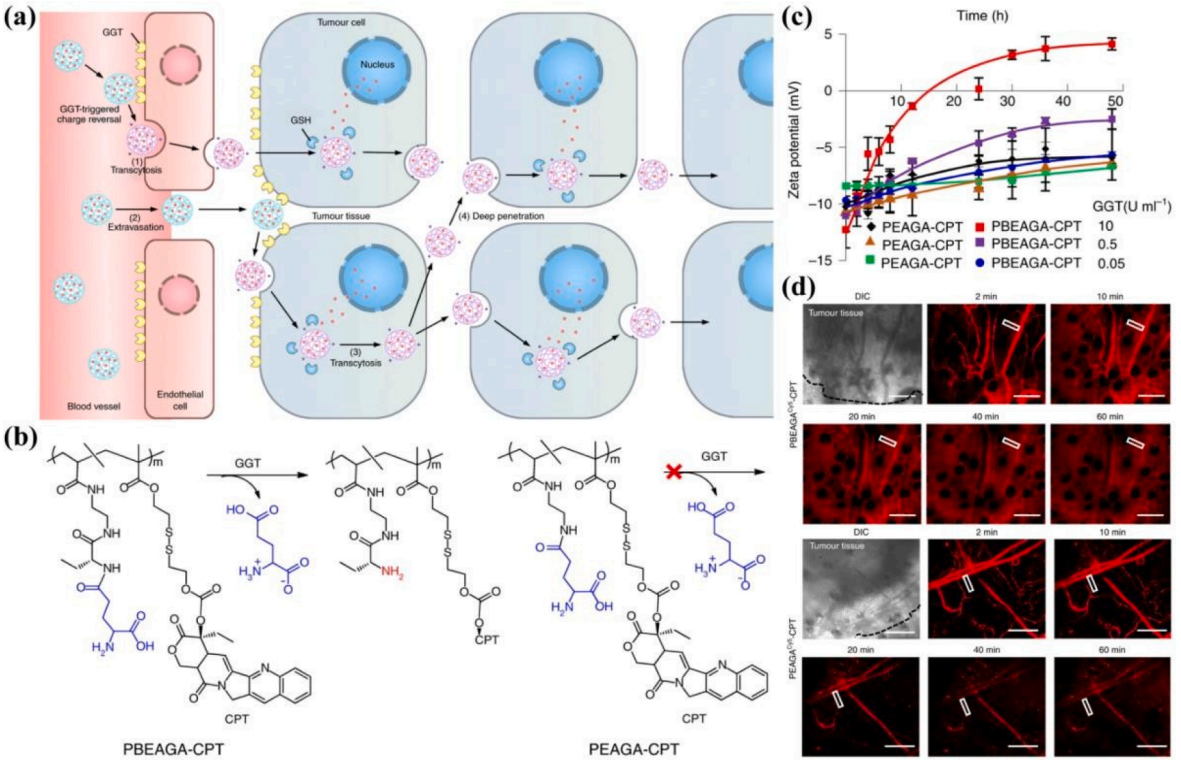

Fig. 11. (a) Schematic illustration of the PBEAGA-CPT with GGT-triggered charge conversion for improved vasculature extravasation and cellular internalization by the active transendothelial and transcellular transport. (b) Mechanism of GGT-responsive charge conversion of PBEAGA-CPT by the cleavage of γ-glutamyl moieties. (c) Zeta potential of PBEAGA-CPT and non-responsive PEAGA-CPT in the presence of GGT with different concentrations. (d) CLSM images of time-dependent extravasation and penetration of PBEAGA^{Cy5}-CPT and PEAGA^{Cy5}-CPT in tumors. Scale bars: 200 μm. Reprinted with permission from 88. Copyright 2019, Springer Nature.

followed the EPR effect of passive diffusion through tumor vascular gaps which was established by Jain's group in 1998 [245]. However, based on the mechanism of EPR effect, the delivery level of NPs is extremely low in animal models, and the corresponding clinical translation is disappointed [246–250]. Encouragingly, in 2020, Chan *et al.* [87] found there are simply not enough endothelial gaps on the wall of blood vessels to support efficient extravasation and accumulation of NPs. In comparison, active transcytosis by endothelial cells, including active uptake intracellular transport and exocytosis, was more efficient for NPs delivery to solid tumors *in vivo* [6]. These results implied that approximately 97 % of NPs were transported into solid tumors by active transcytosis rather than EPR effect. Therefore, the delivery mechanism based on active transcytosis may be more dominant than passive EPR effect.

Inspired by the latest discoveries and the endothelial cell caveolae-mediated transcytosis, Shen *et al.* [88] designed γ-glutamyl transpeptidase (GGT)-responsive zwitterionic polymer-camptothecin (CPT) conjugate (PBEAGA-CPT) for significantly enhanced therapeutic efficacy by the active transendothelial and transcellular transport (Fig. 11a). The PBEAGA-CPT was stable and stealthy in blood circulation due to its zwitterionic nature. On contacting the tumor vessel endothelial cells or extravasating into the perivascular regions contacting tumor cells, the overexpressed GGT on the cell membrane cleaved γ-glutamyl moieties of PBEAGA-CPT to obtain positive surface charge (Fig. 11b,c). The cationized conjugate underwent caveolae-mediated endocytosis and transcytosis for addressing the barrier in vasculature extravasation and achieving uniform distribution along with distal diffusion throughout the tumor. After IV injection of PBEAGA^{Cy5}-CPT, the results of real-time extravasation and tumor penetration demonstrated that the PBEAGA^{Cy5}-CPT (red fluorescence) was initially restricted in the tumor blood vessels, and then gradually extravasated from the vessels and diffused into the distal tumor site (Fig. 11d). Furthermore, other phospholipid-binding zwitterion that is not sticky towards proteins but will weakly bind to cells was developed for enhanced drug delivery in tumor [251]. The antifouling property of zwitterion and the hitchhiking behavior of binding to red blood cells endowed nanocarriers with prolonged blood circulation. Subsequently, the phospholipid affinity allowed nanocarriers to reversibly bind to cell membranes, which could trigger adsorption-mediated active transcytosis for elevated vasculature extravasation and tumor penetration, thus achieving highly efficient delivery from perivascular to avascular and hypoxic regions [252]. These results fully proved that the novel strategy of stimuli-activated transendothelial transport was able to effectively obtain transvascular, deep tumor penetration and enhanced cell uptake ability [253].

3. Size transformation

The size of NPs plays a vital role in the process of vasculature extravasation [254], tissue accumulation [255], deep penetration [256], cellular internalization [257], systemic biodistribution [258], lysosome escape [259], intracellular efflux [260], and nuclear targeting [261]. Normally, the specific optimized size of NPs emerges intrinsically conflicting for different biological barriers. Large NPs with a diameter more than 100 nm are favorable for tissue accumulation/retention [262] and lysosome escape [263], along with limited intracellular efflux [264], but they are disadvantageous for deep penetration, cellular uptake and nuclear targeting [265]. In contrast, small NPs (10–100 nm) display a better vasculature extravasation, deep permeability and cellular uptake [266,267]. However, these small NPs suffer from obvious RES capture (e.g., liver/spleen uptake and renal filtration), unsatisfactory tissue retention, and rapid intracellular efflux, as they readily intravasate back into blood circulation [268]. Likewise, the smaller NPs with a diameter less than 10 nm is required for efficient lymph node delivery and cell unclear uptake [269]. Therefore, the changeable NPs size, whether small to large or large to small, is an ideal strategy to simultaneously overcome versatile barriers *in vivo*. Recently, the novel deformable NPs with turned shape (from spherical to ellipsoidal) have also been developed to efficiently pass through blood vessels and penetrate into the tumor parenchyma.

3.1. Extracellular-triggered size increase

In the previous discussion, we concluded the strategies based on the charge reversible NPs that were introduced to address five biological barriers in 1) blood circulation, 2) vasculature extravasation, 4) deep penetration, 5) cellular internalization, and 6) lysosome escape. Remarkably, the extracellular-responsive size changeable NPs (from small to large) are able to overcome other barrier in 3) tissue accumulation. During blood circulation, the small NPs can efficiently extravasate into lesion region. Once they arrive at the targeted region, under either endogenous or exogenous stimulations, the small NPs can aggregate or swell into large one that can be trapped in tissue for the enhanced accumulation and retention, leading to the improved theranostic efficacy. Normally, the size switching of NPs from small to large may be achieved by the aggregation based on the charge interaction, hydrophobic interaction, hydrogen bonding, DNA assembly and covalent crosslinking. Besides the aggregation, the NPs swelling also can increase their size. Importantly, the size-change behavior of NPs can not only be employed to overcome the barriers *in vivo*, but also often affect their optical and magnetic properties [270], such as photothermal effect in NIR or variable relaxivities for MR imaging.

3.1.1. Charge interaction

The stimuli-responsive aggregation strategy was developed to improve tissue accumulation and retention [271–275]. Grzybowski *et al.* [276] found that the NPs comprising mixed-surface charge (both positive and negative charges) exhibited the controlled pH stability, and they were precipitated sharply at the pH where the charges on the NPs are balanced (pH^{prec}). More importantly, through adjusting the ratio of the positively and negatively charged ligands or changing size of NPs, the flexible pH^{prec} was obtained among about 4.0–7.0 [277], covering the extracellular pH (6.0–6.8) and intracellular pH (5.0–6.0) in cancer cells. By modifying the NP surface with mixed-charge self-assembly monolayers, the Au NPs with tunable pH-induced aggregation behavior were fabricated [278]. Interestingly, under acidic TME, Au NPs could generate aggregates for enhanced tumor accumulation and retention, meanwhile the aggregated Au NPs displayed a red-shift to NIR region which could be applied for efficient PTT of tumor. Moreover, the pH-

sensitive zwitterionic surface of mixed charge was employed to prepare pH-responsive Au NPs, which enabled Au NPs with stealth ability to resist uptake by macrophages and prolong blood circulation. At acidic TME, the pH-responsive Au NPs were quickly aggregated to greatly elevate tumor accumulation and retention, resulting in the efficient PTT of hepatocellular cancer [279].

Moreover, the smart NPs with both positive and negative surface charges also can be formed by pH-triggered surface hydrolysis strategy, and the aggregation of NPs drive by electrostatic attraction. In very recent work, the hydrolysis-susceptible citraconic amide was decorated on the surface of PEG and ethylenediamine modified melanin NPs (PEG-EDA-MNPs) to synthesize pH-responsive melanin NPs (pH-MNPs) (Fig. 12a) [280]. In tumor site, by citraconic amide hydrolysis, the spontaneous aggregation of pH-MNPs occurred for enhanced tumor retention. After the radionuclide ^{68}Ga labeling, the formed ^{68}Ga-pH-MNPs could lead to the enhanced positron emission tomography (PET) imaging of tumor (Fig. 12b).

3.1.2. Hydrophobic interaction

Apart from those aforementioned charge interaction-induced aggregations, the transition between hydrophilicity and hydrophobicity can also be used to induce the aggregation of NPs. For instance, Han *et al.* [281] reported a stimuli-responsive chimeric peptide assembly (PPDT) for superfast tumor accumulation and retention (Fig. 13a). Once the chimeric peptide assembly arrived at acidic TME, their hydrophilic carboxylate anion in PPDT rapidly got protonation to form hydrophobic carboxylic acid groups, resulting in the size increasing and morphology switching from the controlled sphere to spherocylinder (Fig. 13b,c). By fluorescence imaging *in vivo*, the ultrafast accumulation of PPDT in tumor region was observed at 0.5 h post-injection and the fluorescence intensity maintained a high level within 4 h (Fig. 13d). While the fluorescence of non-responsive PPST was relatively low and decreased rapidly. These results indicated that the pH-triggered morphology switch could realize the enhanced tumor accumulation and retention.

In recent years, pH-sensitive prodrugs as hydrophobic blocks were employed to prepare hydrophobic interaction-induced aggregates. The acidic TME triggered the protonation of prodrugs to generate the aggregates due to the increased hydrophobicity [282]. Likewise, by the host–guest interaction, the dual pH-responsive supramolecular prodrug micelles were prepared using extracellular pH-sensitive pillar[5]arene (WP5) and intracellular pH-liable methyl viologen functioned DOX [283]. Upon extracellular pH (about 6.5), the micelles were aggregated due to the protonation of ammonium carboxylate groups of WP5 rim. After cellular uptake, the DOX was dropped from the backbone at endo-/lysosomal pH (about 5.0) by the cleavage of hydrazine bond of linker, improving anticancer activity with low side effects.

Besides that, the enzyme-responsive aggregation strategy also was explored by the *in situ* formation of self-assembled nanofibers for improved tumor accumulation and retention [284,285]. The self-assembled nanofibers were generated by various interaction in response to the overexpressed enzyme in TME, such as gelatinase [286,287], fibroblast activation protein-α (FAP-α) [288,289], MMP [290,291], phosphatase (ALP) [292,293], caspase [294,295], and legumain [296,297] so on. For instance, Wang *et al.* [298] rationally designed a gelatinase-responsive small-molecule precursor for photoacoustic (PA) imaging-mediated therapy of glioma. Under TME, the overexpressed gelatinase selectively cut the small-molecule precursor, that enhanced the molecule hydrophobicity and reduced the steric hindrance, leading to the self-assembly of building blocks to prolong tumor retention time. Moreover, based on the similar responsive structure, a NIR probe with FAP-α-specific responsiveness was fabricated using modular peptide-cyanine probe that consisted of hydrophilic motifs (**1** and **2**), tailoring motif of Gly-Pro-Ala (GPA, a peptide substrate of FAP-α), self-assembly motif, and

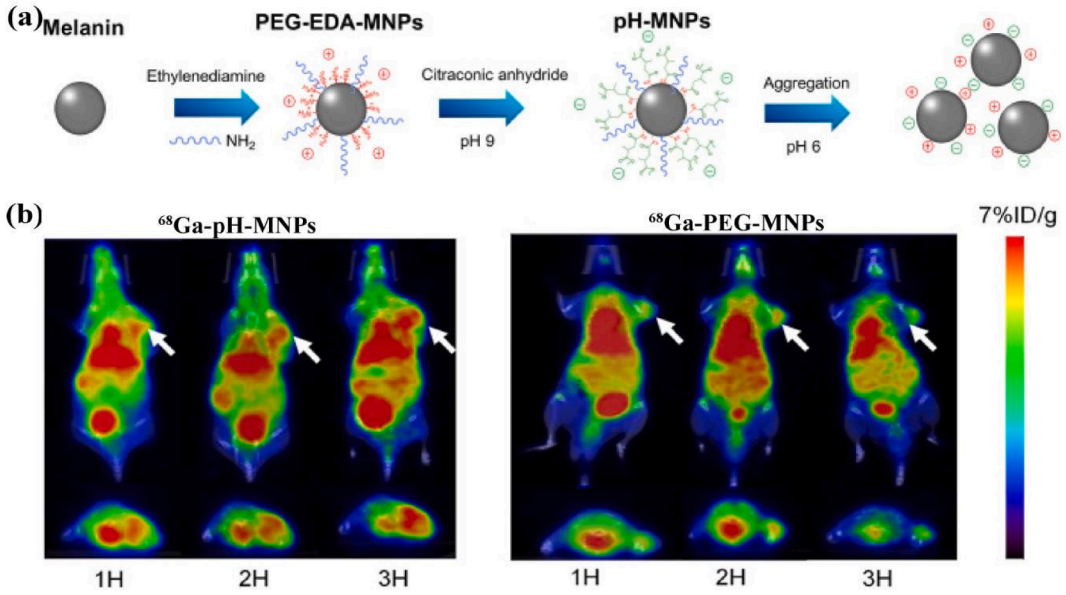

Fig. 12. (a) Schematic illustration of the preparation of pH-MNPs. (b) PET images of tumor-bearing mice after injection of ^{68}Ga-pH-MNPs and non-responsive ^{68}Ga-PEG -MNPs. The white arrow indicates tumor site. Reprinted with permission from 281. Copyright 2020, Frontiers Media S.A.

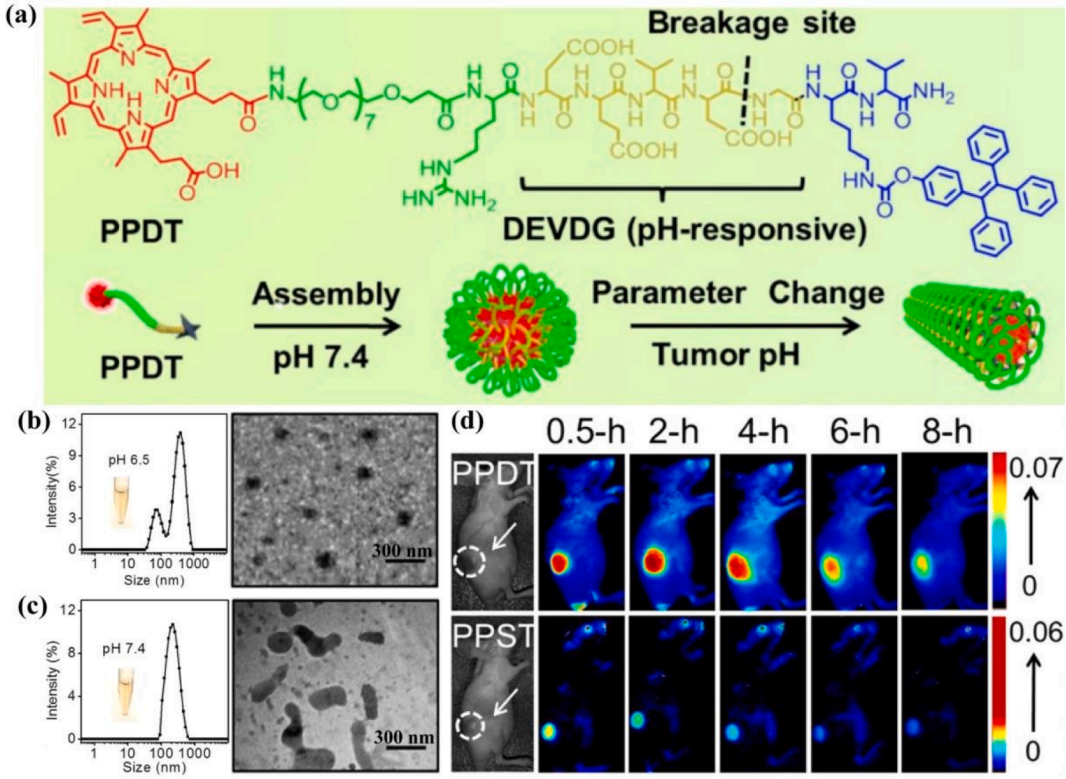

Fig. 13. (a) Schematic illustration of the self-assembly and pH-triggered morphology switching of PPDT. Hydrodynamic size and TEM imaging of PPDT at (b) pH 7.4 and (c) pH 6.5. (d) Fluorescence images of tumor-bearing mice after injection of pH-responsive PPDT and non-responsive PPST. Reprinted with permission from 282. Copyright 2017, American Chemical Society.

cyanine dye (Fig. 14a) [299]. The tailoring motif of GPA is a peptide substrate of FAP-α [300,301]. After FAP-α triggered tailoring, the residues emerged a self-assembly with highly efficient manner into β-sheet nanofibers on the surface of cancer-associated fibroblasts (CAFs) (Fig. 14b) [302,303]. The time-dependent NIR fluorescence imaging *in vivo* revealed that the indocyanine green (ICG) accumulation in tumor was very low, and it was quickly cleared from the body. In contrast, the aggregation-induced retention effect of molecule **1** resulted in a 5.5-fold signal enhancement of tumor at 48 h postinjection compared to that of molecule **4** without FAP-α triggered aggregation (Fig. 14c). More importantly, the small tumor (around 2 mm) could be diagnosed by the precise NIR imaging. In addition, MMP, a common overexpressed enzyme in TME, is considered as the best signal to trigger the aggregation of smart NPs [304,305]. A set of novel peptide-polymer amphiphiles were constructed to obtain MMP-directed assembly *in vivo* for fluorescence imaging of tumors [306,307]. This type of MMP-responsiveness could lead to the assembly of NPs into micrometer-scale aggregates in tumor. Moreover, Christman *et al.* [308] designed smart NPs response to MMP present in the acute myocardial infarction (MI) for prolonged retention in heart tissue.

3.1.3. Hydrogen bonding

Inspired by the abundance of protein assemblies existing in nature, the small peptides with specific structures can self-assemble into well-defined supramolecular architecture by enzyme catalysis for highly efficient drug delivery [309,310]. For instance, Chen *et al.* [311] developed ALP-triggered ICG-doped nanofibers (ICG-nanofibers) for dual-mode fluorescence/PA imaging-guided PTT. When the micelles reached the tumor site, the overexpression of ALP would trigger them to convert into nanofibers *in situ* by head to tail arrangement, thereby achieving the reduced RES capture and enhanced tumor accumulation and retention. Likewise, the Au NPs modified with ALP-responsive peptides were constructed for enhanced retention and PTT of tumor [312]. Once the phosphate group on the side chain of peptides was cleaved by ALP, and then the generated peptides could self-assemble to form large Au NPs aggregates through intermolecular hydrogen bonds.

Additionally, a novel tumor-selective cascade activatable self-detained system (TCASS) was designed for fluorescence imaging-guided drug delivery or surgery (Fig. 15) [313]. The modularized units of the system consisted of tumor-specific recognition motif, enzymatically cleavable linker (DEVD), self-assembly motif, and functional agent (dye or drug). At tumor region, the recognition motif specifically recognized the X-linked inhibitor of apoptosis protein. Subsequently, the recognition process activated downstream caspase-3/7, and then cleaved the DEVD to trigger self-assembly to obtain fibrous superstructures with β-sheet domains by hydrogen bonding. The rational design of the TCASS may optimize tumor accumulation, penetration, and organ competition.

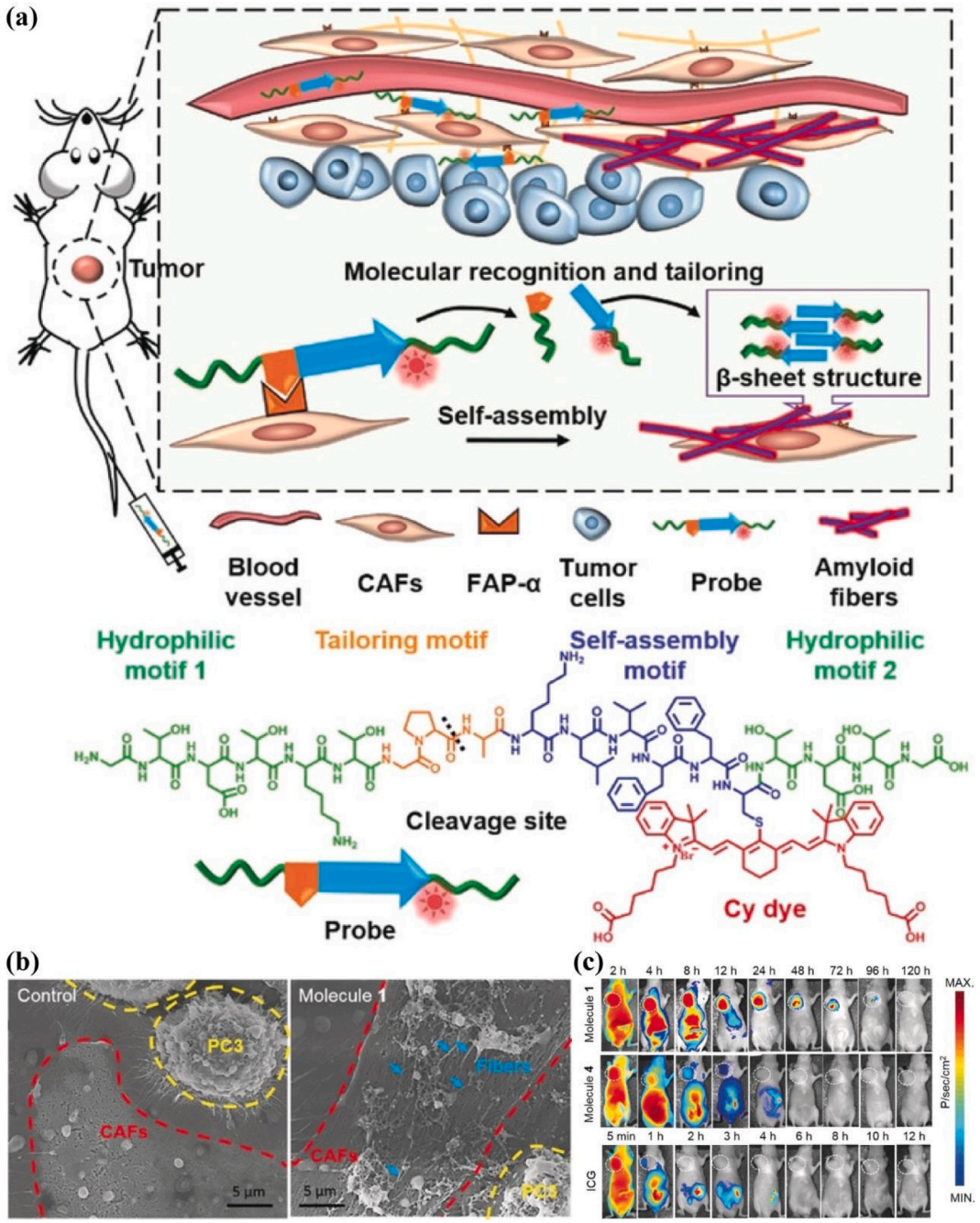

Fig. 14. (a) Schematic illustration of FAP-α-responsive peptide-cyanine probe for enhanced tumor accumulation and NIR fluorescent imaging. (b) SEM images of co-culture cells of CAFs and PC3 treated by the control and **1** group. (c) Time-dependent NIR images of tumor-bearing mice after injection of **1**, **4**, and ICG. Reprinted with permission from 300. Copyright 2019, John Wiley and Sons.

3.1.4. DNA assembly

Recently, the stimuli-responsive DNA assembly strategy has attracted widely attention to assemble the NPs accurately and efficiently, attributing to their sensitive responsiveness to environmental variations, superior biocompatibility, and accessible chemistry for surface modification [314–318]. Among them, cytosine-rich DNA sequences exhibit ideal pH-sensitivity that can drive the aggregation of NPs under acidic TME by the formation of interchain folding [319,320]. However, the DNA crosslinkers have been rarely introduced for biomedical applications *in vivo* since DNA is easily degraded by nucleases during blood circulation [321]. In 2020, a protected and pH-activated DNA assemble strategy was developed to enable the DNA crosslinked aggregation of NPs *in vivo* (Fig. 16a) [322]. The ROS-sensitive PEG and pH-responsive DNA crosslinkers were modified on the NPs surface to form ROS/pH dual-responsive

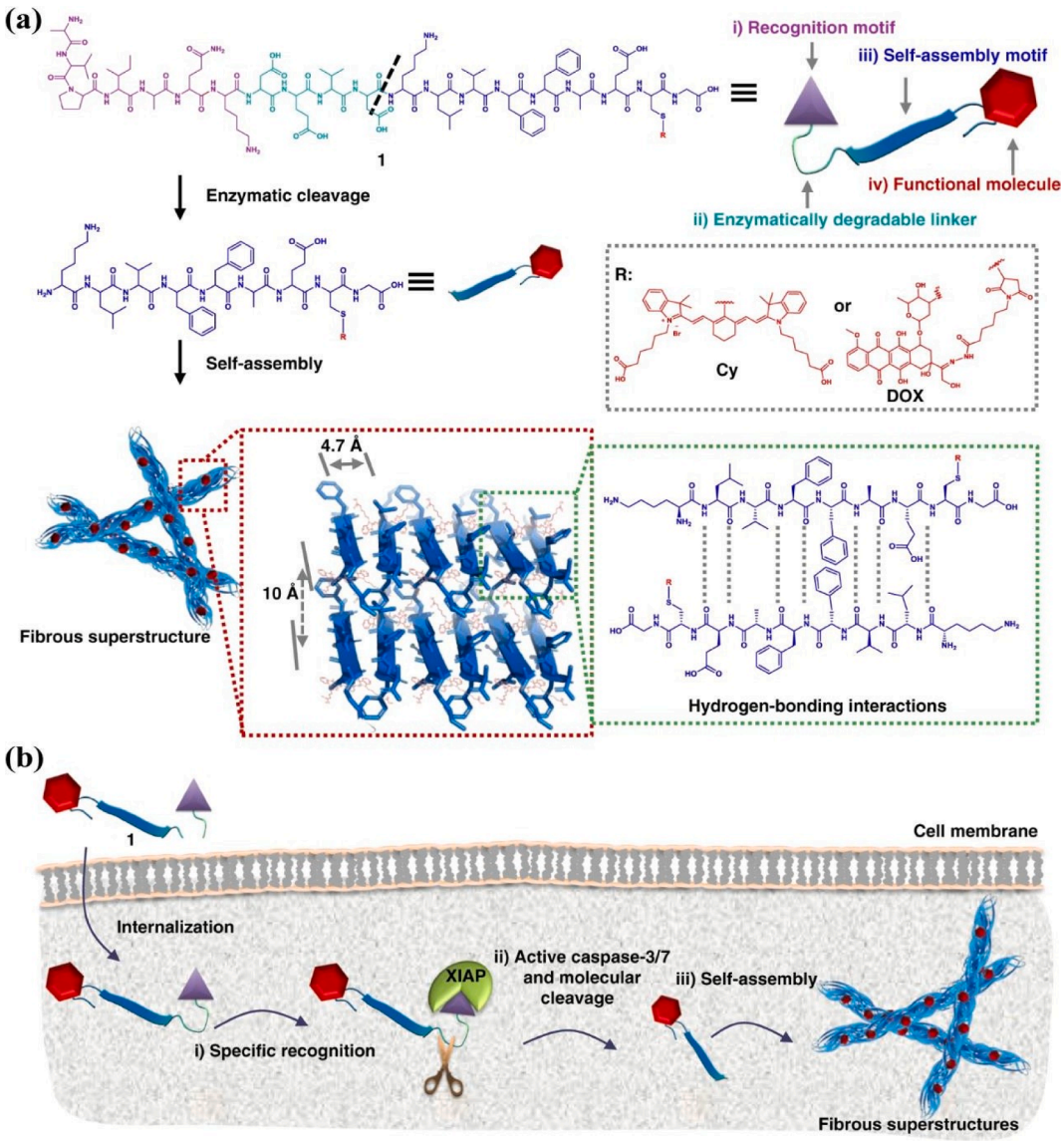

Fig. 15. (a) Schematic illustration of molecular design of TCASS. (b) Schematic mechanism of the specific recognition, molecular cleavage and *in situ* self-assembly of TCASS. Reprinted with permission from 314. Copyright 2019, Springer Nature.

NPs (CuS@mSiO$_2$-DOX/i-motif/TK-mPEG), and the PEG protected DNA from degradation during blood circulation. When arrived at the tumor site, the ROS-sensitive PEG shell was shedded to obtain CuS@mSiO$_2$-DOX/i-motif which could generate pH-responsive aggregation by DNA assembly (Fig. 16b). The results *in vivo* indicated that the single modification with DNA of CuS@mSiO$_2$-DOX/i-motif could enhance the accumulation of NPs twofold in the tumor compared with naked CuS@mSiO$_2$-DOX, while a sevenfold enhancement of tumor accumulation was observed in the dual-modification system of CuS@mSiO$_2$-DOX/i-motif/TK-mPEG (Fig. 16c). Therefore, the strategy of PEG protection and stimuli-activated DNA assembly is important for the enhanced theranostic efficiency.

3.1.5. Covalent crosslinking

3.1.5.1. Endogenous-responsive crosslinking. For the theranostics of the central nervous system diseases, especially brain tumors, the major challenge is to overcome the BBB and enhance the brain retention of nanocarriers [323–326]. To address this, the enzyme-responsive Au NPs were designed for enhanced accumulation and PA imaging-guided chemotherapy of glioma (Fig. 17a) [327]. The legumain-responsive Au NPs (AuNPs-A&C) were comprised of Ala-Ala-Asn-Cys-Lys modified AuNPs (AuNPs-AK) and 2-cyano-6-aminobenzothiazole modified AuNPs (AuNPs-CABT). In the presence of the overexpressed legumain in glioma, the AuNPs-AK would be hydrolyzed to expose the 1,2-thiolamino groups which were reacted with the contiguous cyano groups on the AuNPs-CABT by a click cycloaddition, leading to the formation of Au NPs aggregates. The fluorescence and PA images *in vivo* demonstrated that AuNPs-

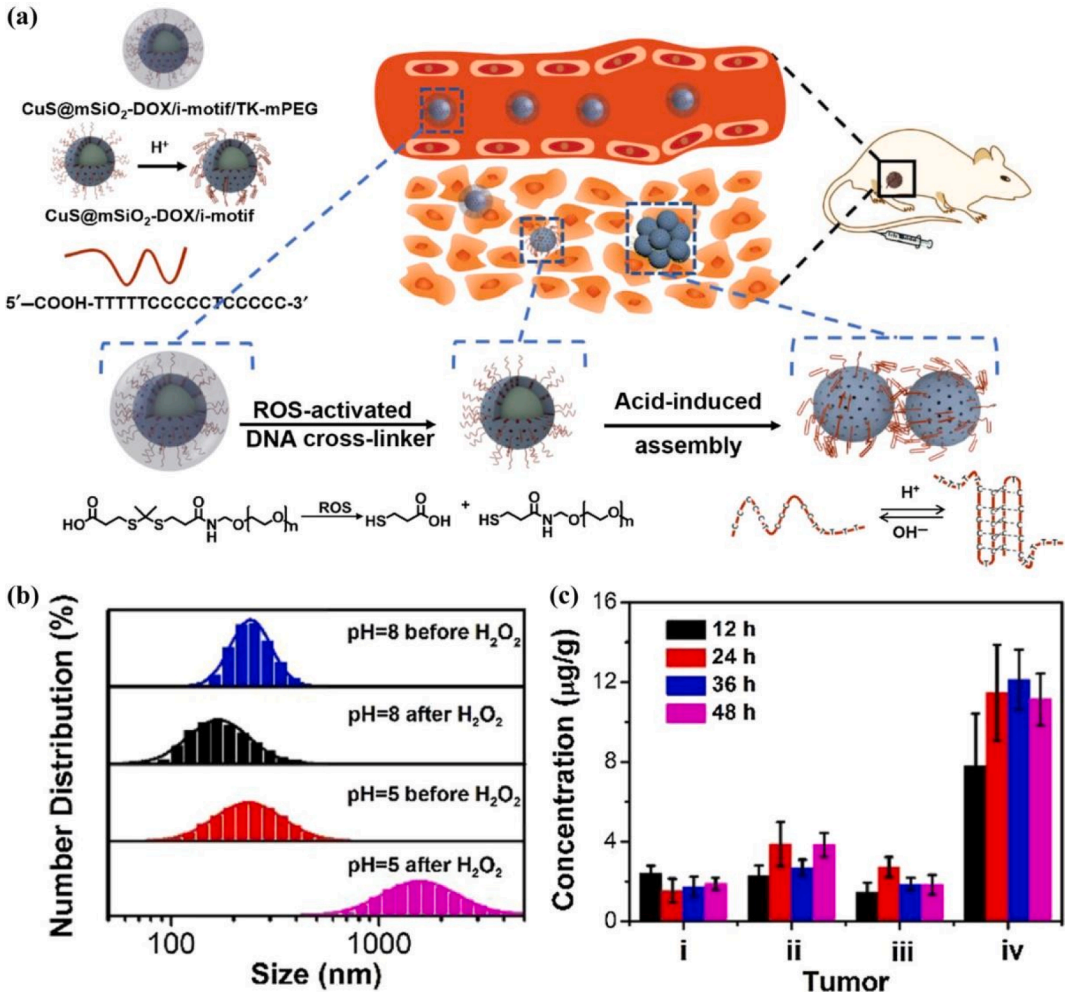

Fig. 16. (a) Schematic illustration of ROS/pH dual-responsive CuS@mSiO$_2$-DOX/i-motif/TK-mPEG for enhanced tumor accumulation. (b) Size distribution of CuS@mSiO$_2$-DOX/i-motif/TK-mPEG at different pHs with or without H_2O_2. (c) The copper contents in tumors tissue at different time points after injection of different samples, (i) CuS@mSiO$_2$-DOX, (ii) CuS@mSiO$_2$-DOX/i-motif, (iii) CuS@mSiO$_2$-DOX/TK-mPEG, and (iv) CuS@mSiO$_2$-DOX/i-motif/TK-mPEG. Reprinted with permission from 323. Copyright 2020, Chinese Chemical Society.

A&C reached a much higher accumulation in the glioma site compared to AuNPs-AK, AuNPs-CABT and AuNPs-PEG, since the legumain-triggered aggregation of Au NPs imped their back-flow out of the target site (Fig. 17b). This strategy may provide a prospective to engineer a nanoplatform for improving accumulation of theranostic agents in brain tumors, resulting in the enhanced theranostic efficiency.

3.1.5.2. Exogenous-responsive crosslinking. Although the endogenous TME-induced aggregation strategies have been reported for enhanced tumor theranostics, the unwanted aggregation of NPs often appears *in vivo* and may further induce immune response after NPs exposure due to the sophisticated biological environments [328–330]. To bypass this hurdle, various light-triggered NPs were developed for highly efficient tumor theranostics [331–334]. More importantly, in virtue of precise spatiotemporal controllability, the light-triggered aggregation strategy can also be applied to most of diseases without specific microenvironments (e.g., neurodegeneration and arthritis), not limited to tumors [254]. To date, some UV-responsive molecules, such as chromophores [335–337], spiropyrans [338–340], and azobenzene [338,341,342], were employed to modify NPs that can self-assembly upon UV irradiation. For instance, Gao *et al.* [329] synthesized novel photolabile NPs using diazirine (DA) conjugated Au NPs for enhanced PA imaging and PTT of breast cancer. Upon 405 nm laser irradiation, the DA groups were transformed into carbene which would form covalent bonds with the ligands of Au NPs by C—C, C—H, O—H, and X—H (X = heteroatom) insertions, resulting in the formation of large Au NPs aggregates.

Remarkably, in 2019, our group designed the light-addressable assemblies of ultrasmall iron oxide (Fe_3O_4 NPs) for enhanced tumor retention and dynamic MR imaging of arthritis (Fig. 18a) [343]. The light-responsive Fe_3O_4-PEG-(DA)-FA NPs were composed of ultrasmall Fe_3O_4 NPs, light-sensitive molecules DA, and targeted agents PEGylated folic acid (PEG-FA). The agglomeration degree of

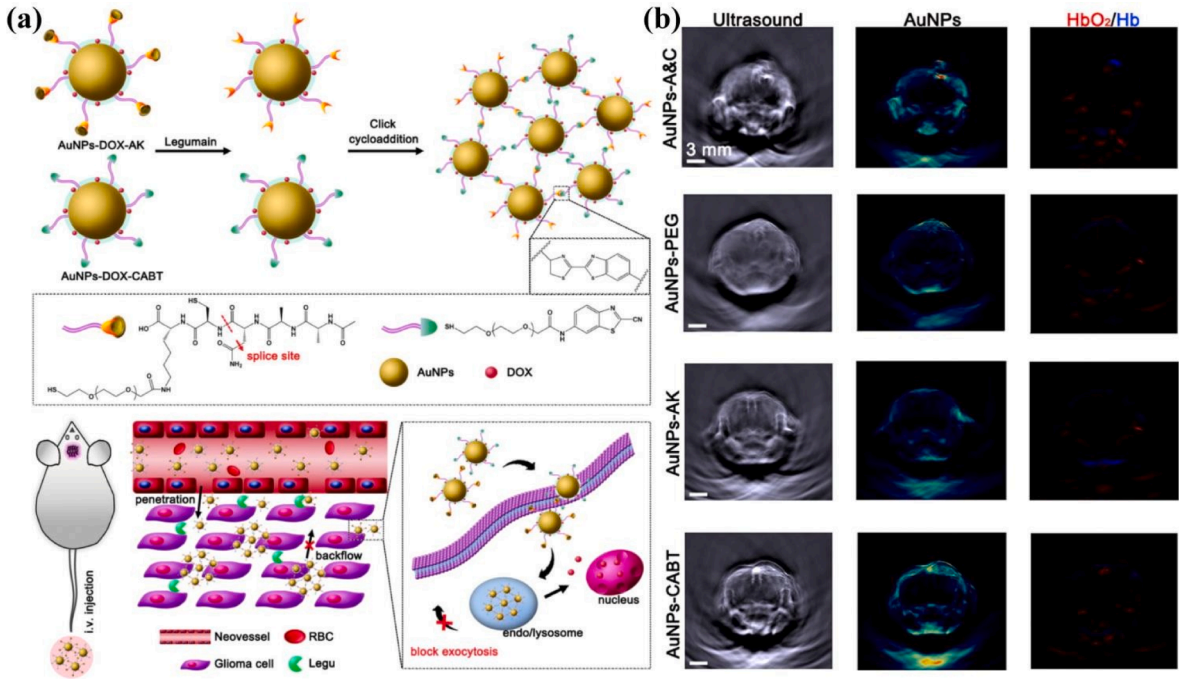

Fig. 17. (a) Schematic illustration of legumain-responsive AuNPs-A&C for improving accumulation in brain tumors after conjugation of DOX for therapeutic efficiency. (b) US, fluorescence, and PA images of glioma after injection of different samples. Reprinted with permission from 328. Copyright 2016, American Chemical Society.

Fe_3O_4-PEG-(DA)-FA NCs could be precisely controlled through the variation of laser irradiation time, that endowed the variable r_1 and r_2 relaxivities, leading to the switching of T_1/T_2-weighted MR imaging. After IV injection, the Fe_3O_4-PEG-(DA)-FA NPs could easily extravasate through the vasculature around arthritis and subsequently penetrate inside the inflammation region by FA-mediated targeting, allowing for enhanced T_1-weighted MR imaging. After 405 nm laser irradiation to induce the formation of Fe_3O_4-PEG-(DA)-FA NCs in the inflammation region, the formed aggregates were not able to intravasate back into circulation and remain in the inflammation region (Fig. 18d), thus allowing for enhanced dynamic T_1/T_2-weighted MR imaging of arthritis (Fig. 18b,c).

3.2. *Intracellular-triggered size increase*

Distinctly from those aforementioned extracellular aggregation for enhanced tissue accumulation and retention, in recent years, several stimuli-responsive intracellular assemble or swelling systems were developed to achieve excellent effect in 6) lysosome escape and 7) intracellular efflux [344–348]. The stimulation change from tissue to cell level may further improve therapeutic efficiency of cancer cells and avoid adverse effects upon normal cells [349–351]. The intracellular aggregation itself was proven to have cytotoxicity that can induce cancer cell apoptosis. Notably, the conversion from biocompatible to cytotoxic only occur inside cancer cells, that could be promising in reducing the unexpected side effects induced by traditional chemotherapy. Likewise, by the intracellular assembly or swelling strategy, the intracellular efflux and exocytosis of the aggregated NPs are inhibited to overcome multidrug resistance (MDR) which is a major hurdle for the successful chemotherapy of tumors.

3.2.1. *Aggregation-induced apoptosis*

According to the unique microenvironment in cancer intracellular, the smart NPs with intracellular-triggered aggregation behavior were designed. For instance, Maruyama *et al.* [352] prepared enzyme-responsive precursor peptide which could be cleaved by the extracellular MMP to obtain supramolecular gelator. The resulting gelator was taken up by cancer cells, and self-assembled to nanofibers in cells, leading to the cellular function impairment and cell apoptosis. Moreover, the intracellular self-assemble nanofibers using small hydrophobic molecules could disrupt the dynamics of microtubules due to the Warburg effect [353], and thus selectively caused apoptosis of glioblastoma cells [354]. Furthermore, by the host–guest interaction, the redox-triggered Au NPs aggregates were achieved responding to intracellular GSH [355]. The formed Au NPs aggregates displayed the prolonged cell retention and induced cell apoptosis due to their size increasing. Meanwhile, the aggregation of Au NPs generated the enhanced absorption in NIR region, that increased their potency for PTT. These results revealed that the intracellular self-assembly strategy of nanoplatforms not only can elevate retention but also may have potential as nanomedicines for the treatment of cancer. Recently, using two reactions to control supramolecular self-assembly has attracted widely interest. Among them, the dephosphorylation/phosphorylation cycle catalyzed by the ALP/kinase switch has been applied to control the self-assembly of NPs [356–358]. By ALP-triggered dephosphorylation and GSH-

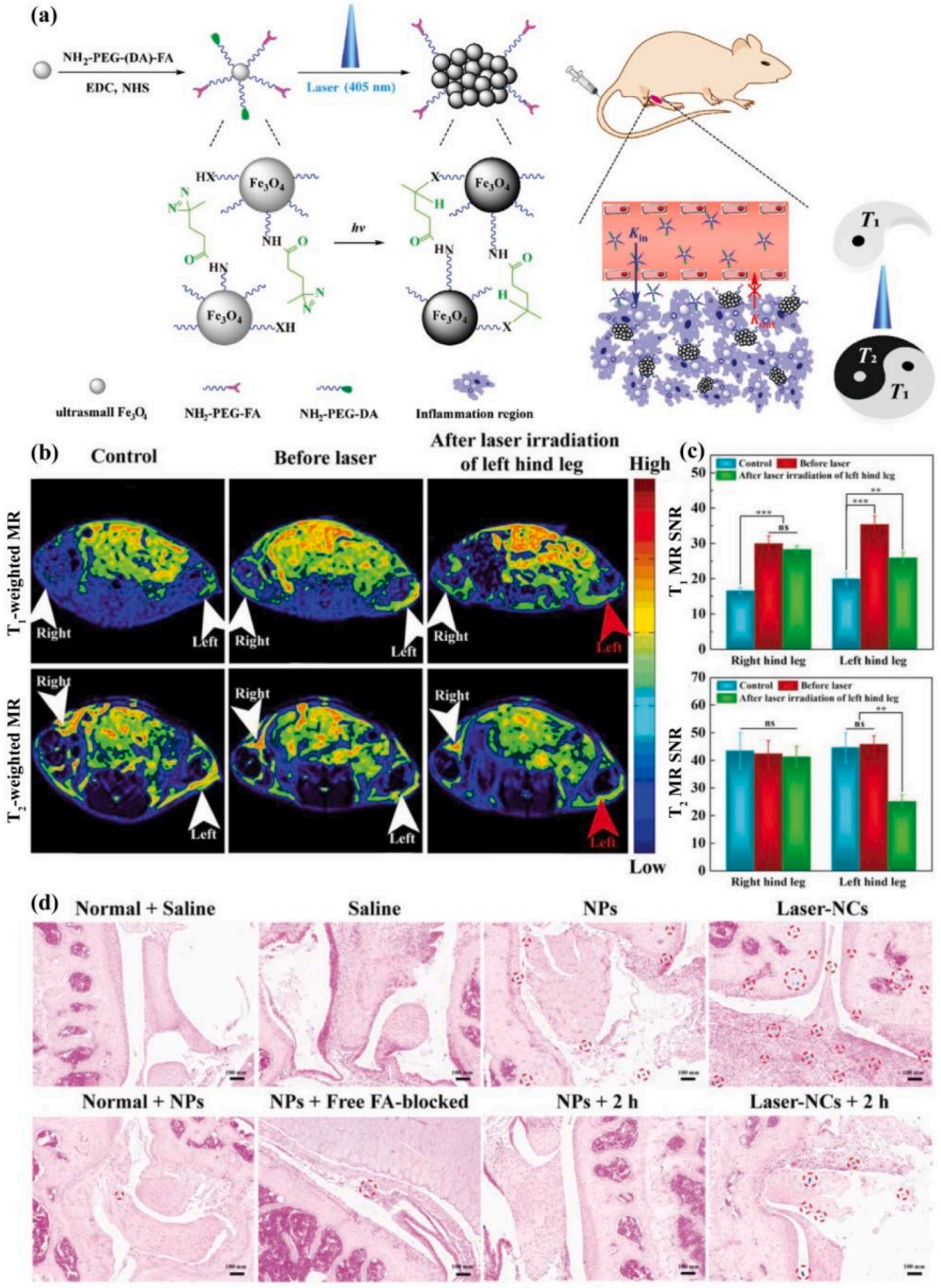

Fig. 18. (a) Schematic illustration of the preparation of Fe_3O_4-PEG-(DA)-FA NPs for enhanced retention and dynamic T_1/T_2-weighted MR imaging of inflammatory arthritis. (b) T_1/T_2-weighted MR imaging, and (c) the corresponding SNR of MR images of arthritis before and after injection of Fe_3O_4-PEG-(DA)-FA NPs. (d) Safranin O and Prussian blue-stained section of arthritis after different treatments. Reprinted with permission from 344. Copyright 2019, John Wiley and Sons.

triggered condensation reaction, the extracellular/intracellular environment-differentiated molecular self-assembly was developed [359], that can be used for enhanced intracellular retention and aggregation-induced apoptosis of hepatocellular carcinoma [312].

In very recent work, the intracellular pH-driven transformable nanovaccine (NTV) was fabricated for cancer immunotherapy (Fig. 19a) [360]. The pyrene-conjugated D-peptide (PDP) was modified onto polymer by acid-sensitive acetal bond, and then the formed polymer-peptide conjugates were used to load antigenic peptide (AP). At intracellular pH of 5.6, the PDP was released from NTV by the acetal bond cleavage, and then re-assembled into nanosheets due to their strong π-π stacking interactions. The dramatic morphological change of NTV from nanospheres (about 100 nm in diameter) into nanosheets (several micrometres in length or width) mechanically disrupted the endosomal membrane and directly delivered AP into the cytoplasm (Fig. 19b). More importantly, the formed nanosheets also boost tumor immunity *via* activation of specific inflammation pathways, furtherly providing an safe and efficient cancer immunotherapy (Fig. 19c).

3.2.2. Aggregation-enhanced therapy

Due to the fact that a certain amount of MMP and GSH generally exist in both extracellular and intracellular sites [361,362], it is difficult to precisely distinguish them by the differences of MMP and GSH concentrations. Currently, some more accurate biosignals within cancer cells were found, that could effectively trigger the intracellular assembly to realize retention enhancement and active tumor therapy until NPs enter cancer cells completely. The mRNA, which is overexpressed in the intracellular of cancer cells but undetectable in the extracellular of cancer cells or normal cells, comes into view as an appropriate candidate [363–365]. Inspired by these findings, the mRNA-responsive Au NPs were constructed using a pair of different molecular beacon sequences-functionalized Au NPs (GNP-1 and GNP-2) for controllable aggregation-induced exocytosis inhibition and enhanced PTT of breast cancer (Fig. 20a) [366]. In the MiRNA-21 positive cancer cells (Control group), the rapid intracellular accumulation of Au NPs was observed, and the exocytosis of Au NPs aggregates was greatly inhibited (Fig. 20b), while the dispersive Au NPs escaped from the MiRNA-21 negative

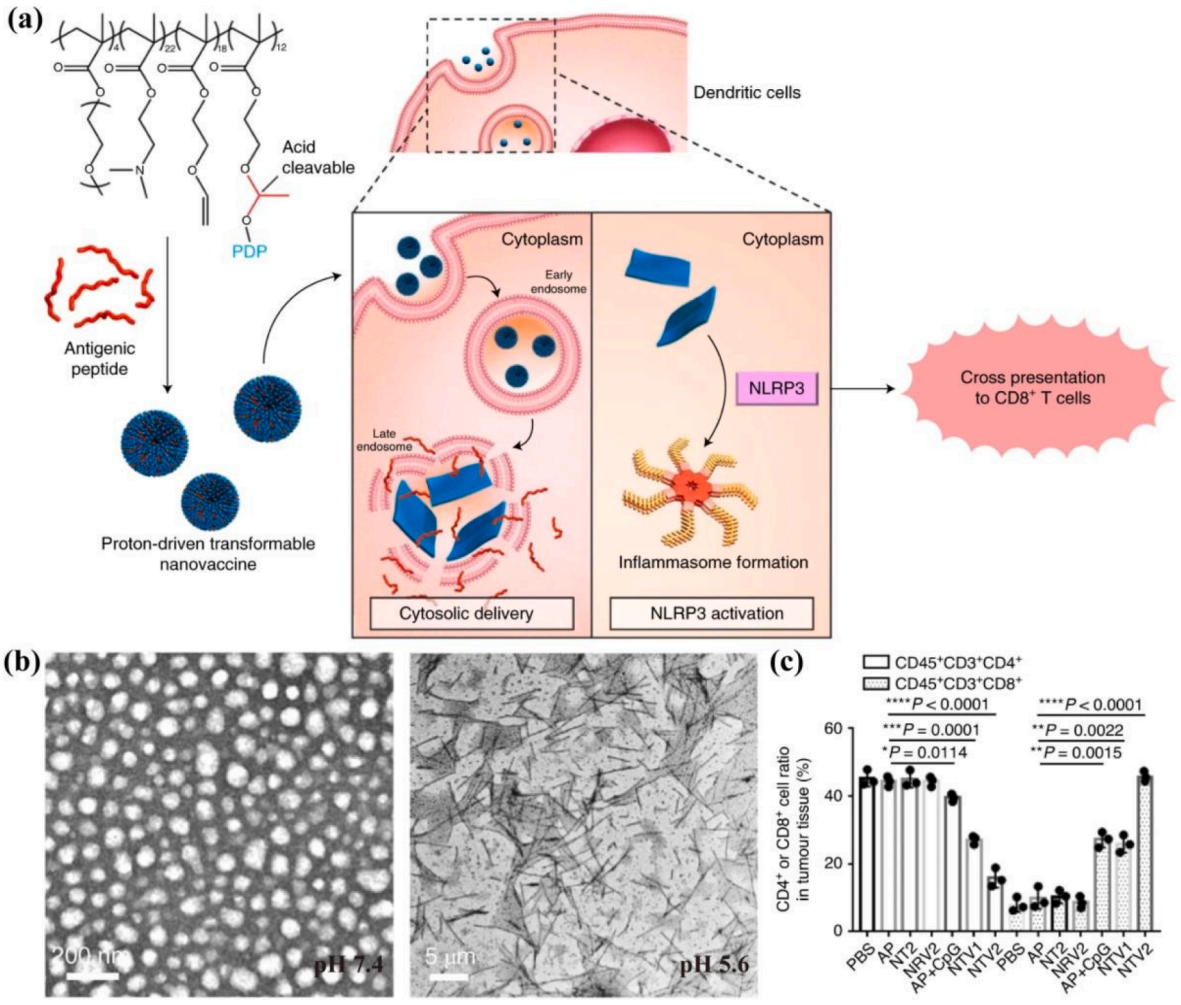

Fig. 19. (a) Schematic illustration of pH-driven NTV for cancer immunotherapy. (b) TEM images of NTV at pH 7.4 and 5.6. (c) T-cell infiltration in the tumor tissue at day 23 using a flow cytometer. Reprinted with permission from 361. Copyright 2020, Springer Nature.

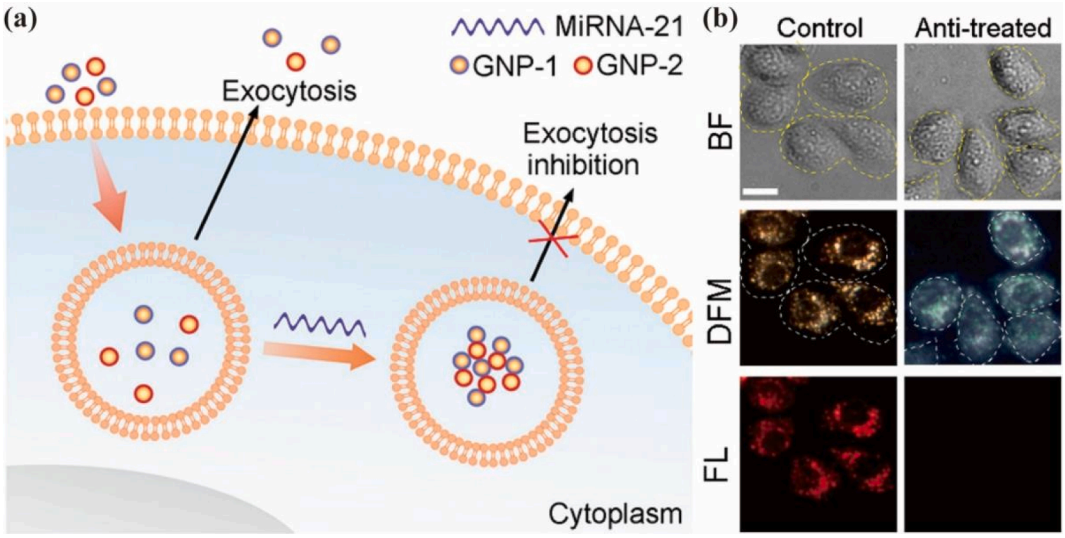

Fig. 20. (a) Schematic illustration of mRNA-responsive Au NPs (GNP-1 and GNP-2) for exocytosis inhibition. (b) Microscopic images of cells in Control and MiRNA-21-treated groups incubated with Au NPs (GNP-1 and GNP-2) (BF: bright-field images, DFM: dark-field microscopeimages, FL: Cy5 fluorescence images). Reprinted with permission from 367. Copyright 2018, American Chemical Society.

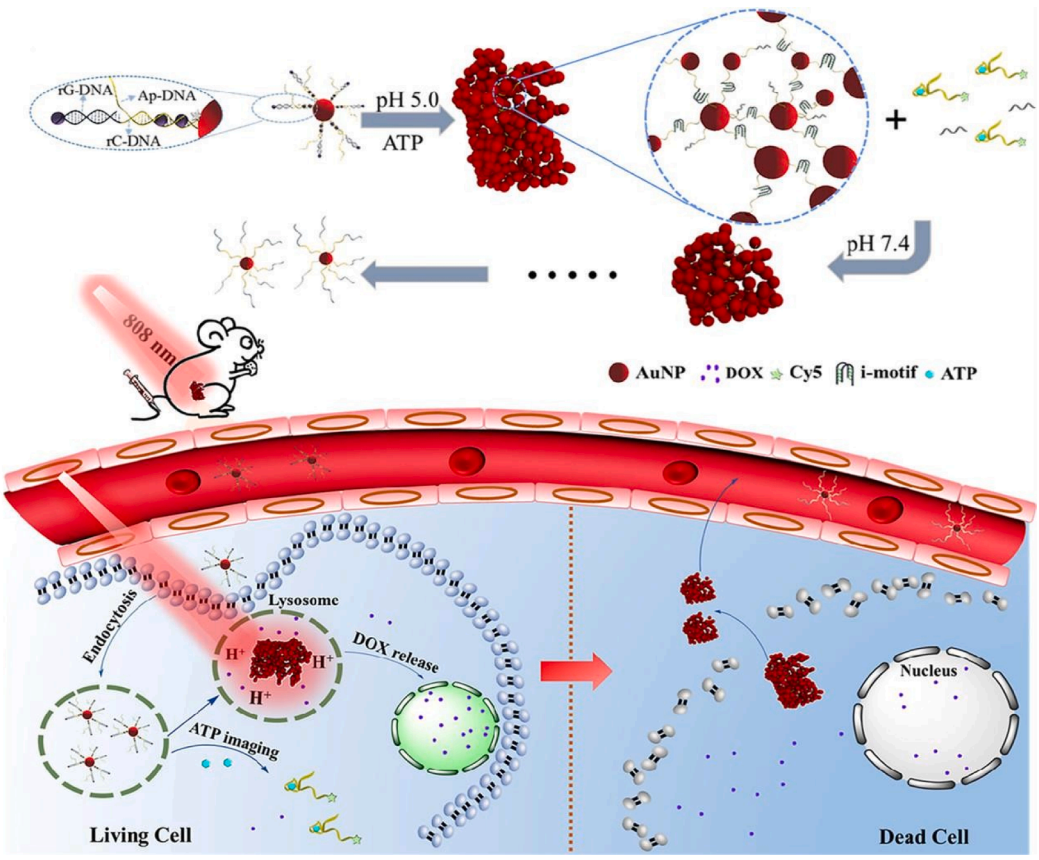

Fig. 21. Schematic illustration of DNA-modified AuNPs with pH-responsive reversible assembly for combined chemotherapy and PTT of tumor. Reprinted with permission from 371. Copyright 2019, American Chemical Society.

cells (Anti-treated group). What's more, other mRNA-responsive DNA-modified Au NPs were designed for intracellular self-assembly and enhanced retention [367]. Besides the promoted retention behavior and activated photothermal effect attributed to the intracellular aggregation, the formation of double strand with survivin mRNA may also interrupt its normal function and cause down-regulation of survivin expression, leading to the improved apoptosis of cancer cells by combined therapy. Moreover, the intracellular assembly of drug conjugates limited their expelling from cytosol through efflux proteins, avoiding the MDR [368].

These stimuli-responsive assembles or aggregations were developed for selectively inducing apoptosis or combined therapy of cancers *via* the enhanced cell uptake and intracellular retention, efficient lysosome escape, and limited cellular efflux. However, the large size of these assembles or aggregations also are difficult to be excreted through human system after therapy, that may lead to some potentially adverse effects for normal organs [369]. To solve the contradiction, Kong *et al.* [370] designed ternary DNA complex-modified Au NPs with controlled reversible assembly for combined chemotherapy and PTT of tumor (Fig. 21). After being delivered

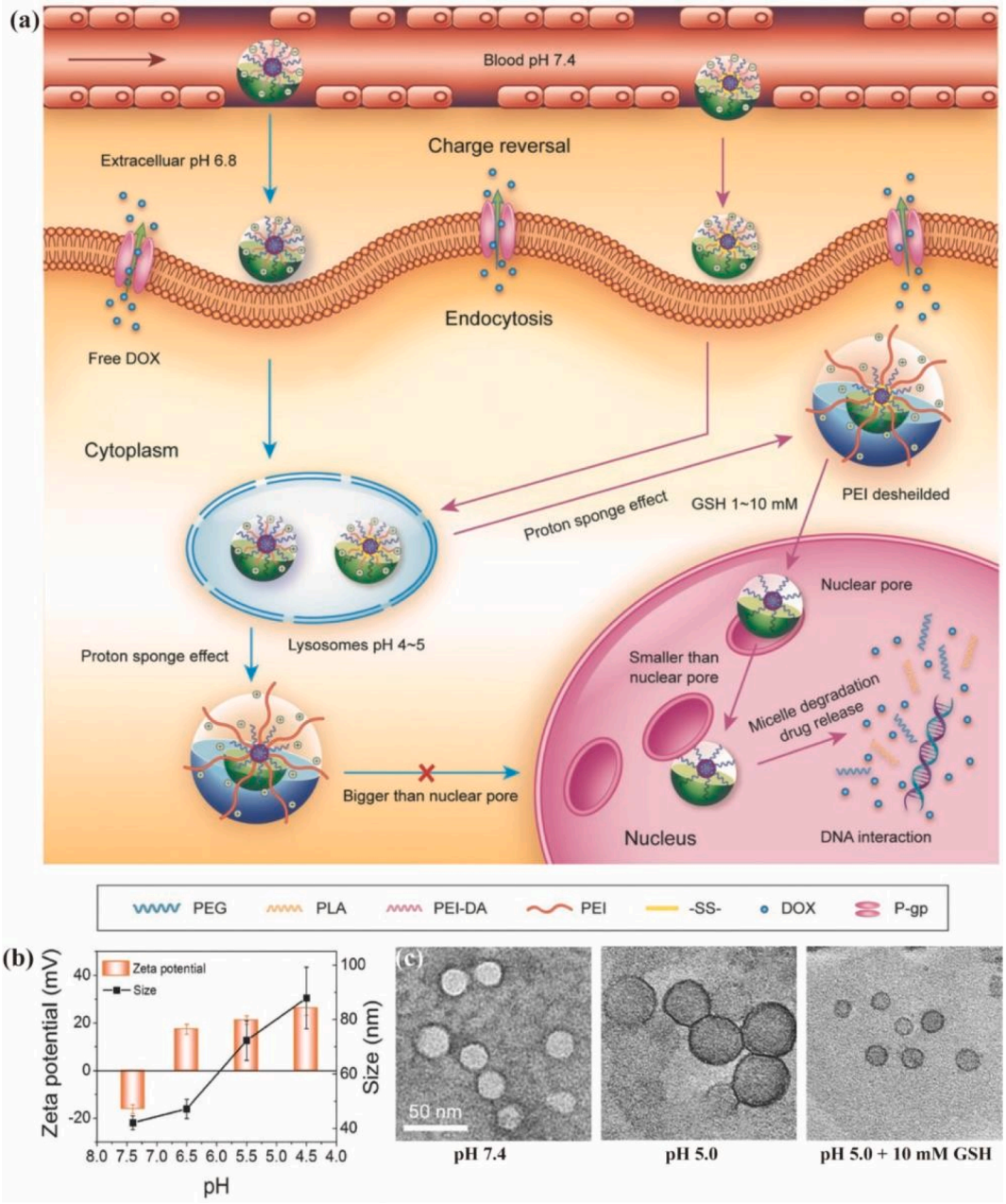

Fig. 22. (a) Schematic illustration of multi-responsive size changeable micelles for nuclear delivery and drug release of MDR breast tumor. (b) Zeta potential and size of micelles as a function of pH. (c) TEM images of micelles at pH 7.4 and 5.0 in the presence or absence of GSH. Reprinted with permission from 373. Copyright 2015, John Wiley and Sons.

into tumor cells, the DNA crosslinked aggregation of Au NPs took place by the synergetic contributions of pH and overexpressed ATP. Encouragingly, the DNA crosslinking and decrosslinking were reversible. When returned back to neutral physiological environment, the Au NPs aggregates could be reversibly disassociated to monodispersed NPs that were relatively easier to excrete *via* renal clearance.

3.2.3. Swelling-controlled release

Apart from those aforementioned intracellular-responsive aggregated NPs, several NGs or micelles with intracellular-triggered swelling behavior were explored for efficient lysosome escape, limited intracellular efflux, and controlled drug release. For instance, Zhang *et al.* [371] reported the intracellular pH-responsive reversible swelling-shrinking NGs (NLSC-NGs) for controllable drug delivery. The diameter of core/shell NLSC-NGs was sharply increased by 10-fold at endosomal (pH5.0–6.0) or lysosomal pHvalue (pH4.0–5.0), due to the pH-triggered swelling of polyelectrolyte core. The extensive volume expansion and positive surface charge of NLSC-NGs led to the endo-lysosomal bursting and rapid drug release in cancer cells. Moreover, multi-responsive size changeable micelles were designed for facilitating nuclear delivery and drug release of MDR breast tumor (Fig. 22a) [372]. The micelles hold well-defined core-corona structure, in which biocompatible polylactide is selected as core, and whose one end is linked with PEG and other end is conjugated with DMMA modified polyethylenimine (PEI) *via* a disulfide bond as corona. The micelles exhibited negative surface charge (−16.24 mV) at the physiological pH of 7.4, and the significant charge reversal from negative to positive was observed at extracellular pH of 6.5 due to DMMA cleavage for enhance deep penetration and cell uptake. More importantly, after lysosomes uptake (pH 4.0–5.0), the micelles were swelled from 42.1 to 87.9 nm by proton sponge effect of PEI to realize the lysosomes escape and limited efflux (Fig. 22b). Subsequently, the disulfide bonds were broken, triggered by intracellular GSH, leading to PEI shell deshielding and size decreasing (Fig. 22c). Finally, the smaller micelles were able to entry cell nuclear and release the cargo intranuclearly.

3.3. Size decrease

For highly efficient cargo delivery *in vivo*, in addition to the size increased strategy (from small to large) that is employed to

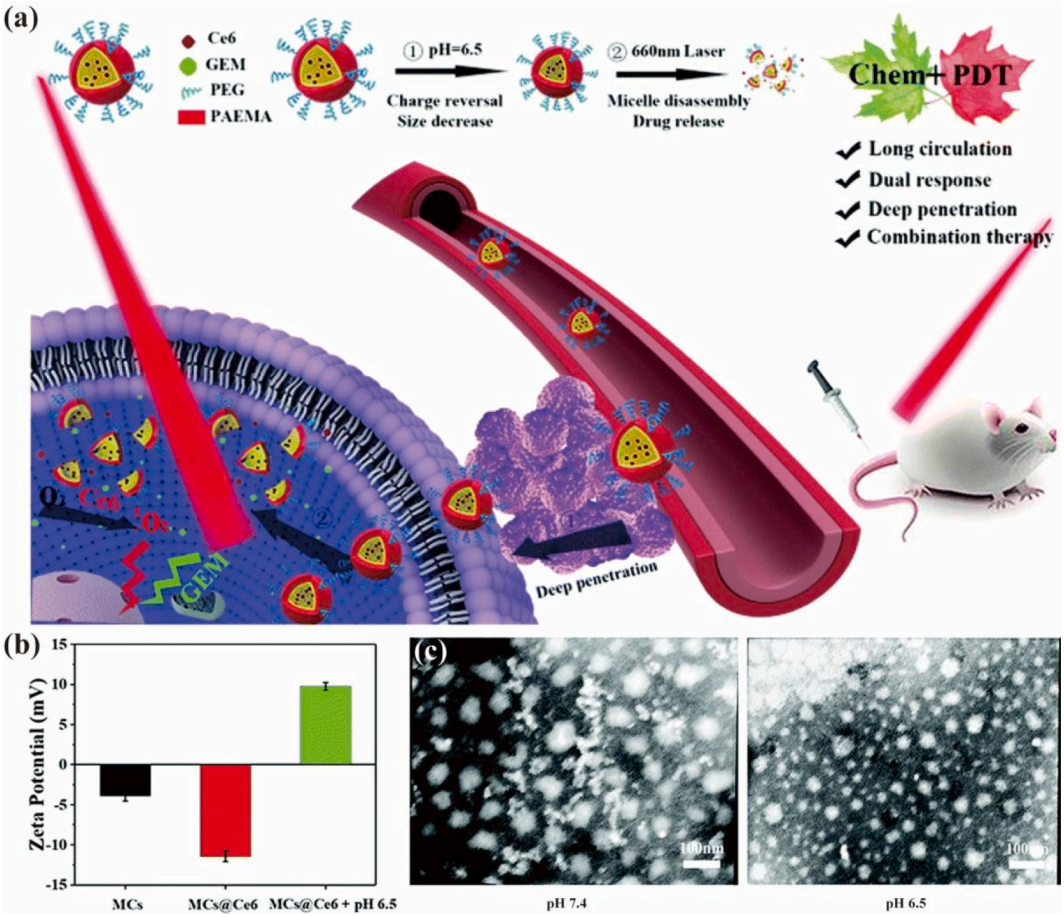

Fig. 23. (a) Schematic illustration of pH-sensitive MCs@Ce6 for combined PDT and chemotherapy of tumor. (b) Zeta potential of MCs@Ce6 in media with different pHs. (c) TEM images of MCs@Ce6 at pH 7.4 and 6.5. Reprinted with permission from 376. Copyright 2020, Royal Society of Chemistry.

overcome the barriers in 3) tissue accumulation, 6) lysosome escape, and 7) intracellular efflux, other stimuli-responsive size decreased strategy (from large to small) should also be considered to improve theranostic efficiency by the optimized properties in 4) deep penetration, 5) cellular internalization, and 8) nuclear targeting [373]. The initial NPs with larger size can reduce renal clearance and enhance accumulation in targeted region. After that, their size will be decreased into a smaller one with higher tissue permeability, cellular uptake, and nuclear targeting. Under endogenous or exogenous stimulations, the smaller NPs can be obtained by the reversible shrinkage, shield removal, satellite release, and clusters bomb.

3.3.1. *Reversible shrinkage*

3.3.1.1. Endogenous TME. It is well known that the dense collagen-rich extracellular matrix in some diseased tissues (e.g., tumor) significantly hinders the penetration and diffusion of nanocarriers, leading to the limited thernaostic efficacy [374]. To address this issue, the smart nanocarriers with stimuli-responsive size shrinkage behavior were developed to enhance tissue penetration *in vivo*. For instance, based on pH-sensitive "switch" molecules 2-(azepan-1-yl)ethyl methacrylate (PAEMA), the smart micelles (MCs@Ce6) were synthesized for combined PDT and chemotherapy of tumor (Fig. 23a) [375]. During blood circulation, the drug (GEM) entrapped micelles were hydrophobic and closed to protect the GEM from leaking. When the MCs@Ce6 reached the tumor region, the acidic TME made the PAEMA "switch" open, and then the reversal charge (−3.88 mV to 9.89 mV) and decreased size (92 nm to 51 nm) of MCs@Ce6 together promoted the tumor penetration and cellular uptake (Fig. 23b,c).

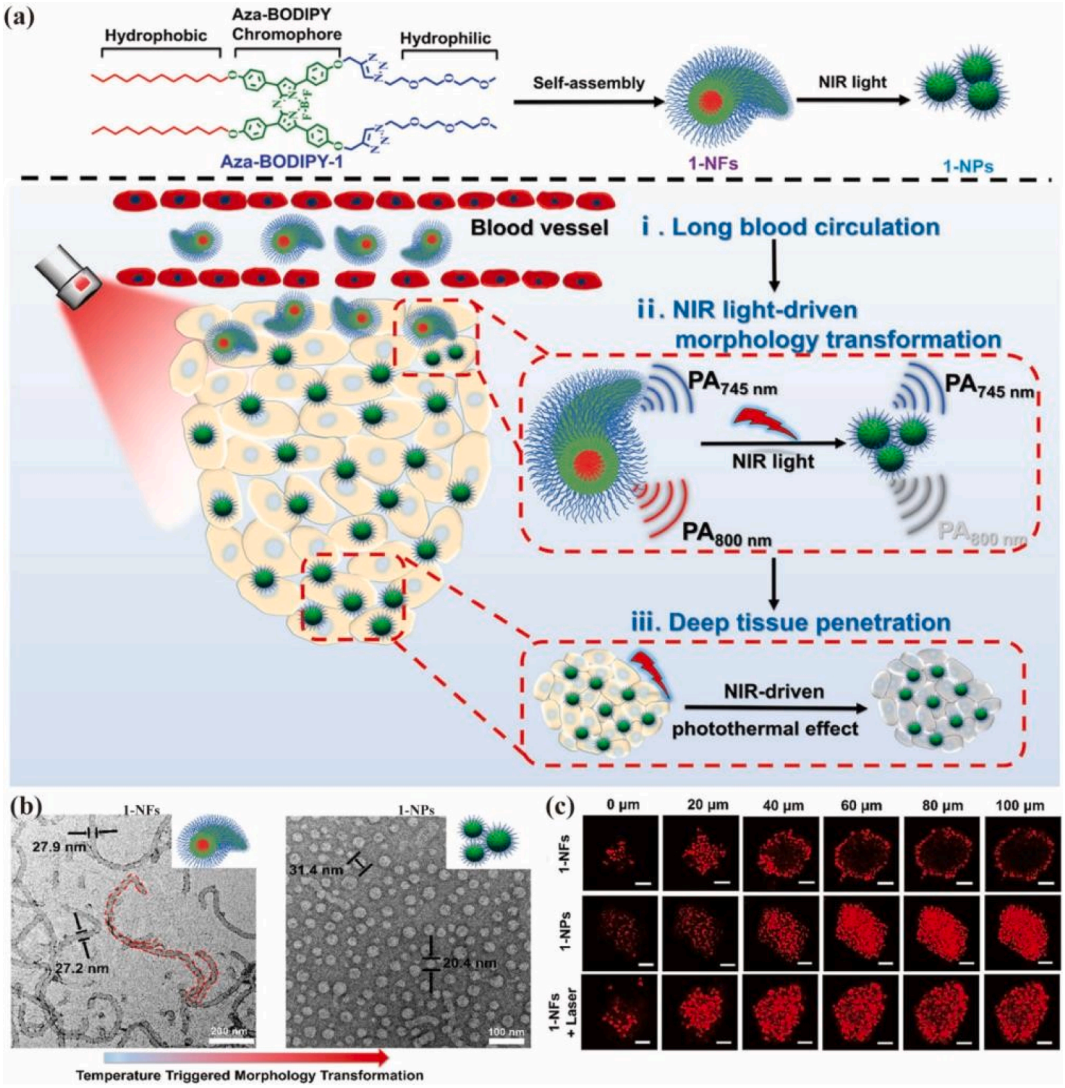

Fig. 24. (a) Schematic illustration of NIR-responsive aza-BODIPY aggregates for PA imaging-guided PTT of breast cancer. (b) TEM images of 1-NFs and 1-NPs. (c) CLSM images of multicellular tumor spheroids incubated with 1-NFs and 1-NPs with or without NIR irradiation. Scale bar: 100 μm. Reprinted with permission from 385. Copyright 2020, American Chemical Society.

3.3.1.2. Exogenous stimulations. Additionally, the size shrinkage NPs responding to exogenous stimulations, such as thermal or light, also were explored for enhanced theranostics of other diseases. In our previous work [376–378], various thermal- or/and light-responsive MGs were prepared using thermosensitive monomers VCL or/and photosensitive molecules (spiropyran, SP). At relatively high temperature (more than body temperature of 37.5 °C) or UV laser irradiation (365 nm), the hydrodynamic diameters of these MGs were shrunk. Likewise, Kohane *et al.* [379] developed photoswitchable NPs (SP NP_Hs) consisting of SP and lipids for enhanced drug delivery and diffusion of cornea. UV-triggered ring-opening in the hydrophobic SP to form zwitterionic merocyanine (MC), which caused the SP NP_Hs shrink to form smaller MC NP_Hs. However, the resulting MC is less stable than SP, and the MC NP_Hs will spontaneously revert to SP NP_Hs in darkness or under visible light, with an increase in size. To address this dilemma, the introduction of cholesterol increased the hydrophobic interaction among SP and lipids to limit the reversion of size increase in absence of light irradiation [380]. A higher efficient antitumor efficiency with low side effects was observed *in vivo* due to the favorable tumor penetration and reduced drug leakage. Notably, the photochromic conversion of SP could be potentially triggered at depths up to several centimeters by NIR lasers using two-photon technology (wavelength of about 720 nm), through soft tissues, bone, and intact skull [381].

To avoid unnecessary damage caused by UV in normal tissues, Chen *et al.* [382,383] developed a class of amphiphilic aza-BODIPY dyes which exhibited dimorphic aggregation behavior and distinct NIR absorption property. Furthermore, they reported the NIR-responsive aza-BODIPY aggregates for PA imaging-guided PTT of breast cancer (Fig. 24a) [384]. The amphiphilic property enabled aza-BODIPY molecules to self-assemble into fibrous aggregates (1-NFs). Compared to spherical 1-NPs, the 1-NFs displayed prolonged blood circulation and enhanced tumor accumulation [385,386]. Upon NIR irradiation, with temperature increasing to around 48 °C, the *in situ* morphology transformation from 1-NFs into 1-NPs was achieved for deep tumor penetration and enhanced antitumor outcome (Fig. 24b,c).

3.3.2. Shield removal

3.3.2.1. PEG. Normally, the long hydrophilic or negative chains, such as PEG or natural polymers, were introduced as shield to cover the surface of NPs to resist protein adsorption in blood circulation, thereby reducing the RES capture, improving blood stability and enhancing tissue accumulation *in vivo*. However, the shell shielding also suppresses the deep penetration and cellular uptake of these NPs. To overcome the dilemma, some stimuli-responsive shell-detachable NPs were developed to achieve the satisfactory blood circulation, tissue accumulation, deep penetration and cellular internalization simultaneously. As a typical example, the surface PEGylated NPs were prepared by the stimuli-responsive covalent bonds or noncovalent interactions that could be destroyed to induce PEG removal under endogenous microenvironments or exogenous simulations [387].

In our previous work, pH/GSH dual-responsive platform based on antifouling dendrimer-copper sulfide (CuS) nanohybrid was fabricated for combined chemotherapy and PTT of breast cancer (Fig. 25) [388]. The targeted RGD peptides were modified onto G5 PAMAM dendrimer, and then the pH-responsive PEGylated zwitterion and GSH-responsive DOX were conjugated on the dendrimer, respectively. Finally, the CuS NPs were loaded within dendrimer to form intelligent system. During blood circulation, the antifouling property of PEGylated zwitterion endowed the system with extended blood circulation. When reached tumor region, both acidic TME-triggered PEGylated zwitterion removal and RGD-mediated targeting improved tumor penetration and cell uptake of the system. The intracellular GSH-responsive DOX release was realized by disulfide bond cleavage. With these properties owned, the intelligent system is able to break different barriers *in vivo* for combination therapy of tumors.

3.3.2.2. Natural polymers. As an alternative strategy, the natural polymers, such as HA [389], polyglutamic acid [390], polyacrylic acid [391], and dextran [392], as non-toxic and biodegradable shields also can be used to coat on the surface of NPs by endogenous or exogenous stimuli-sensitive covalent bonds or noncovalent interactions. Among them, the HA is not only a targeted agent for several malignant cancer cells with the overexpression of HA-binding receptors (e.g., CD44 or RHAMM) [393–395], but also can be degraded

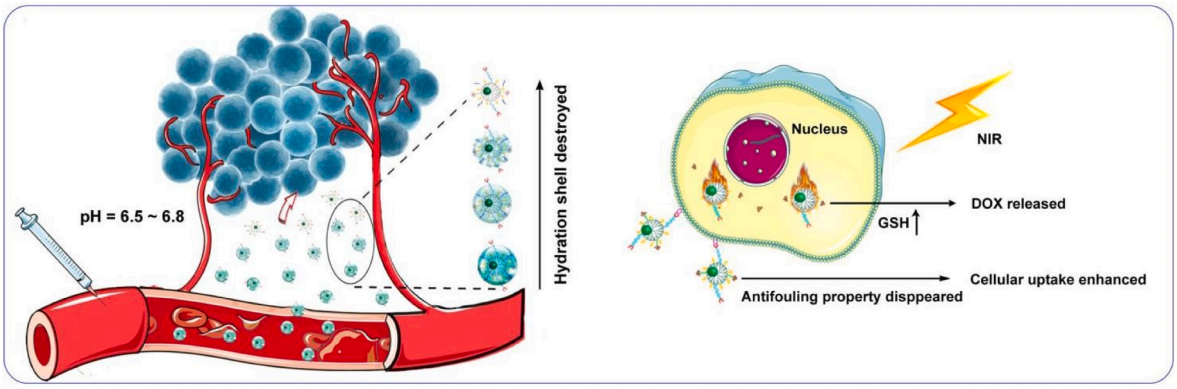

Fig. 25. Schematic illustration of pH/GSH dual-responsive system for combined chemotherapy and PTT of breast cancer. Reprinted with permission from 389. Copyright 2021, John Wiley and Sons.

by the HAase in TME [396,397]. For instance, the smart NPs (IDDHN), containing NIR-sensitive NO donor, dendrimeric prodrug and ICG, were engineered for photothermal associated DOX and NO delivery (Fig. 26) [398]. In tumor site, the HA shell was degraded by HAase to form small-sized dendrimeric prodrug for elevated deep penetration. Meanwhile, NIR laser enhanced NO release synergistically triggered deep penetration due to strong photothermal effect of ICG. The results *in vivo* illustrated that the IDDHN showed a much better antitumor efficiency with low side effects upon NIR irradiation. Remarkably, the shedding of PEG or natural polymers also may lead to the surface charge conversion of NPs, which further promotes drug release.

3.3.3. Satellite release

3.3.3.1. Surface cleavage. The above strategies of size shrinkage and shield removal were developed to decrease the size of NPs for augment deep penetration and cell uptake, but the reduction in the size of NPs is restricted, and the final size of NPs is still in dozens of nanometers. Generally, the smaller NPs (<10 nm) can further improve the ability of deep penetration and cellular internalization, and even achieve efficient lymph node migration and cell unclear delivery [399–401]. Therefore, the satellite release strategy, that ultrasmall NPs can be released from a large subject under endogenous microenvironments or exogenous stimulations, was explored in extensive disease Theranostics Compared to other ultrasmall NPs, dendrimers have attracted widespread interest in biomedical applications due to their unique features, such as ultrasmall size, highly branched architecture, and protein biomimetic property [402]. In 2019, the core-releasable satellite nanovehicles were rational constructed for relieved tumor hypoxia and enhanced chemotherapy and PTT [403]. At acidic TME, the surface small dendrimer-based satellites (about 6 nm) were emancipated from large subject *via* the pH-triggered polydopamine dissociation for deep tumor penetration.

Moreover, by self-assembly approach, the amphiphilic dendrimers that consisted of hydrophobic polymer, pH- or enzyme-sensitive linker, and hydrophilic drug-loaded dendrimer were employed to fabricate satellite releasable dendrimer vesicles [343,404]. For instance, the pH-responsive dendrimer vesicles (iCluster/Pt) were synthesized through the assembly of platinum (Pt)-conjugated poly (amidoamine)-graft-polycaprolactone (PCL-CDM-PAMAM/Pt), polycaprolactone (PCL), and PEG-*b*-PCL (Fig. 27a) [405]. The formed iCluster/Pt could release single PAMAM/Pt (about 5 nm) from the iCluster/Pt subject by acid-sensitive CDM linker cleavage in acidic pH of 6.8 (Fig. 27b,c). At 90 min postinjection of two dyes (red RhB and green Flu) labeled iCluster/Pt ($^{RhB}iCluster_{Flu}$), nearly 50 % of green fluorescence intensity from the released Flu-labeled PAMAM could be detected at the blood vessels surrounding tumor, whereas red fluorescence from the residual large subject labeled with RhB were not detectable beyond blood vessels (Fig. 27d). As a comparison, both green and red fluorescence from non-responsive $^{RhB}Cluster_{Flu}$ were confined to blood vessels. These results indicated that the dendrimer satellite release was able to greatly enhance tumor penetration and therapeutic outcome. More importantly, in the primary tumor, the resulting single dendrimer PAMAM after satellite release could be promoted to deliver further effectively into tumor lymphatics and migration into lymph nodes, leading to the inhibition of tumor metastasis (Fig. 27e). Post-injection of $iCluster^{RhoB}$ for 4 h and 12 h, the released PAMAM (red) from $iCluster^{RhoB}$ accumulated in the sentinel lymph nodes was clearly observed by fluorescence imaging (Fig. 27f) [406].

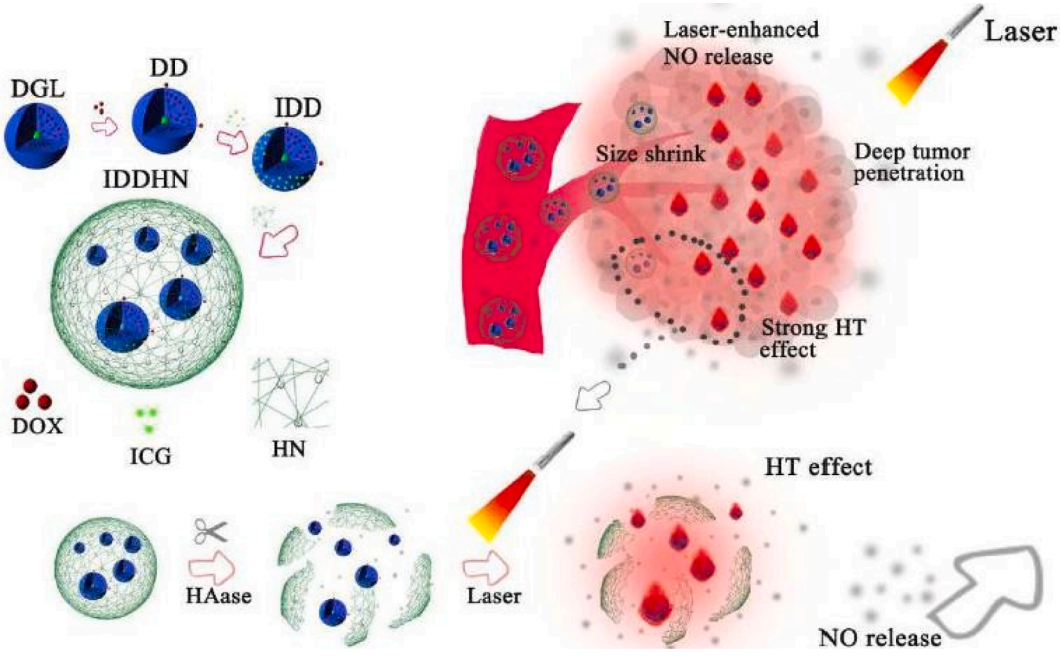

Fig. 26. Schematic illustration of the preparation of HAase/NIR-responsive IDDHN for deep tumor penetration and photothermal associated drug delivery. Reprinted with permission from 399. Copyright 2018, Elsevier.

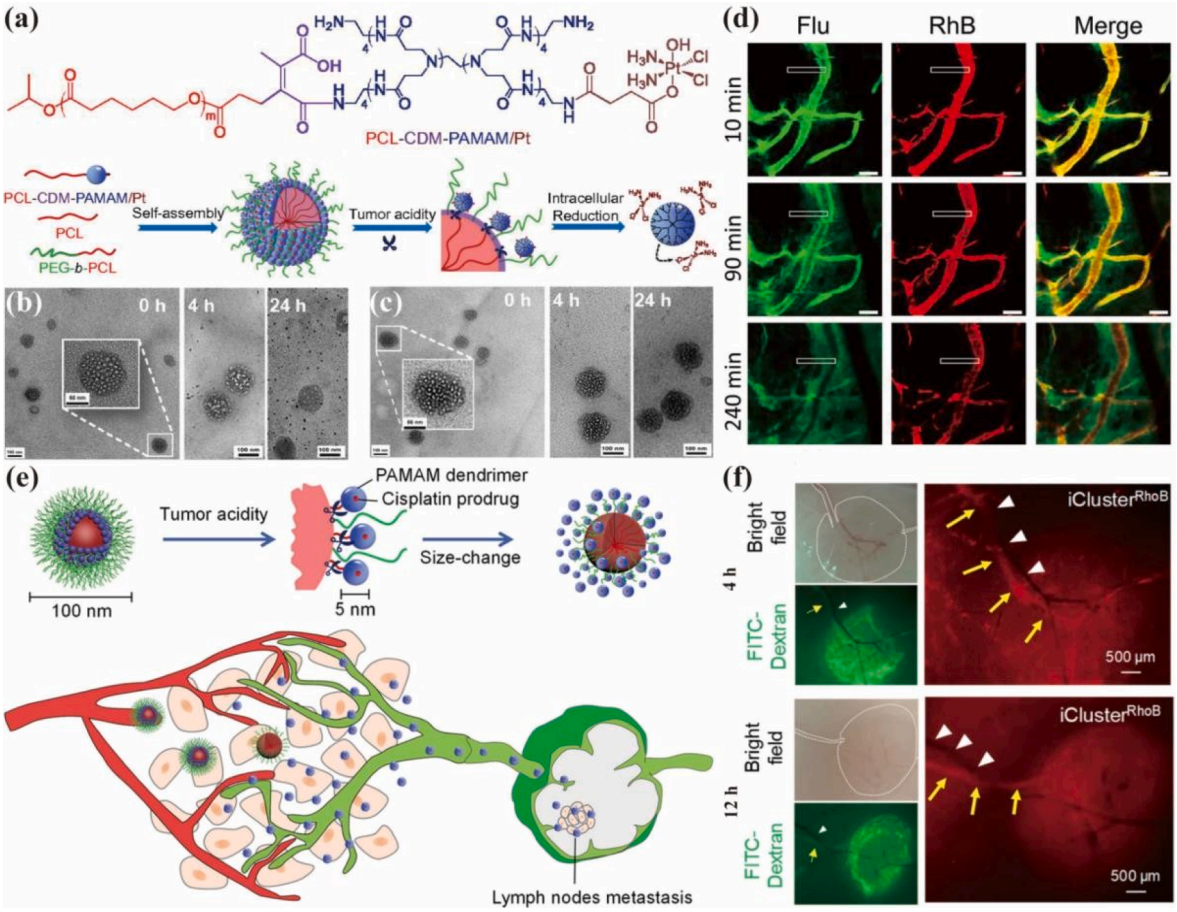

Fig. 27. (a) Schematic illustration of the preparation of pH-responsive releasable dendrimer vesicles and redox-triggered cisplatin release. TEM images of (b) iCluster/Pt and (c) non-responsive Cluster/Pt. Scale bar: 100 nm, and for the Inset images: 50 nm. (d) CLSM images of iCluster/Pt (^{RhB}iCluster$_{Flu}$) at blood vessels surrounding tumor. Scale bar: 100 μm. Reprinted with permission from 406. Copyright 2016, National Academy of Sciences. (e) Schematic illustration of pH-triggered releasable dendrimer vesicles iCluster for promoted delivery into tumor lymphatics and the inhibition of tumor metastasis. (f) Fluorescence images of sentinel lymph nodes in tumor-bearing mice after injection of iCluster^{RhoB} after 4 h and 12 h. Reprinted with permission from 407. Copyright 2019, American Chemical Society.

In very recent work, PAMAM-conjugated ICG (PAMAM-ICG) was bound with the PEG-*b*-PCL through a singlet oxygen ($^1O_2$)-sensitive thioketal (TK) bond to obtain $^1O_2$-responsive amphiphilic dendrimers (PEG-PCL-TK-PAMAM-ICG) that was further loaded with Ce6 and self-assembled to form light-responsive dendrimer-based NPs (SNP$_{ICG/Ce6}$) for combined PDT/PTT in the hypoxic TME (Fig. 28) [407]. When the SNP$_{ICG/Ce6}$ accumulated at tumor site, the $^1O_2$ produced by Ce6 upon 660 nm laser could kill cancer cells in the normoxic tumor region by PDT, and the single PAMAM-ICG satellite was simultaneously released due to the TK bond cleavage, allowing the penetration into the internal hypoxic area and efficient ablation of cancer cells by PTT under 808 nm irradiation.

3.3.3.2. Core degradation. Apart from the satellite release by surface shearing, the ultrasmall NPs can also be released from subject surface through core degradation. Gelatin, a substrate of MMP-2, can be completely degraded in TME. By virtue of this advantage, the MMP-responsive core-satellite NPs with a core composed of gelation and surface covered with small NPs (e.g., quantum dots [408], Au NPs [409] or dendrimers [410]) were engineered for efficient drug delivery and precise imaging of various tumors, such as fibrosarcoma, glioma, melanoma, or breast cancer. Among them, Gao *et al.* [411] synthesized MMP/pH dual-responsive drug delivery system (G-AuNPs-DOX-PEG) based on gelatin as core and DOX tethered Au NPs (AuNPs-DOX-PEG) as satellites. Through MMP-triggered degradation of gelatin, the release of single AuNPs-DOX-PEG from the surface was achieved for improved tumor penetration (Fig. 29). When AuNPs-DOX-PEG stayed in tumor region or internalized by cancer cells, the DOX was released *via* the cleavage of pH-sensitive hydrazone bonds from AuNPs-DOX-PEG for controlled chemotherapy of melanoma and breast cancers.

3.3.4. Cluster bomb

3.3.4.1. Cleavable covalent bond. For satellite release strategy, the residual large subject after small NPs release is often useless, and

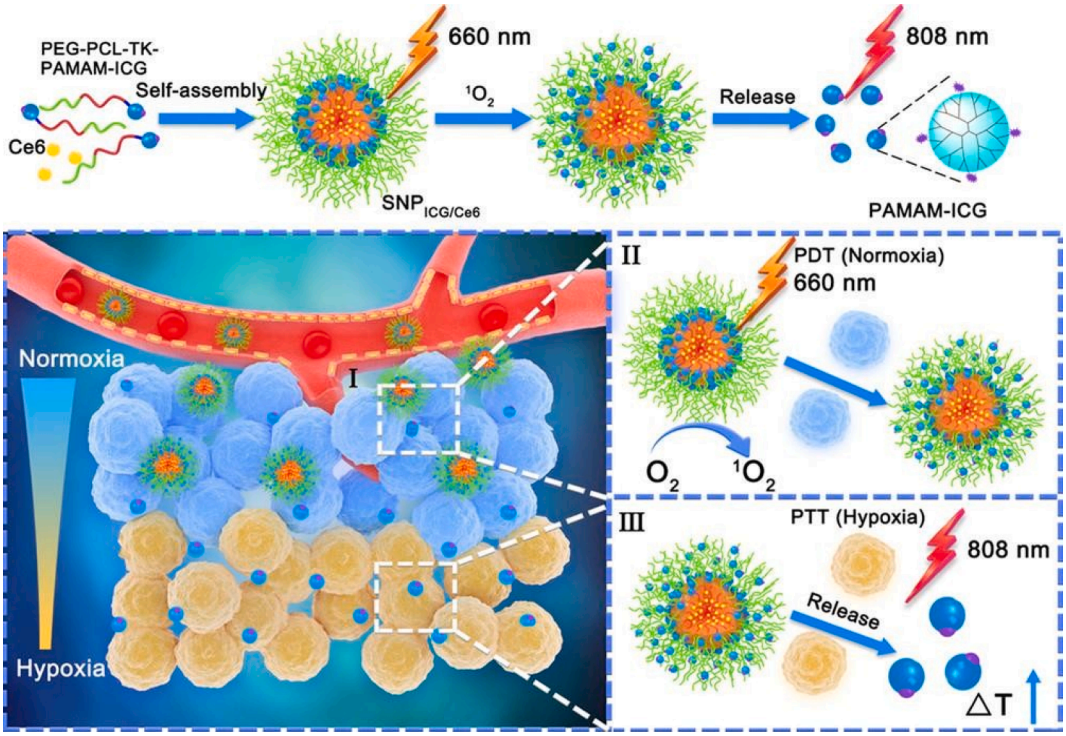

Fig. 28. Schematic illustration of the preparation of light-responsive dendrimer NPs for the combined PDT/PTT of hypoxic tumor region. Reprinted with permission from 408. Copyright 2020, American Chemical Society.

may cause long-term retention toxicity and increase metabolic burden. Some studies have revealed that most large NPs (more than 20 nm) were unfitted for renal clearance [412]. Therefore, the cluster bomb strategy was developed that the large clusters were thoroughly disintegrated into small NPs without residual subject. Through covalent crosslinking, noncovalent assembly or shell encapsulation of small NPs, the large clusters with suitable size (50–200 nm) were constructed for reducing RES capture and enhancing tumor accumulation. Under either endogenous microenvironments or exogenous simulations, these clusters could be completely dissociated into single NPs for improved deep penetration and cellular uptake [413]. In our group, the redox-responsive Fe_3O_4 clusters were prepared by crosslinking of ultrasmall Fe_3O_4 NPs (about 3.3 nm) with cystamine dihydrochloride (Cys) for dynamic T_2/T_1 MR imaging [414]. Under reducing TME, the large Fe_3O_4 clusters with high r_2 relaxivity (26.4 mM^{-1} s^{-1}) were dissociated to single ultrasmall Fe_3O_4 NPs with high r_1 relaxivity (3.9 mM^{-1} s^{-1}). Importantly, the splitting of Fe_3O_4 clusters could not only improve the permeability, but also endowed T_2 and T_1 MR imaging transformation ability attributing to relaxivity change.

Moreover, by the formation of acid-sensitive hydrazine linkage, Ling *et al.* [415] synthesized pH-responsive dynamically reversible Fe_3O_4 clusters (IONAs) assembled by extremely small-sized Fe_3O_4 NPs (about 7 nm) (Fig. 30). Similarly, after the splitting of IONAs in acidic TME, their r_1 and r_2 relaxivities showed obvious change. Meanwhile, the IONAs could amplify MR signal intensity as the postinjection time increased. It is assumed that the improved T_1 MR diagnosis of tumor based on IONAs can be attributed to the enhanced tumor penetration and augment r_1 relaxivity by pH-triggered disassembly.

3.3.4.2. Structure-switchable DNA. Besides that, the small NPs also can be crosslinked to form smart clusters by the stimuli-responsive noncovalent bond. Differed from the dissociate mode of covalent bond cleavage that is always irreversible and slow, the crosslinking/splitting process by noncovalent interaction is simple, reversible and fast [416–419]. DNA, a representative noncovalent linker, was used to fabricate stimuli-responsive clusters [420–422]. Through hybridization between i-motif DNA and i-motif binding oligodeoxynucleotides, the pH-responsive dynamic Au clusters were prepared for gene-chemotherapy of tumor [422]. By acidic TME-triggered DNA dissociation, the Au clusters were disassembled into signal Au NPs to improve tumor penetration and cellular uptake, as well as achieve controllable release of gene and drug. Likewise, the pH/enzyme dual-responsive clusters (pTSNA) based on pH-responsive triplex DNA [423] and telomerase-sensitive hairpin DNA co-conjugated Au NPs were developed to realize two-step responsive on the tissue and cell levels (Fig. 31a) [424]. At acidic TME, due to pH-triggered disassembly, the pTSNA was dissociated into single Au NPs for enhanced tumor penetration and cell uptake. After cellular internalization, the telomerase-responsive intracellular DOX release was obtained. Through immunofluorescence staining analysis of tumor *in vivo*, the red fluorescence of DOX in the pTSNA-DOX group existed in both the peripheral and central area of tumor tissue, demonstrating the better permeability of disassembled NPs and efficient drug release (Fig. 31b). As a comparison, the main accumulation of DOX in pH-insensitive nTSNA-DOX group was observed at the periphery of tumor tissue, due to the limited penetration of large size. The extremely low red fluorescence in

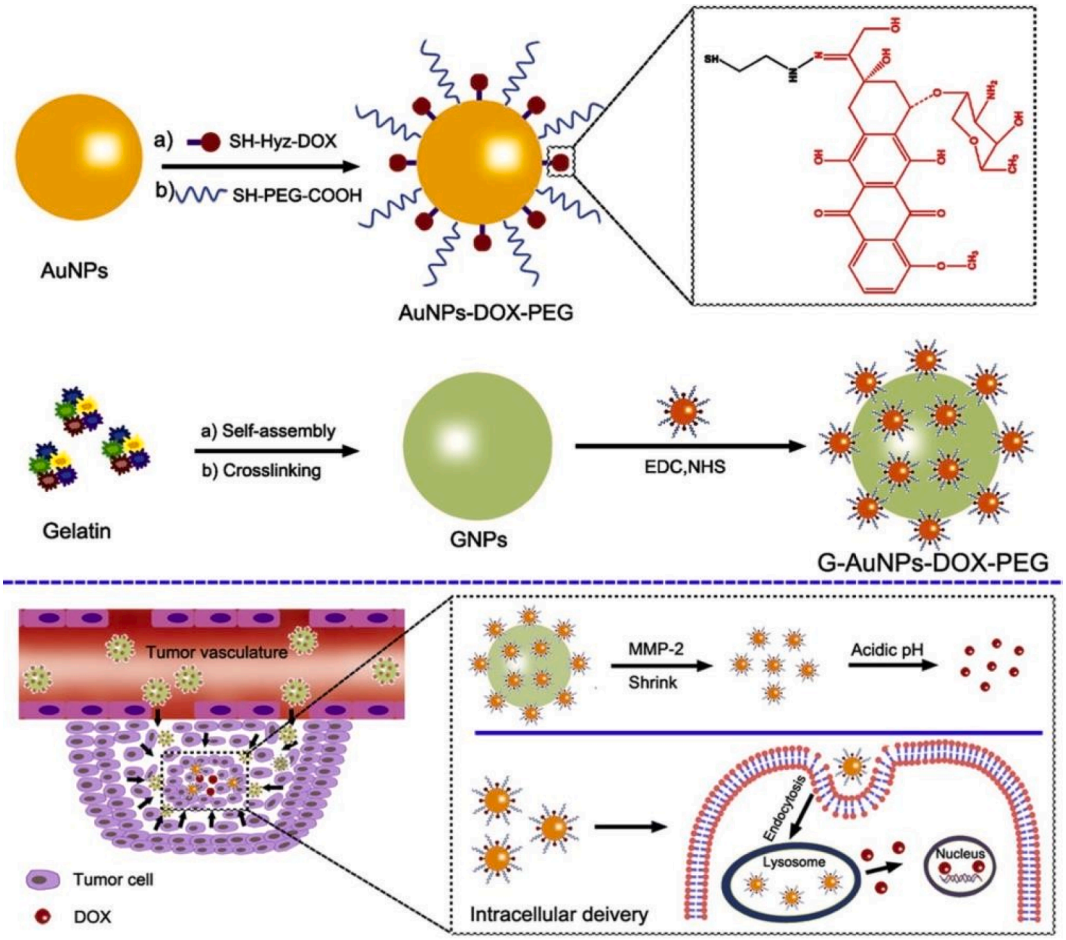

Fig. 29. Schematic illustration of the preparation of MMP/pH dual-responsive G-AuNPs-DOX-PEG for deep penetration and controlled chemotherapy of melanoma and breast cancers. Reprinted with permission from 412. Copyright 2015, Elsevier.

telomerase-nonresponsive pSNA-DOX group indicated that a small amount of drug was released.

What's more, based on i-motif DNA-assisted pH-responsive Fe_3O_4 clusters, Ling *et al.* [425] proposed the inverse contrast enhancement concept for precise MR diagnosis of hepatocellular carcinomas.The acidic TME triggered the disassembly of clusters to elevate tumor penetration and achieve the conversion from T_2 to T_1 MR imaging. More importantly, under T_1 MR imaging mode, the darkening of normal liver and the simultaneous brightening of hepatocellular carcinomas enabled highly sensitive diagnosis of small hepatocellular carcinomas (less than 1 cm). The innovative concept will facilitate the development of next-generation intelligent MR imaging contrast agents with inverse contrast enhancement properties.

3.3.4.3. Hydrophobicity change. Additionally, the hydrophobicity change of the assemblies by protonation was employed as other strategy to design smart cluster bomb. In the previous work, a series of ultra-pH-sensitive nanoprobes based on tertiary-amine-containing polymers that displayed sharp and superfast pH-responsiveness (on the scale of milliseconds) were established for rapid and effective tumor delineation [426–428]. For instance, Gao *et al.* [429] synthesized ultra pH-responsive micelles conjugated with near-infrared dye by self-assembly. Under acidic TME, the micelles could be dissociated, and then the released dye with the activated state as nanoprobe was achieved for magnified fluorescence imaging. The stimuli-responsive nonlinear signal amplification strategy to greatly increase the detection accuracy of pathophysiological signals of TME to achieve a broad specificity of tumor visualization. In 2022, Wang *et al.* [430] synthesized the amphiphilic copolymers with ionizable hydrophobic blocks and then encapsulated with photosensitizers to obtain acid-activatable nanophotosensitizer. The nanophotosensitizer could spatiotemporally target distinct stages of endosomal maturation (pH 7.0–5.0), thus achieving highly specific PDT-mediated tunable cancer cell pyroptosis.

Besides, the ultra-pH-sensitive dendrimer-based cluster nanobombs were constructed for cisplatin delivery [431]. The splitting of nanobombs (about 80 nm) into single dendrimer (less than 10 nm) in acidic TME was superfast which can be completed within seconds, due to the rapid protonation of tertiary amine groups. The resulting dendrimers displayed the improved tumor penetration and cell uptake. Furthermore, to optimize the therapeutic efficacy, the pH-triggered immunostimulatory nanocarrier was developed using dendrimer-based cluster nanobombs to spatially deliver BLZ-945 and Pt-prodrug to tumor-associated macrophages (TAMs) and

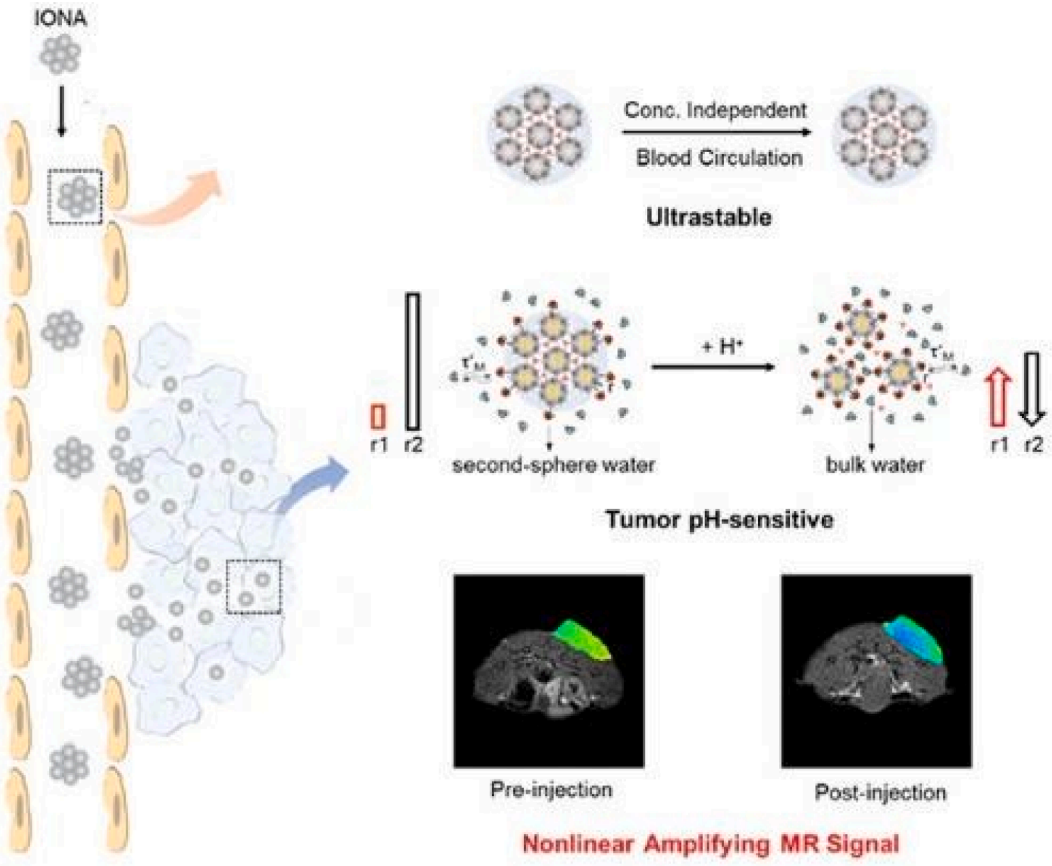

Fig. 30. Schematic illustration of pH-triggered disassembly of IONAs for targeted amplification of T_1 MR imaging of hepatocellular carcinoma. Reprinted with permission from 416. Copyright 2019, American Chemical Society.

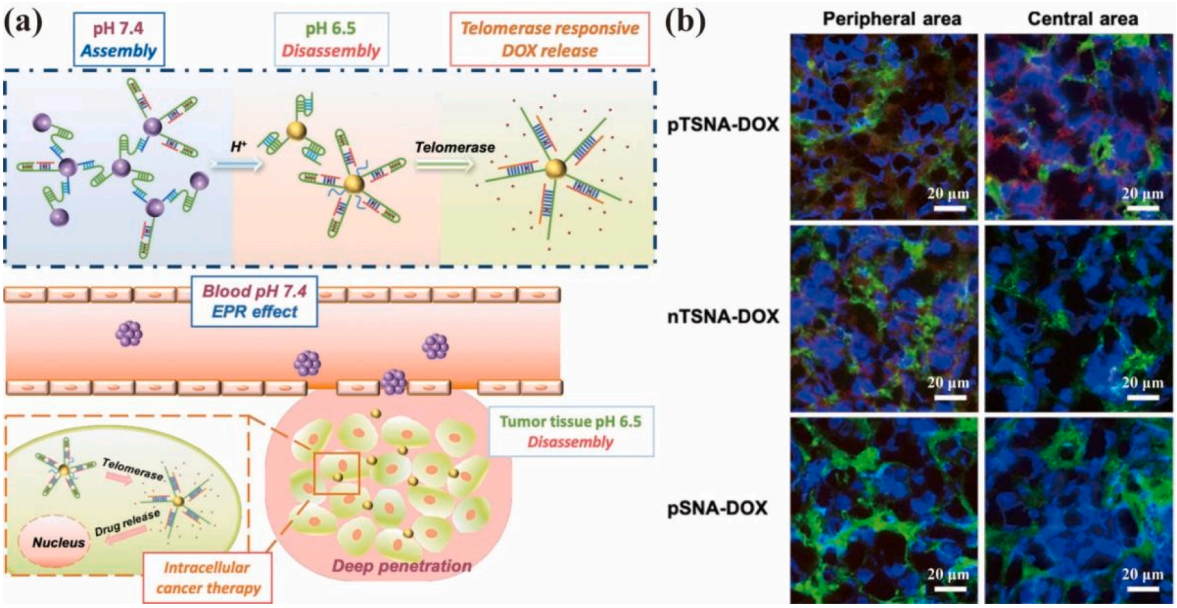

Fig. 31. (a) Schematic illustration of pH/enzyme dual-responsive pTSNA-DOX for enhanced tumor penetration and efficient drug release. (b) Immunofluorescence staining images of tumor tissue at peripheral and central area after injection of pTSNA-DOX, nTSNA-DOX and pSNA-DOX group. Reprinted with permission from 425. Copyright 2020, American Chemical Society.

tumor cells for cancer chemo-immunotherapy [432]. In 2020, Liu *et al.* [433] reported pH-responsive splitting clusters (RNPs) based on the self-assembly of ultrasmall Au_5 NPs (~ 5 nm) and pH-responsive polymers for enhanced cancer radiotherapy (Fig. 32). The acidic TME could trigger the dissociation of RNPs into individual Au_5 NPs by the rapid protonation of pH-sensitive fragment. The formed Au_5 NPs displayed high permeability to deep avascular tumor region through passive extracellular diffusion and active transcytosis, thereby enriching local irradiation dose and boosting the susceptibility of cancer cells to radiotherapy. Meanwhile, these Au_5 NPs could monitor the feedback of favorable radiotherapy responsiveness by detecting the activated apoptosis after radiation. Overall, the strategy provided a promising paradigm for drug delivery in deep tissue and personalized radiotherapy.

3.3.4.4. Parcel rupture. Apart from those aforementioned endogenous-triggered nanobombs, the nanoparcel which could be ruptured in response to exogenous stimulations was prepared by physically encapsulation of small NPs [434]. In very recent work, a NIR-triggered disintegratable liposomal nanoparcel that Pt-grafted dendrimer prodrug (PAM/Pt) was encapsulated in ICG-based lipid [435]. When irradiated by NIR laser at tumor site, ICG heating detonated the thermosensitive liposomes to release the small sized PAM/Pt (about 8.6 nm) for tumor deep penetration. Moreover, the PA shockwave triggered decomposable nanoparcel was developed for synergistic chemotherapy and mitochondria-targeting PA therapy of breast cancer (Fig. 33a,b) [436]. The nanoparcel (Den-Cy5.5/Pt@PFH) with a diameter of 100 nm was synthesized based on the liquid perfluorohexane (PFH) and small dendrimer NPs (Den-Cy5.5/Pt) with a BSA shell. Under 606 nm laser irradiation, the PFH underwent a liquid–gas phase transition to release Den-Cy5.5/Pt (about 10 nm) for deep tumor penetration due to shockwave generation from Den-Cy5.5/Pt@PFH (Fig. 33c). After that, the internalized Den-Cy5.5/Pt was further reduced intracellularly to release cisplatin and kill tumor cells (Fig. 33d). Noteworthy, the positively charged Den-Cy5.5/Pt could localize in the mitochondria of cancer cells owing to mitochondrial transmembrane potential. Upon laser irradiation again, the resulting PA shockwave mechanically damaged the mitochondria simultaneously to produce localized cytotoxicity in cancer cells. A combination of chemotherapy and mitochondria-targeting PA therapy might offer robust antitumor efficacy.

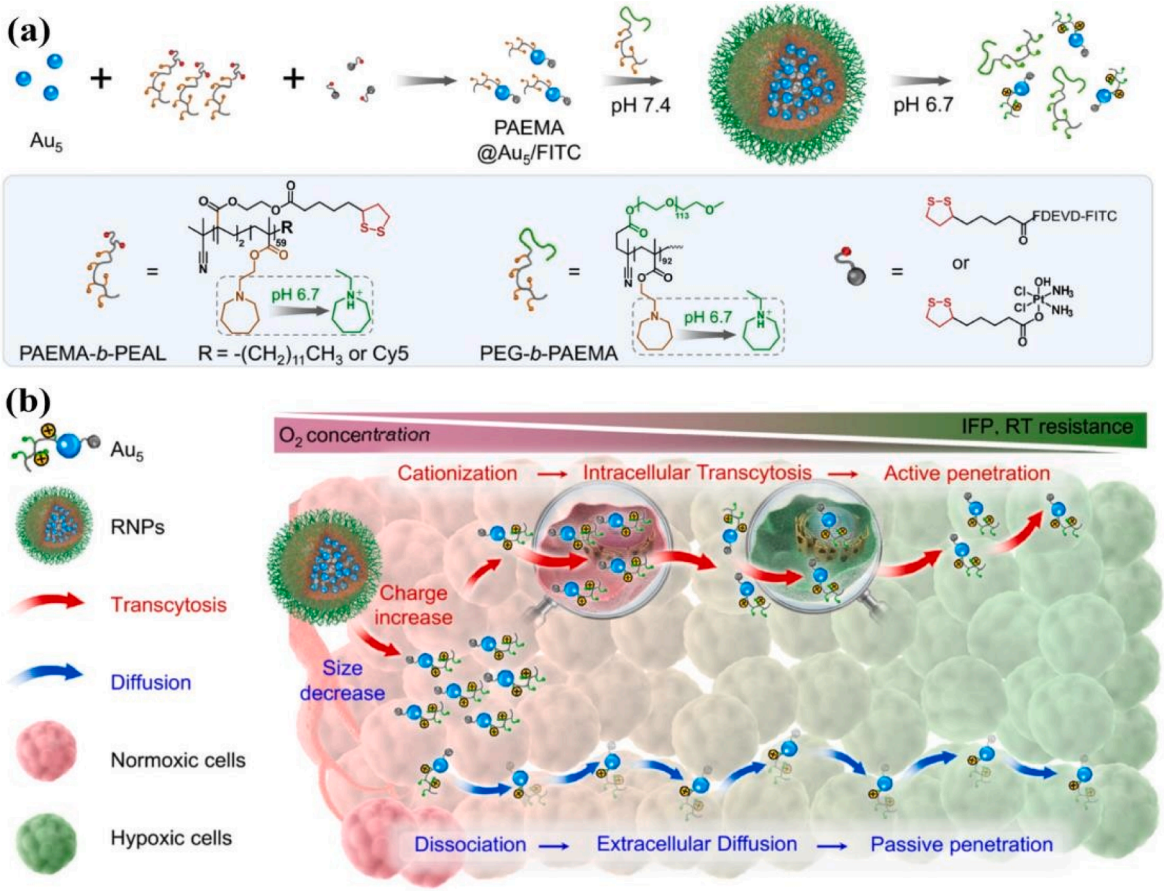

Fig. 32. (a) Schematic illustration of the preparation of RNPs with pH-responsive morphological transformation. (b) The TME-triggered dissociation of RNPs into individual Au_5 NPs for improved tumor deep penetration by extracellular diffusion and intracellular transcytosis. Reprinted with permission from 434. Copyright 2020, American Chemical Society.

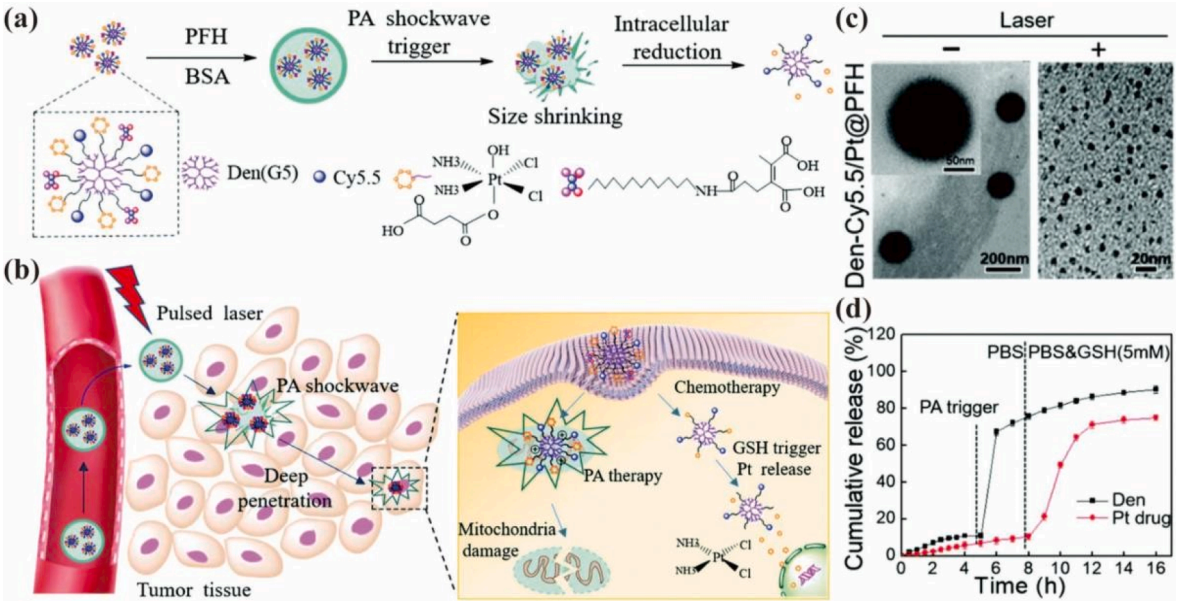

Fig. 33. (a) Schematic illustration of Den-Cy5.5/Pt@PFH. (b) Schematic illustration of Den-Cy5.5/Pt@PFH nanoparcels for the combination of photoacoustic therapy and chemotherapy. (c) TEM images of Den-Cy5.5/Pt@PFH before and after laser irradiation. (d) Cumulative release of Den-Cy5.5/Pt and cisplatin under different conditions. Reprinted with permission from 437. Copyright 2019, Royal Society of Chemistry.

3.4. Soft deformation

In recent years, a rather new field, tailoring the mechanical properties of NPs for improved tumor theranostics, has attracted increasing attention [433]. The flexibility (soft or stiff) and shape (spherical or ellipsoidal) of NPs can significantly affect their delivery behaviors in 1) blood circulation, 3) tissue accumulation, 4) deep penetration, and 5) cellular internalization [437–439]. Similarly, the novel smart NPs with soft deformability may meet the requirement of overcoming different barriers. Some previous studies [418,440] have shown that the smart NPs with mechanical pressure-responsive deformation displayed excellent transvacular ability and deep penetration behavior in the tumor ECM. In 2018, Lu *et al.* [441] constructed flexible and deformable hollow mesoporous organosilica NPs (HMONs) that underwent morphological change (from spherical to oval) during cellular internalization. In compared with undeformable counterparts, the cell uptake of deformable HMONs by breast cancer cells improved 26-fold, leading to highly efficient anticancer activity. Furthermore, they systemically investigated the biological behaviors of deformable HMONs *in vivo* (Fig. 34a) [442]. The comparative studies between soft (SMONs-HA-Cy5.5, 24.2 MPa) and stiff (MONs-HA-Cy5.5, 79.2 MPa) counterparts were conducted. Apart from exhibiting a twofold increase in cancer cell uptake, the SMONs-HA-Cy5.5 also displayed a remarkable pharmacokinetic advantage due to their unique fluid mechanics, with a fivefold increase in blood drug concentrations compared to MONs-HA-Cy5.5, resulting in considerably improved tumor accumulation (Fig. 34b,c). Moreover, the *ex vivo* intratumoral distribution results indicated that the SMONs-HA-Cy5.5 significantly improved extravasation behavior and intratumoral penetration, generating a 16-fold increase in diffusion distance in TME (43 vs. 2.72 μm), relative to MONs-HA-Cy5.5 (Fig. 34d). This is because that the deformation of soft ones to ellipsoids may contribute to a rotational motion in complex crowded media.

In addition to this, the soft and deformable NPs also can be achieved by coating a layer of shell with certain elasticity (e.g., liposomes, vesicles, or cell membranes) [443,444]. The yolk-shell NPs (CCM@LM) with an mesoporous silica (MSNs)-supported PEGylated liposome core and cancer cell membrane (CCM) coating were developed for homologous targeted chemotherapy of breast tumor (Fig. 35a) [445]. The deformation of CCM@LM was measured using atomic force microscropy. Under the loaded force, the CCM and liposome-coating LM (L@LM) deformed irregularly, whereas LM deformed negligibly. In contrast, the CCM@LM with moderate rigidity and elasticity might help to transform into an ellipsoidal shape frequently during tumor penetration (Fig. 35b) [446]. As expected, the CCM@LM displayed superior penetration throughout multicellular spheroids *in vitro* (Fig. 35c).

Moreover, the MGs or NGs exhibiting 3D crosslinked network, soft architecture and deformable shape also can be used as nanocarriers to enhance tumor penetration [443]. In our group, a series of MGs or NGs with tunable crosslinking densities were constructed using functional monomers or polymers, and crosslinkers [384,447,448]. These MGs or NGs with different crosslinker contents may control the mechanical property. Giasson *et al.* [449] synthesized four NGs that showed increased mechanical property (18 kPa to 211 kPa) with crosslinker increase (1.7 % to 15 %). The MGs with larger size in micrometer displayed relatively lower mechanical property [450]. By virtue of these intrigued characteristics, we developed various functionalized soft NGs for improved tumor theranostics due to their prolonged blood circulation, enhanced tumor accumulation and deep penetration [451–456]. Notably, some research work [457–459] demonstrated that the NPs with termediate rigidity may possess better tumor penetration than stiffer and/or softer counterparts. For instance, Gao *et al.* [460] constructed three hybrid NPs with different mechanical properties of 5, 50, and

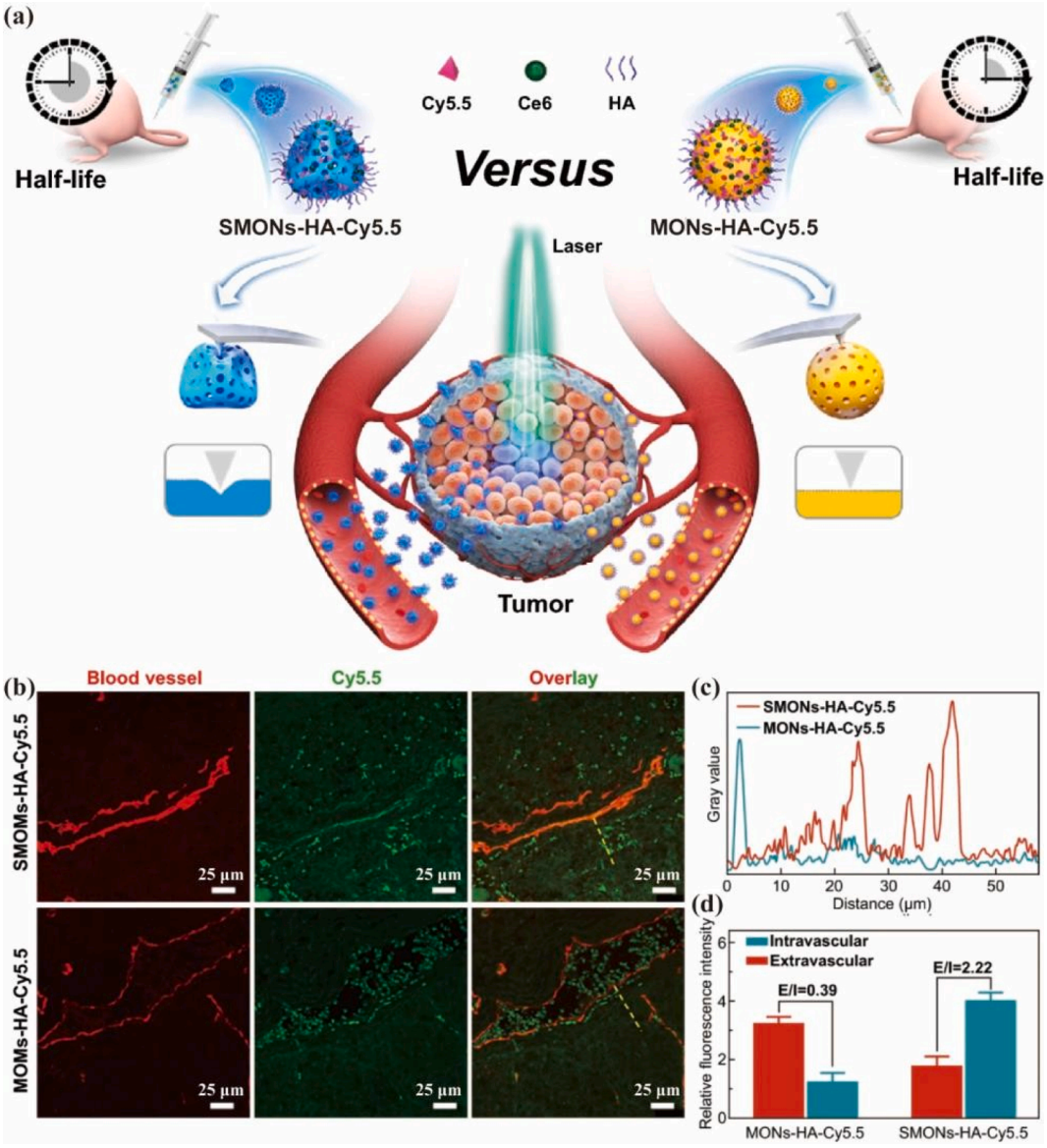

Fig. 34. (a) Schematic illustration of SMONs-HA- Cy5.5 for prolonged blood circulation, enhanced accumulation and deep penetration of tumor. (b) CLSM images and (c) the corresponding grey value profiles in extravascular areas of tumor tissues after injection of different samples. (d) Fluorescence intensities of Cy5.5 in intravascular and extravascular areas of tumor tissue after treated with different samples. Reprinted with permission from 443. Copyright 2020, Springer Nature.

110 MPa. By super-resolution high-speed confocal microscopy, the deformation of 50 MPa hybrid NPs from spherical to ellipsoids was directly observed, that facilitated their rotation and penetration, whereas 110 MPa hard hybrid NPs distorted negligibly, and 5 MPa soft hybrid NPs deformed excessively and irregularly.

4. Bioinspired systems

4.1. Biomimetic systems

Although these aforementioned smart NPs and novel strategies have been developed to overcome some biological barriers *in vivo* for highly efficient theranostics of diseases, these synthetic NPs still face the risk of activating the undesired immune responses, leading to the rapid elimination by the immune system and the serious toxic effects [461–463]. In recent years, the engineering of smart NPs using biomimetic strategies has attracted extensive attention due to their unique biological properties and functions [464–466]. Normally, the biomimetic systems were constructed to mimic natural biological systems (e.g., virus, bacterial, or cells) using the

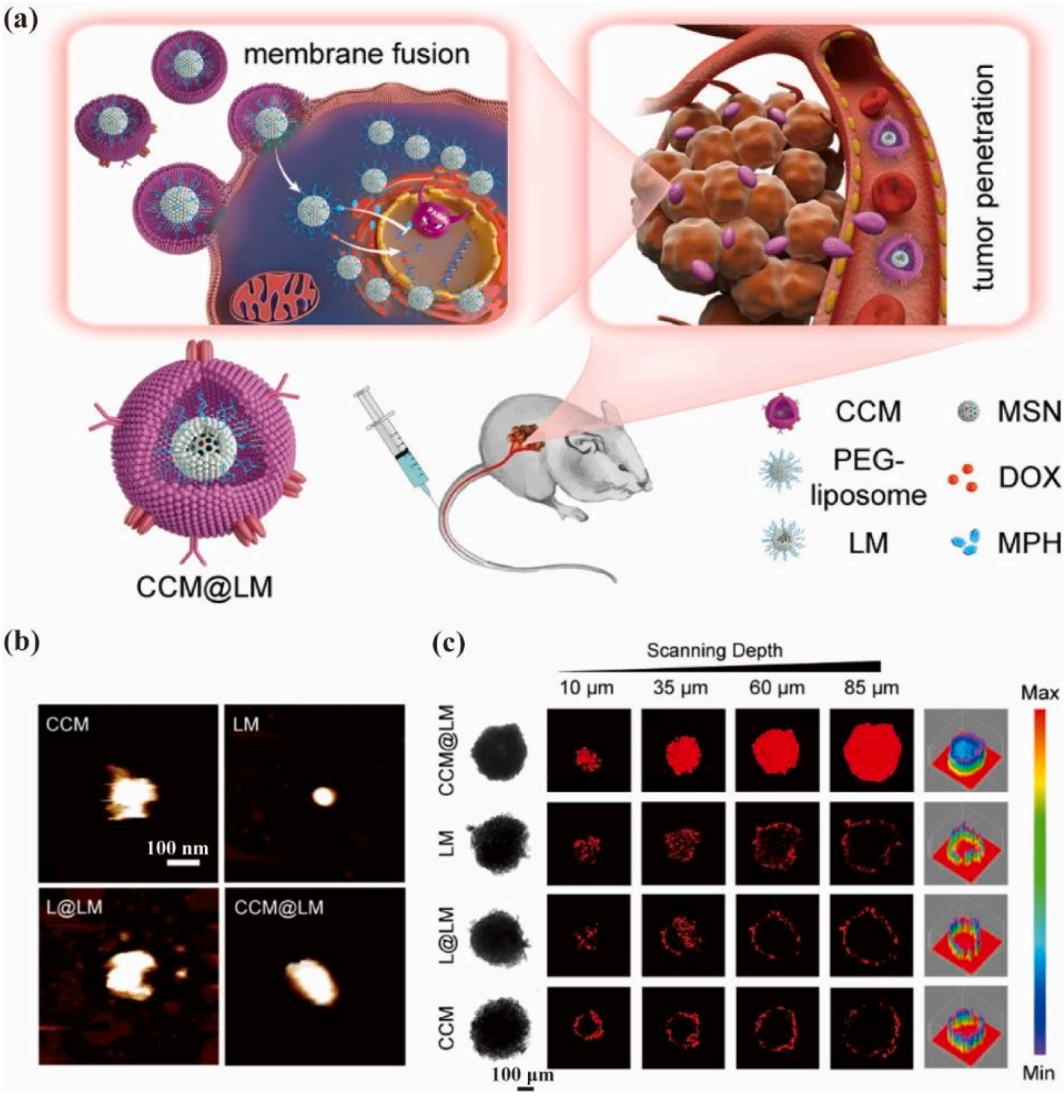

Fig. 35. (a) Schematic illustration of deformable CCM@LM for deep penetration and homologous targeted chemotherapy of breast tumor. (b) Atomic force microscopy images of different samples. (c) CLSM images of multicellular tumor spheroids treated by different samples. Reprinted with permission from 446. Copyright 2020, American Chemical Society.

biomimetic blocks [467,468] or the combination of biomimetic coating and synthetic NPs [469,470] (Fig. 36a,c). As a result, the biomimetic systems are capable of overcoming the barriers in 1) blood circulation, 3) tissue accumulation, 5) cellular internalization, 6) lysosome escape, and 8) nuclear targeting by the strong protein resistance, homologous and subcellular targeting, ideal cell membrane fusion, and excellent immune evasion.

4.1.1. Biomimetic block

By virtue of the distinctive structure that is close to globular protein [471,472], the polypeptide-based dendrimers as biomimetic block can be utilized to construct the mimics of natural biological systems [473–475]. Recently, Gu *et al.* [476,477] developed a versatile strategy to prepare the viral capsid-like biomimetic nanoarchitectures by the self-assembly of PLL dendrimers with linear poly (L-leucine) (Fig. 37). Furthermore, they synthesized the smart virus mimics (CTVMs) based on the self-assembly of DMMA-modified amphiphilic dendritic lipopeptides (DLPs) for systemic drug delivery [478]. The CTVMs is expected to offer the following benefits: (1) stealthy negative corona to obtain protein resistance and hydrophobic core to encapsulate bioactive drugs, (2) acidic TME-triggered surface charge conversion to improve deep penetration, (3) receptor-mediated targeting to enhance cell uptake mimicking viral internalization, and (4) supramolecular lysine-rich architectures to generate virus-like subcellular targeting (i.e., endosomal escape and unclear targeting). With the excellent properties owned, the CTVMs after systemic administration hold great potentials to improve antitumor efficacy, reduce cancer metastasis and side effects. Moreover, the arginine-containing DLPs were also employed to prepare virus mimics for gene delivery with high transfection efficiency, serum resistance and low cytotoxicity [475].

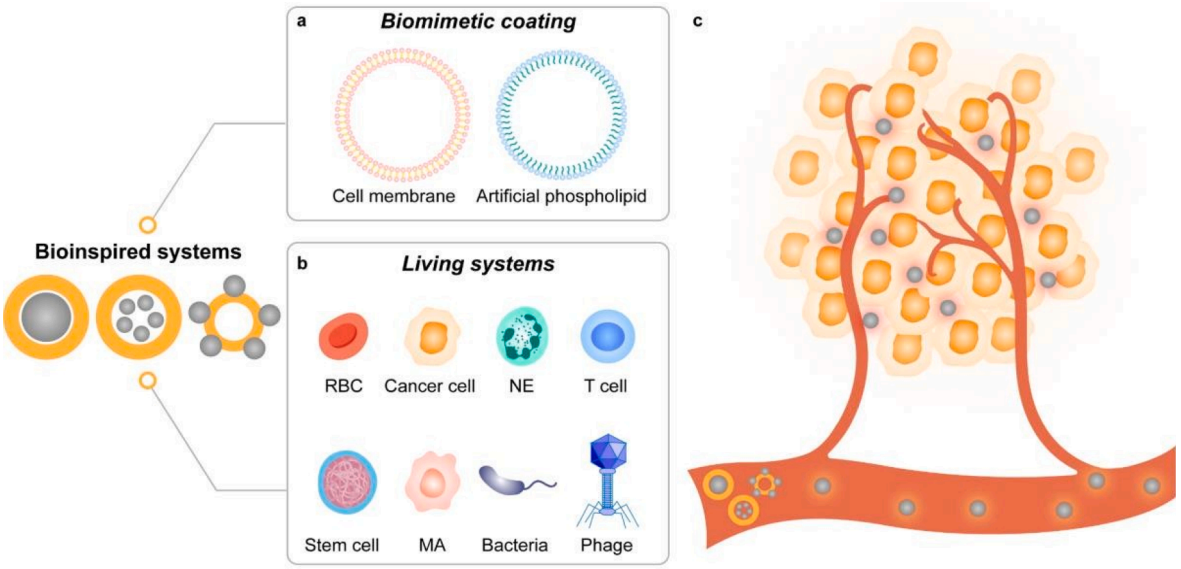

Fig. 36. Schematic illustration of (a,b) the construction of bioinspired systems (biomimetic and living systems) and (c) their applications for overcoming biological barriers and enhancing disease Theranostics.

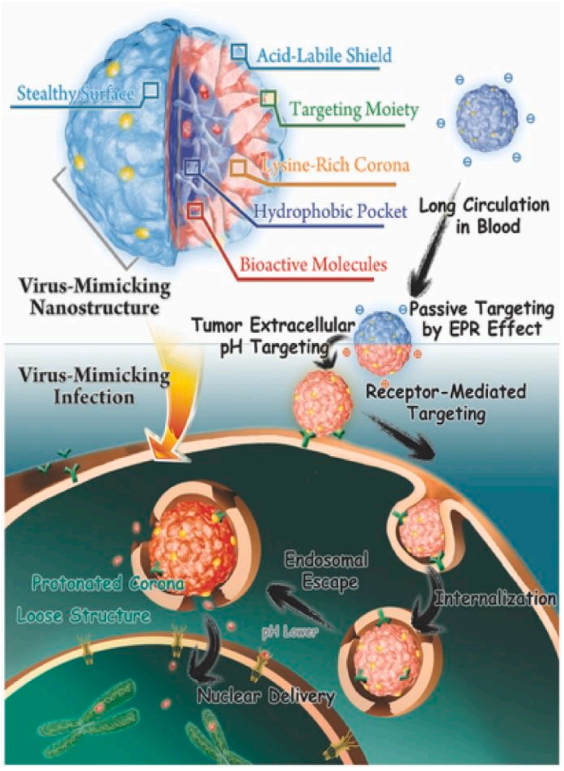

Fig. 37. Schematic illustration of CTVMs for improved antitumor efficacy. Reprinted with permission from 478. Copyright 2014, John Wiley and Sons.

4.1.2. Biomimetic coating

Inspired by the natural cell membranes that are responsible for intercellular communication, immune defence, and metabolism through the life circle, the biomimetic coating has been extracted and coated on the synthetic NPs to prepare cell-like systems from biomimetic perspective [479]. These created biomimetic coating-covered NPs are regarded as other novel class of biomimetic systems

to realize the smart functions from natural cell membranes and achieve the relevant biomedical applications [480–482]. The biomimetic coating provides a convenient method to endow the NPs with prolonged blood circulation, good biocompatibility, deep penetration and cancer-targeting properties [483,484]. Recently, the artificial lipid bilayers or natural cell membranes (e.g., the membrane source from red blood cells, platelets, immune cells, cancerous cells, and bacteria) have been developed to construct biohybrid delivery systems. Notably, red blood cells membranes-coated biomimetic systems display prolonged blood circulation and immune-evasive properties, however they often lack the specific targeting and immunological ability [485].

4.1.2.1. Artificial phospholipid. The artificial lipids are most clinically used for formulating nanocarriers and also used as biomimetic coating [486–490]. For instance, Zhao *et al.* [491] chose fusogenic phospholipid 1,2-dioleoyl-*sn*-glycero-3-phosphoethanolamine (DOPE) to coat biodegradable dendrimer nanoassembly (DLC-PEG) for highly efficient DOX delivery (Fig. 38a). The DOPE rendered the formed DLC-PEG/DOX with stealthy and stable in the blood. Once inside tumor tissue, the DOPE was expected to peel off by fusion to release single dendrimer for improved tumor penetration and cellular uptake. The result suggested that the DOX intensity inside the tumor treated with DLC-PEG/DOX was about 10 times more than that treated with a standard long-circulating nanocarrier with similar size (PCL_{2k}-PEG_{2k}/DOX) (Fig. 38b). Due to the pH-responsive protonation, the formed cationic dendrimer could further promote cellular internalization in acidic TME, thereby shipping the DOX into the cytosol and circumventing the MDR.

Multivalent displays of glycan ligands from the surface of biological membranes can be emulated by glycopolymers [492–494] and glycodendrimers [495–497], that are efficient for recognition of the carbohydrate-binding proteins and lectins. In recent years, a simple method for the assembly of amphiphilic Janus glycodendrimers to fabricate artificial phospholipid was reported [498–500]. Eighteen amphiphilic Janus glycodendrimers with different topologies were synthesized though an accelerated modular strategy [450]. These formed assemblies as biomimetic membranes exhibited the specific and potent bioactivity, that is expected to be of interest for targeted drug delivery and vaccines [501,502].

4.1.2.2. CCM. Compared with traditional artificial lipid bilayers, the biomimetic coating from natural cells contain various functional moieties (e.g., proteins and antigens) which can be used for intracellular communication, specific recognition, bioantifouling, and protection [503]. The conventional cells, such as platelet [504–506], leukocyte [507,508] or red blood cells [509,510], have been employed for biomimicking the NPs. However, these biomimetic NPs may not have the ability to recognize and target cancer cells. Remarkably, in recent years, the CCM have attracted widespread attention in the formation of biomimetic NPs for highly efficient tumor theranostics attributing to their long blood circulation time, homologous targeting, and immune escape [511–513]. The combination of CCM and NPs has inspired a new strategy to develop biomimetic smart NPs to address some barriers *in vivo*. By specific recognition function of membrane protein on CCM, the novel biomimetic NPs (CPPNs) were constructed from 4T1 cell membranes and paclitaxel (PTX)-loaded polymeric NPs for chemotherapy of the primary and metastatic tumors [514]. The CPPNs displayed the

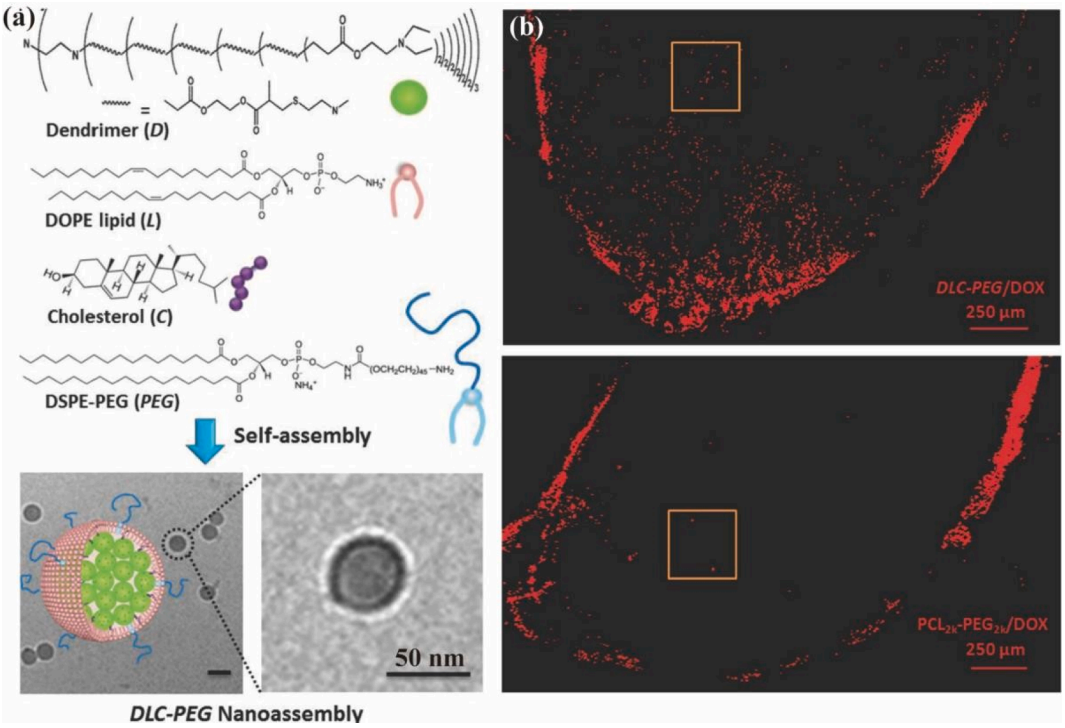

Fig. 38. (a) Schematic illustration of the preparation of DLC-PEG/DOX, and their SEM images. (b) CLSM images of the tumor tissues after injection of DLC-PEG/DOX and PCL_{2k}-PEG_{2k}/DOX. Reprinted with permission from 492. Copyright 2014, John Wiley and Sons.

decreased phagocytic uptake, increased blood circulation, and homologous targeting of breast metastatic cancers. Likewise, based on HeLa cell membranes and nanoscale metal–organic frameworks, the O_2 self-sufficient cell-like biomimetic NPs were developed for targeted PDT of tumor [515]. After IV injection, the biomimetic NPs were beneficial for tumor accumulation and uptake by the immune escape and homologous targeting. To obtain better antitumor efficacy, Liu *et al.* [516] prepared B16-F10 cell membranes camouflaged MSNs for combined starvation therapy and immunotherapy of melanoma with low side effects.

In 2020, our group reported a versatile nanoplatforms (USIO NCs/DOX@CM) based on pH-responsive ultrasmall Fe_3O_4 clusters loaded with DOX and surface-coated with B16 cell membranes for UTMD-promoted precise tumor theranostics (Fig. 39) [517]. The versatile nanoplatforms were quite unique: 1) the ultrasmall Fe_3O_4 clusters with pH-responsive benzoic-imine bonds could be used for dynamic T_2/T_1 MR imaging and simultaneous rapid DOX release by the dissociation of clusters; 2) the CCM-coating enabled the immune evasion-resulted pharmacokinetics and homologous tumor targeting; and 3) the enhanced tumor delivery was achieved by UTMD effect. Moreover, membrane-related tumor antigens and specific functional proteins are of great importance, that should be considered for the constructing anticancer vaccines [503]. Summary, the emerging CCM-coated biomimetic nanotheranostics represent a safe and effective strategy for tumor Theranostics

4.1.2.3. BM. Similar to cell membrane, the bacteria membrane (BM) with protein shells was also employed to cover the NPs for highly efficient theranostics of tumor or inflammatory [518]. Especially, bacterium-based systems survived in anaerobic environments and along oxygen taxis to reach anoxic tumor *in vivo* [519,520]. Moreover, several investigations implied that the bacteria naturally possessed tumor-targeting features mediated by adhesion proteins, antigens, or other molecules on the surface of protein shells [521]. Therefore, the BM-coating strategy improves a new perspective to design the biomimetic NPs for enhanced disease Theranostics For instance, He *et al.* [522] developed novel biohybrid micromotors using the combination of living neutrophils with BM-camouflaged MSNs for targeted drug delivery by the chemotactic motion. The *E. coli* membrane coating not only enabled the drug encapsulation in MSNs without undesired leaking, but also promoted the uptake of the resulting MSNs into neutrophils without loss of their bioactivity and chemotaxis ability. Excitingly, the micromotors could effectively move along the chemoattractant gradients produced.

Additionally, BM can also be introduced as appealing vaccination coating as they contain a large number of immunogenic antigens with intrinsic adjuvant properties and exhibit various pathogen associated-molecular patterns that play a key role in stimulating innate immunity and promoting adaptive immune responses [523–525]. With these excellent properties, the BM-coated NPs will mimic the natural antigen presentation by bacteria to the immune system [526]. For instance, Zhang *et al.* [527] prepared the BM-coated AuNPs (BM-AuNPs) as antibacterial vaccine for modulating antibacterial immunity (Fig. 40). When subcutaneously injected into mice, the BM-AuNPs traveled to adjacent draining lymph nodes and rapidly activated dendritic cells residing in the lymph nodes. Furthermore, the vaccination with BM-AuNPs in the animal model generated strong and durable antibody responses with high avidity.

4.2. Living systems

4.2.1. Cell-based systems

To address the lack of cellular activity in biomimetic systems, some endogenous living cells (e.g., red blood cells (RBCs),

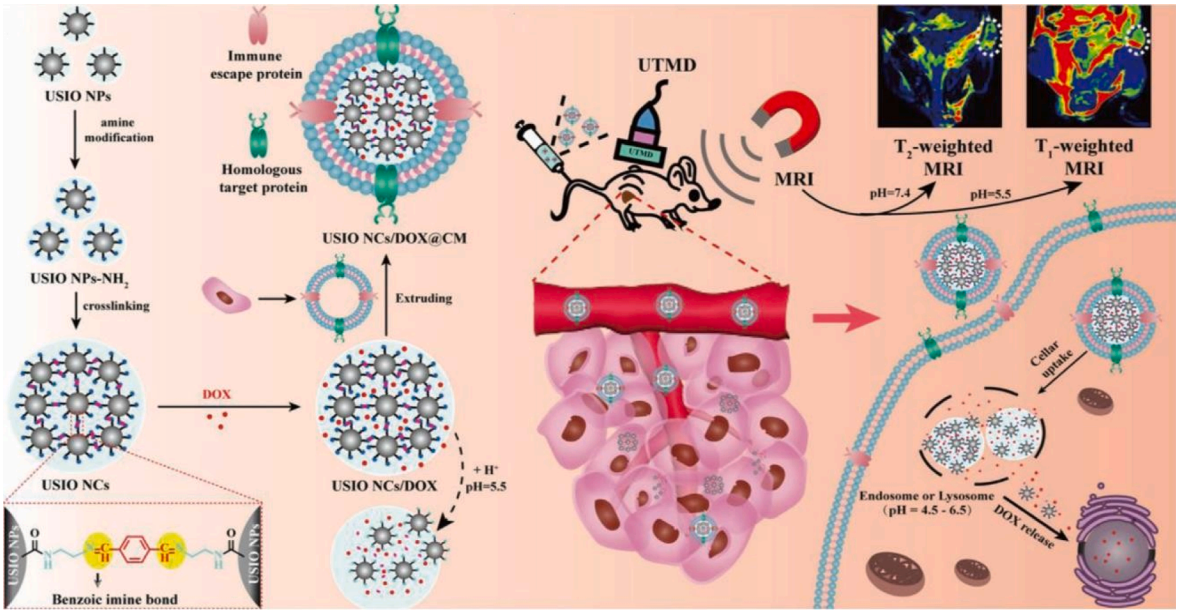

Fig. 39. Schematic illustration of the preparation of cell membranes coated versatile nanoplatform USIO NCs/DOX@CM for UTMD-promoted dynamic MR imaging-guided chemotherapy of tumor. Reprinted with permission from 518. Copyright 2021, Elsevier.

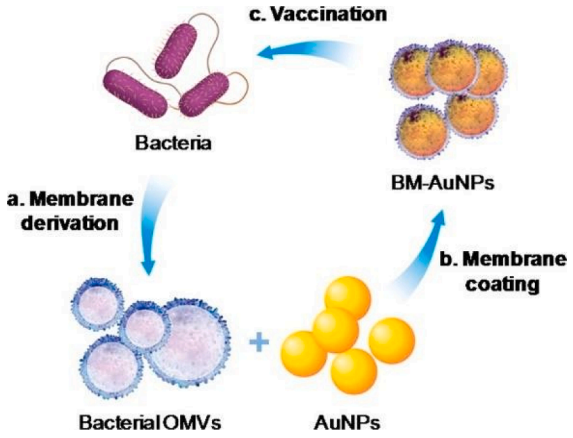

Fig. 40. Schematic illustration of BM-AuNPs for modulating antibacterial immunity. Reprinted with permission from 528. Copyright 2015, American Chemical Society.

macrophages (MAs), neutrophils (NEs), T cells and stem cells) as delivery systems were employed to attach or phagocytose various nanoplatforms (Fig. 36b,c), aiming to overcome the barriers in 3) tissue accumulation, 4) deep penetration, 5) cellular internalization, and 6) lysosome escape [75,76]. These cell systems have significant advantages of phagocytic nature, abundance, disease homing, minimal immunogenicity and nontumorigenicity. For tumor theranostics, they can migrate/chemotax through tumor areas and to metastatic tumor cells in response to tumor-associated chemokines, that may severely thwart tumor function and metastatic potential. Moreover, immune cells including MAs and NEs can also be more actively recruited to the inflammation region. Notably, the genetically engineered cells that display chemoattractant receptors and endothelial cell-binding molecules are effective vehicles for the targeted delivery of imaging agents and therapeutics [528].

4.2.1.1. RBCs. RBCs are the most abundant cells in the body and account for more than 99 % of the total blood cells. They carry large amount of hemoglobin molecules which bind with O_2, and therefore serve as the major O_2 transporter throughout the body [529]. RBCs are regarded as ideal cell carriers for their high availability, long circulating half-life, large surface area and interior volume

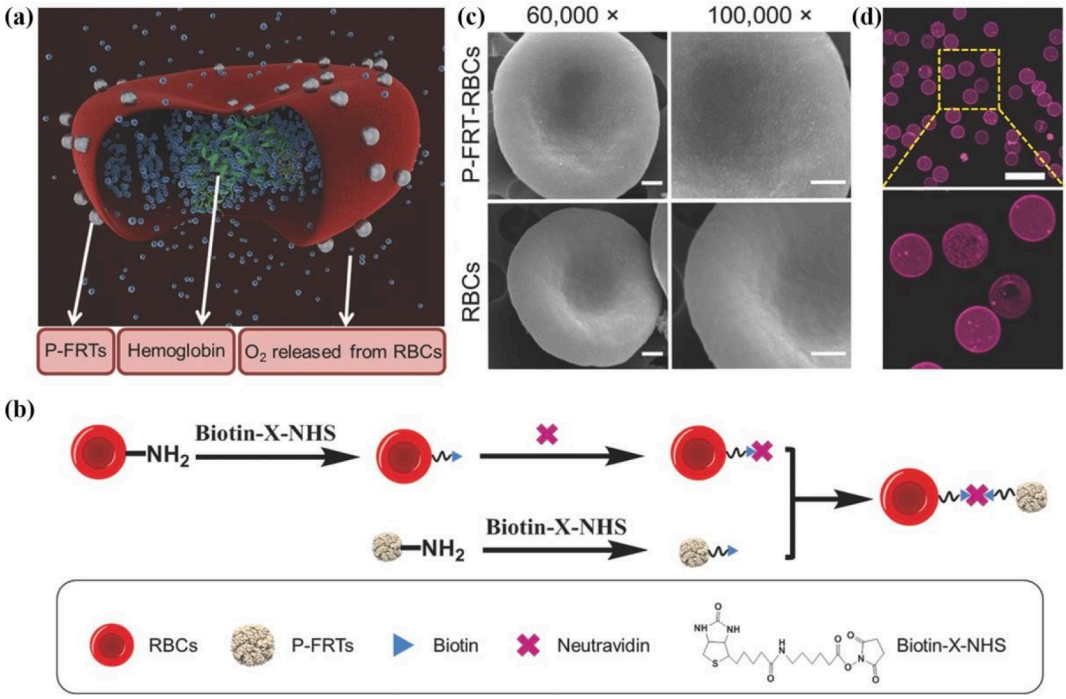

Fig. 41. (a) The illustration and working mechanism of P-FRT RBCs. (b) The preparation P-FRT- RBCs (not to scale). (c) SEM images of P-FRT-RBCs and RBCs. (d) Confocal microscopy images of Cy5.5-labeled P-FRT-RBCs. For c-d, Scale bar: 20 μm. Reprinted with permission from 534. Copyright 2016, John Wiley and Sons.

[530]. Various bioactive molecules can be loaded onto or into RBCs to improve their circulating behavior in blood stream. For instance, Au NPs could be physically loaded into RBCs using a simple hypotonic dialysis method for improved dynamic X-ray imaging of blood pool [531]. Meanwhile, aging or broken RBCs were easily uptake and cleared by the scavenger cells in the RES organs. In this way, non-specific drug uptake and side-affects might happen in the delivery process. It is important to minimize the damages to RBCs within the loading process, and therefore several mild strategies such as antibody or penetrating peptide-based loading were developed [532].

In addition to loading NPs and drugs inside the RBCs, it is also feasible to attach large amount of NPs onto their surface. In a recent work by Xie *et al.* [533], the unique function of RBCs as O_2 transporter was exploited and combined with nanomedicine to relieve tumor hypoxia and facilitate highly-efficient PDT (Fig. 41). They first loaded $ZnF_{16}Pc$ photosensitizers in ferritins (with a ferritin to $ZnF_{16}Pc$ molar ratio of 1:40), and then the ferritins nanocages (P-FRT) were conjugated onto the surface of RBCs using a biotin-neutravidin-mediated coupling strategy to get the P-FRT-loaed RBCs (P-FRT RBCs). RBC-loading significantly extended the circulation half-life of P-FRT lead to an improved the biodistribution of NPs, in which there was a relatively high content of NPs in the blood at both early time point (1 h) and longer time point (24 h). Meanwhile, more accumulation of P-FRT in hyper-vascular tissues such as tumor was found. As a result, carrying a large amount of photosensitizers (up to 5×10^5 photosensitizer per each cell) and oxygen in RBCs, the generated nanosystem showed efficient production of $^1O_2$ even under low oxygen conditions, thus realizing enhanced PDT against cancer cells both *in vitro* and *in vivo* in a hypoxia tumor model.

5.2.1.2. MAs. Immune cells, such as MAs, NEs, T cells, as part of the body's immune system, play important roles in the innate and adaptive immune response against to various diseases such as cancer, inflammation and infection. Many of them possess innate homing ability, favorable circulating behavior and special immune-activities, and thereby can be served as interesting living delivery systems to cross the barriers *in vivo* for improved biomedical applications.

MAs are the major scavenger cells within the body, responsible for phagocytosis and disposal of dead cells, cell debris and foreign substances. Generally, they are the first immune cells to respond to invading pathogens, secreting cytokines to recruit other leukocytes into inflammation or tumor area. MAs are among one of the most abundant infiltrating leukocytes in the TME and play a vital role in

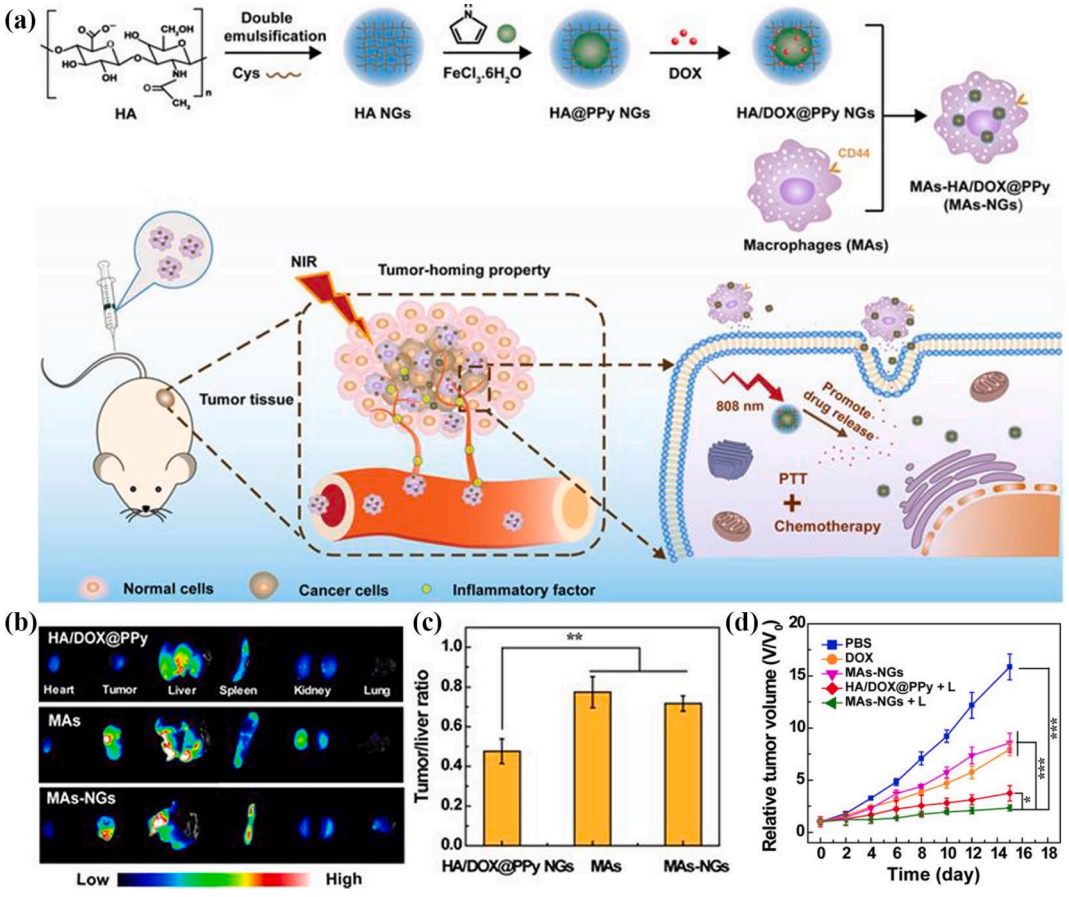

Fig. 42. (a) Schematic illustration of the preparation of MAs loaded with HA/DOX@PPy NGs (MAs-NGs) for combination PTT/chemotherapy of tumors. (b) *Ex vivo* fluorescence images of major organs and tumors and (c) corresponding tumor/liver fluorescence ratio (MAs and MAs-NG were stained with DiR, and Cy7-labeled HA/DOX@PPy were used as control. (d) Relative tumor volume of 4T1-tumor bearing nude mice after different treatments. Reprinted with permission from 539. Copyright 2021, Ivyspring International Publisher.

tumor progression. Importantly, they are found to have natural immune evasion property as well as tumor-homing and infiltration ability through the recognition of certain kinds of cytokines and chemokines released by tumor cells [534,535], thus holding great potential in the tumor delivery of nanocarriers.

The challenge for MA-mediated delivery is to enhance the loading content in MAs, because many drugs or NPs can be toxic to MAs, resulting in low uptake or damage of cell viability. Earlier studies have taken strategies in modification and structure reorganization of NPs to reduce their cytotoxicity and improve MA uptake [536]. In a recent study, Xie *et al.* [537] reported the application of a nanocapsule strategy to solve MAs loading obstacles, in which a DOX-silica nanocomplex (DSN) was constructed and then incubated with MAs to prepare the MA-loaded DSN. Using this approach, the loaded DOX within MAs could be high up to 16.6 pg/cell, and the DSN would do no harm to the migration ability of MAs within the first 6–12 h that they need for tumor homing.

While these abovementioned MA-based delivery systems are mainly focused on the single drug-loaded NPs with limited therapeutic modalities. In recent years, to render the MA-mediated drug delivery systems with multifunctionality toward a highly-efficient therapy or theranostics, the hybrid nanomedicine was also combined with MAs for effective treatment of diseases, especially cancers. In a recent work by our group, the NGs-loaded MAs were formed for the combination therapy of tumor [538]. In this work, cystamine dihydrochloride-crosslinked HA-based NGs were first prepared through a double emulsification method, then loaded with the photothermal agent of PPy by an *in situ* oxidization polymerization and physically encapsulated with DOX. The created HA/DOX@PPy NGs were then endocytosed by MAs under regular cell culture condition to generate the MAs-NGs (Fig. 42a). The MAs-NGs displayed high drug-loading efficiency and specific targeting ability for enhanced tumor accumulation (Fig. 42b), thereby achieving the improved therapeutic efficiency based on the combined PTT with chemotherapy (Fig. 42c,d).

However, the preparation of NGs-loaded MAs *ex vivo* is labor-intensive, and the migratory capacity of MAs can also be impaired. To avoid the high cost within the *ex vivo* procedures. In 2020, Tan *et al.* [539] developed a vectorization strategy to realize *in vivo* loading of MAs with nanocarriers. The cancer cell-derived apoptotic bodies (ABs) as biological vehicles of nanocarriers were readily engulfed by the MAs. After intravenous injection, the nanocarriers-loaded ABs can be rapidly phagocytized by the MAs during blood circulation, leading to the enhanced tumor accumulation and inhibited tumor metastasis as well as recurrence based on the MAs-mediated delivery. In addition, tumor-associated MAs (TAMs) have received special interests for its role in remodelling the TME. Given different activation pathways, macrophages can be polarized into M1/M2 phenotypes. M2 macrophages are the main phenotypes in TME and can promote tumor angiogenesis, invasion, and metastasis. In comparison, M1 macrophages can produce cytotoxic cytokines and chemokines, such as tumor necrosis factor-α (TNF-α) and intracellular NO to suppress tumor growth [540]. Hence, inducing macrophages toward the M1 differentiation can bring about extra benefits in MA-mediated delivery. Recently, some researchers found that Au NPs-based nanoplatforms possessed the ability to induce MA polarization toward the M1 anti-tumor phenotype. In a work by Wang *et al.* [541], the authors demonstrated that MAs loaded with dendrimer entrapped Au NPs could effectively trigger the M1 differentiation of MAs to facilitate immunotherapy under the guidance of CT imaging, which helps to improve the outcome of

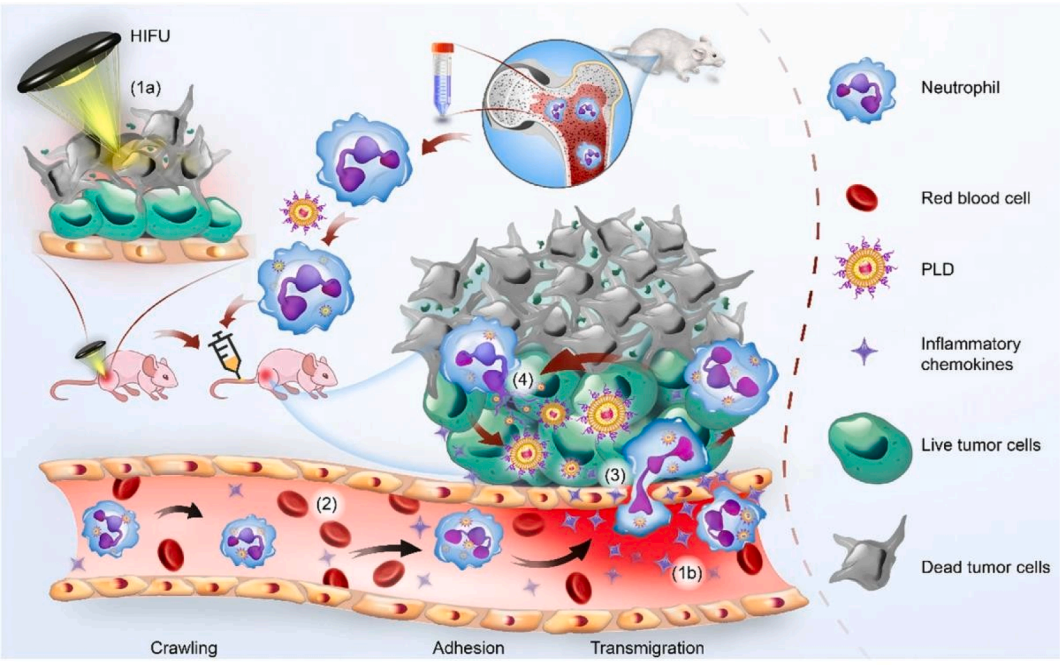

Fig. 43. Schematic illustration of NE-mediated drug delivery for suppression of tumor recurrence after HIFU ablation. (1a,b) HIFU ablates tumor to generate an inflammatory environment, and (2) the released chemokines induce the migration of NEs to tumor region; (3) PLD@NEs transmigrate to the vascular barrier and penetrate into the tumor along the chemotactic gradient; (4) PLD is released from NEs for antitumor by the formation of neutrophil extracellular traps. Reprinted with permission from 544. Copyright 2021, Springer Nature.

chemotherapeutics in a orthotopic osteosarcoma model.

4.2.1.3. NEs. NEs are another type of natural phagocytes, which have a higher abundance than MAs. Similar to MAs, they present in tumor tissue and have a positive effect on the continuous recruitment of circulating leukocytes. NEs display a native ability to traverse BBB and BTB for targeting tumor and other diseases in the central nervous systems. For instance, Zhang *et al.* [542] reported NEs loaded with liposomes entrapping PTX can penetrate into the inflamed brain after surgical resection of glioma, suppressing the recurrence of tumors in mice. The NE-mediated PTX delivery led to an 86-fold higher drug accumulation in the glioma area than free PTX, which indicates the superior brain tumor targeting ability of NE carriers. In a latter study, Cai *et al.* [543] proposed a strategy to use NEs loading PEGylated liposome doxorubicin (PLD) for a targeted therapy of residual liver tumors after HIFU ablation, which also realized the improved therapeutic outcomes (Fig. 43). With the liposome package, the PLD (the first liposome-based nanodrug approved by the FDA) did not show appreciable harm to the viability and morphology of NEs. After HIFU ablation, the generated inflammatory response could promote the chemotactic migration of PLD@NEs to the residual tumor area, and then the PLD was released by inflammatory stimuli, thereby resulting in the targeted postoperative chemotherapy.

Remarkably, smart nanoplatforms can also be designed to hijack the NEs *in vivo*. For example, Wang *et al.* [544] demonstrated that albumin NPs could be actively internalized *via* NEs through the interaction of Fcγ receptors, provoking a new route to deliver therapeutic NPs into the tumor microenvironment. In 2021, Brenner *et al.* [545] reported a novel design criteria to induce selective phagocyte of NPs by NEs marginated to inflamed lungs. The work showed that the supramolecular arrangement of proteins in NPs could serve as a guidance for accumulation in NEs in lung inflammation. Revealing such an interplay between agglutinated protein on NPs and complement proteins raises the potential for novel approaches to NE-related immunotherapy.

4.2.1.4. T cells. In comparison with the above two immune cells, T cells are the most important component in cell-mediated immunity and they have been readily isolated and expanded *in vitro* [546]. Remarkably, T cells can not only serve as vehicles for augmenting the tumor delivery of NCs, but also directly recognize and kill cancer cells with surface modification or through certain stimuli. Surface engineering technologies of T cells such as T cell receptor (TCR) and chimeric antigen receptor (CAR)-engineered T cell have been regarded as milestone progress in cancer immunotherapy. Several functional NPs such as Au NPs [547] and magnetic NPs [548] have been used to label T cells for tracking the fate of T cells *in vivo*, and it is found that surface-engineered T cells can be used as the vehicle for delivery of therapeutics into tumors. In a work by Cohen *et al.* [549], the authors transduced T cells to express a melanoma-specific TCR and labeled the cells with glucose-coated Au NPs. The labeling process did not harm the T cell function. After labeling, the T cells were then injected intravenously to mice with a melanoma xenograft to track the distribution, migration, and kinetics of T-cells through CT imaging. As compared to the nontransduced T cells counterpart, the transduced T-cells were observed to efficiently accumulate in the tumor area and the tumor growth was significantly suppressed.

Apart from the strategy of loading NPs inside T cells, backpacking NPs on the T cell surface may be another option. Irvine *et al.* [550] developed a stable conjugating strategy to the surface of T cells *via* cell-surface thiols, in which the adjuvant-loaded NPs were successfully conjugated and enhanced the efficacy of T cell adoptive therapy. Also taking advantage of the T cell surface thiols, they further utilized polyclonal T cells as carriers to deliver drug-loaded into lymphoma tumors [546]. In this study, the authors first expanded primary T cells isolated from mice in the presence of IL-2 and a mTOR inhibitor rapamycin to retain the CD62L and CCR7 expression on T cells during IL-2-mediated cell proliferation. Phosphatidylglycerol lipid, maleimide-headgroup lipid, and SN-38 were fused together to form the drug-loaded nanocapsules with free maleimide groups on the surface, which can be covalently reacted with the T cell thiol groups (Fig. 44). This T cell-based live delivery strategy greatly improved the pharmacokinetics of SN-38, in which the drug accumulation was greatly increased in tumor-bearing lymph nodes, reaching a 63-fold higher concentrations than free nanocapsules at 20 h and retaining for at least 4 days. This improved drug pharmacokinetics then help to inhibit tumor growth and increase survival greatly.

4.2.1.5. Stem cells. Many types of stem cells, including mesenchymal stem cells (MSCs) and neural stem cells, have been shown to have the ability to migrate to the tumor microenvironment, and are therefore widely used for tumor-specific drug delivery. Currently, a gene-engineered stem cells system has been approved by FDA to treat recurrent high-grade gliomas in clinical trials. Moreover, many types of NPs, such as poly-lactic acid NPs, lipid nanocapsules [551] and Au nanorods [552] *etc.*, have been loaded in stem cells toward the transportation of tumor area for precise Theranostics In a study by our group, MSCs-mediated delivery system of Fe_3O_4 NPs-loaded PEI NGs was constructed for improved T_1 MR imaging in a subcutaneous breast tumor and orthotopic glioma models [553]. The results showed that the NGs with good biocompatibility did not influence the possible differentiation of BMSCs, with no remarkable change on CD34 and CD44 observed, thus may facilitate a safe long-term tracking the fate of cell migration *in vivo*.

Differently from the nanomedicine-internalized stem cells, the strategy of anchoring NPs on stem cells surface may allow for more effective delivery and less toxicity of NPs to stem cell carriers. In an early study, Tang *et al.* [554] modified MSCs with DOX-loaded silica NPs and successfully transported the system into glioma cells for chemotherapy. Recently, Liu *et al.* [555] synthesized mesoporous silica-coated super-paramagnetic Fe_3O_4 NPs (Fe_3O_4@MSNPs) to serve as nanocarriers for drug delivery, which possessed pH-responsive release and MR imaging properties. Then, the Fe_3O_4@MSNPs were conjugated to human adipose-derived stem cells (hADSCs) based on antigen–antibody reactions using anti-CD44 antibody to generate the living delivery system (Fig. 45a). The living system can be actively driven to tumor site through the tumor-tropic behavior of hADSCs, and DOX can be controllably released in the tumor area to exert killing effects. Likewise, the super-paramagnetic Fe_3O_4 core with good MR imaging property allowed real-time monitoring of live drug delivery, and it was found that the live system containing both antibody and stem cells could migrate and

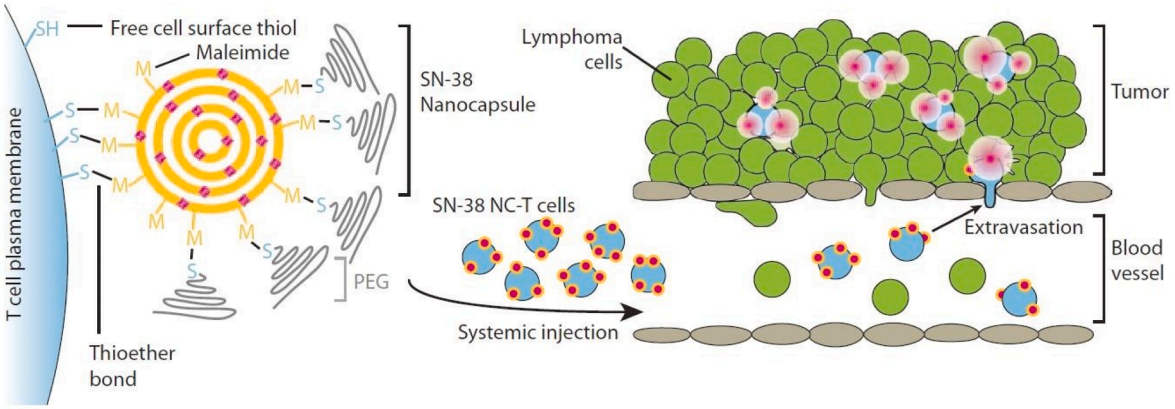

Fig. 44. Schematic illustration of T cell functionalization and cell-mediated delivery of SN-38-loaded NPs into tumors. Reprinted with permission from 547. Copyright 2015, AAAS.

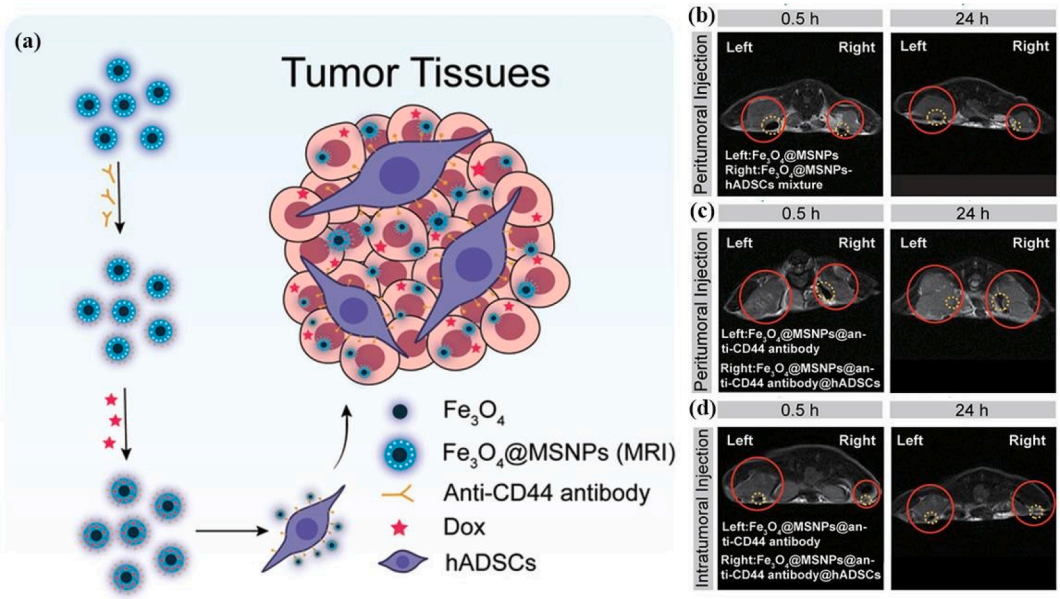

Fig. 45. (a) Schematic illustration of the design of hADSCs-based living system for real-time monitoring of tumor. (b–d) T_2 MR imaging of tumor. The tumor region and materials are marked with red and yellow circle, respectively. Reprinted with permission from 556. Copyright 2022, John Wiley and Sons.

retain at tumor site after injection of 24 h (Fig. 45b–d), which can contribute to the diagnosis of small or dispersed tumors.

Remarkably, in 2021, Klemke *et al.* [528] developed a genetically engineered and enucleated cell for the targeted delivery of therapeutic agents. Using bioengineering techniques, the engineered MSCs were able to express multiple chemoattractant receptors and endothelial cell-adhesion molecules. Afterwards, the nuclei of bioengineered MSCs were removed to obtain cell nuclei-free delivery vehicles named as "cargocytes" that could display the intrinsic cellular functions for energy and protein production, and delivery of NMs to inflamed and pathological tissues *via* the active chemotaxis and endothelial adhesion. Overall, the cargocytes combine cell bioengineering and enucleation techniques, thus representing a multifunctional carrier that exhibit the potential to treat a range of diseases in a controllable and effective manner, with higher safety.

4.2.2. Bacterial-based systems

In recent years, the development of synthetic biology can engineer bacteria into drug carriers for efficient and targeted delivery [556–558]. In the field of drug delivery, the commonly used engineering bacteria include *E. coli*, Salmonella, and Lactococcus. These engineered bacteria as gene carriers also have easy editing property [559,560]. Importantly, the engineered bacteria are able to selectively colonize tumor tissue due to hypoxia and immunosuppressive TME, and then survive for up to several weeks, thus achieving tumor specific delivery and retention [561,562]. For instance, Liu *et al.* [563] developed double-modified *E. coli* to reprogram the

immunosuppressive TME for improving antitumor efficacy. Through integrating the synthetic biology and interfacial chemistry, both the interior and exterior of the bacteria were modified to express melanin as photothermal agent and anchor immune checkpoint inhibitors on their surface. The *in vivo* animal experiments shown that two therapeutic agents could be distributed homogenously and durably within tumors due to the colonization properties of bacteria in hypoxic TME.

Another type of bacteria, Salmonella, exhibit the natural advantage in delivering proteins into cancer cells because of their unique physiology, such as active cell invasion, specific tumor accumulation, and *in situ* production of protein drugs [564–566]. Different from conventional delivery carriers, the capacity of *in situ* protein drug production of Salmonella allows for more drugs to be delivered and accumulated in tumors than those initially injected. The specificity is contributed by the tumor growth, coupled with the clearance from healthy tissues simultaneously [567]. In 2021, Forbes *et al.* [568] designed the engineered Salmonella that can target necrosis/hypoxic region of cancer cells for intracellular delivery of proteins (Fig. 46). In this work, three genetic circuits were carried out to control protein production, invade cells, and release protein drugs. The intrusion control *via* the main regulator flhDC increased delivery efficiency by more than 500 times. After the uptake by cancer cells, the protein drugs directly accumulated in the cancer cells and then killed them. Subsequently, the bacteria will be automatically eliminated without affecting normal cells. Although the engineered bacteria as living delivery systems have attracted great interest of the researchers, their clinical transformation is highly controversial. The key reason is that some potential challenges have not been systematically assessed, such as the administration route and dose of bacterial, the mechanism of bacterial distribution within tumors, and biosafety issues.

4.2.3. Phage-based systems

The phages are capable of infecting and lysing bacteria, replicating and degrading biofilm matrix, which is a promising strategy for the treatment of bacterial infectious diseases [569]. Unlike antibiotic-based treatment, the phage strategy is also effective against multidrug-resistant bacteria. Moreover, most phage have been shown to be specific to target bacteria without infecting commensal microflora [570]. Due to these unique properties, the phages have also been developed as drug carriers for specific delivery to microbiota, enabling programmable remodeling of microbiota to enhance the therapeutic efficacy of bacterial infectious diseases and tumors [571]. For instance, García *et al.* [572] reported an engineered phage-loaded polymer microparticles for deep lung delivery. Through the pulmonary administration of dry powder inhalation, active phages can deposit throughout the lungs and effectively reduce *P. aeruginosa* infection and related inflammation, preventing pneumonia-associated death of mice.

As everyone knows, the microbiota plays an important role in human physiology and is closely related to acute infection, chronic disease occurrence, and tumor progression [573,574]. In the TME, the abnormal proliferation of some bacteria directly induces the failure of chemotherapy in tumor [575], while the secretion of some bacteria induces antitumor immune response and inhibits tumor growth [576]. In a recent work, a phage-guided hybrid nanocarrier was prepared based on the biorthogonal reaction of irinotecan-encapsulated dextran NPs and phages [577], which could enhance the chemotherapy efficacy by regulating the gut microbiota (Fig. 47). By the colonization of tumor microbiota of *F. nucleatum*, the hybrid nanocarrier increased the accumulation in colon tumors by approximately three times, thereby augmenting chemotherapy efficacy with low side effects. Meanwhile, the phages also eliminated intratumoral *F. nucleatum* in tumor areas, enhancing their response to chemotherapy through the regulation of the gut microbiota.

5. Conclusion and perspective

In this review, we have summarized the comprehensive approaches for the construction of smart and bioinspired systems. Three innovative strategies of surface charge conversion, size transformation, bioinspired systems are emerged to overcome various barriers of BVTDCLIN (e.g., blood circulation, vasculature extravasation, tissue accumulation, deep penetration, cellular internalization, lysosome escape, intracellular efflux, and nuclear targeting) for highly efficient theranostics of different diseases, including cancer, neurodegeneration, myocardial infarction, inflammation, and infection. Among them, smart nanoplatforms with endogenous (pH, enzyme, mRNA, redox, hypoxia, $^1O_2$, ATP, and intracellular mechanical pressure) and exogenous (light, US, PA shockwave, thermal,

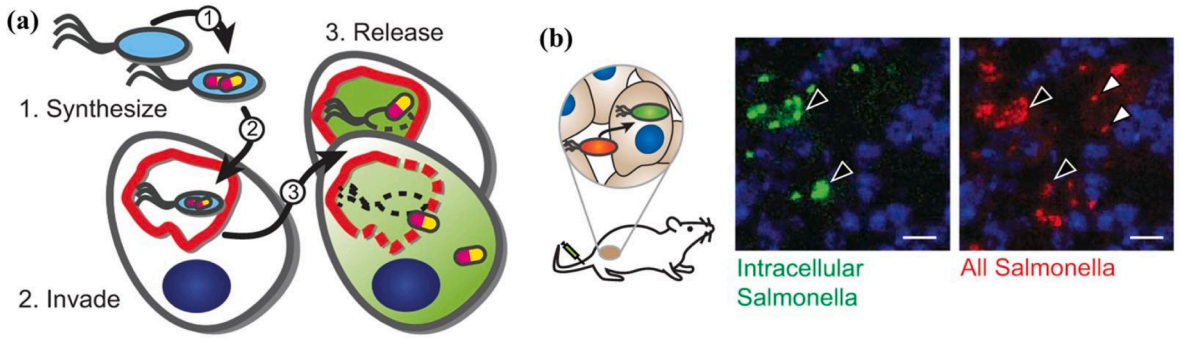

Fig. 46. (a) Schematic illustration of genetic engineering of bacterial vectors. (1) Production of protein drug in bacteria; (2) Active invasion of cancer cells; (3) Release of drug. (b) After injection of intracellular-reporting Salmonella, more bacteria (red) are intracellular (green, black arrows) than extracellular (white arrows). Reprinted with permission from 569. Copyright 2021, Springer Nature.

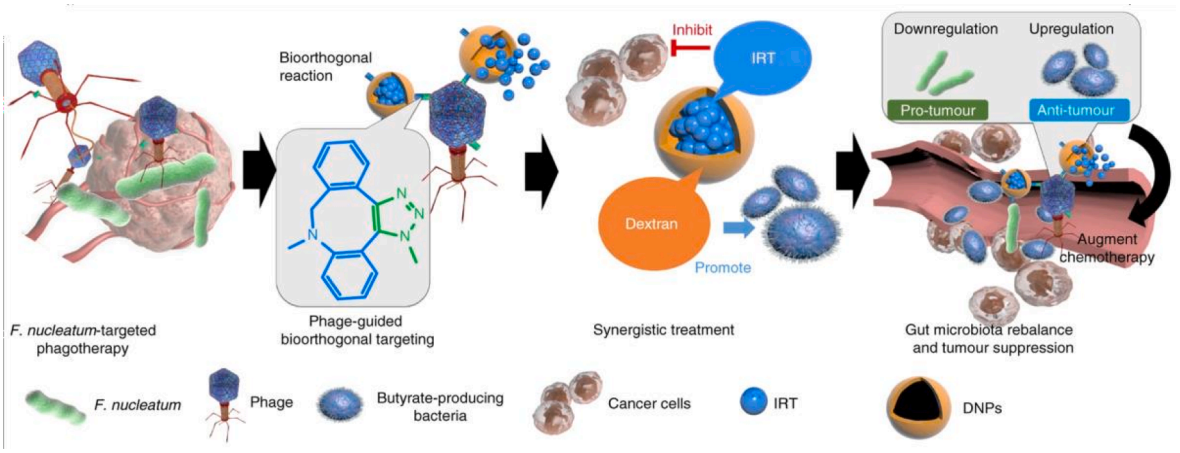

Fig. 47. Schematic illustration of phage-guided hybrid nanocarrier for enhanced chemotherapy efficacy of colorectal cancer by modulating gut microbiota. Reprinted with permission from 578. Copyright 2019, Springer Nature.

and specific additives) responsiveness were constructed. On the basis of these massive research works, such a general "*step-by-step*" design principle can be highlighted for smart nanoplatforms to overcome the biological barriers [578]: (1) Draw a comprehensive background knowledge of the target lesion or disease and clarify one or more critical features (e.g. macro- or microstructure abnormity and genetic mutation) as the guideline for the design of nanoplatforms. (2) Take specific size, shape and/or charge control or transformation strategies of nanoplatforms according to the chosen features of the target diseases. (3) Flexible ulitization of endogenous and exogenous components as constructing blocks or stimulus to incorporate the nanoplatforms with targeting, immune escaping and/or responsive functionalities. (4) Take careful consideration of the balance between safety and functionality and design nanoplatforms with viable biocompatibility for barrier-crossing.

Despite the recent progresses achieved, these challenges that remain need to be addressed before the clinical application of these smart NPs. Firstly, the *in vivo* safety of smart NPs, containing biodegradability, tissue biodistribution, metabolism, and long-term effects need to be evaluated in a standardized manner. For achieving higher requirement of precise and personalized medicine, the novel multistage-responsive NPs should be designed to combine multiple strategies simultaneously, to systematically overcome all barriers *in vivo*. Likewise, the increasingly complex composition and synthetic process of these smart NPs have obviously limited their clinical translation. To promote the substantial progress of smart NPs in clinical practice, the smart NPs should be as simplified as possible under the premise of ensuring efficient Theranostics As a typical, the simplest composition-assisted exogenous stimulation technology (e.g., NIR laser or US) for crossing versatile barriers *in vivo* and evaluating theranostic efficiency should be explored.

Secondly, the mechanical properties of NPs have emerged as a novel key attribute for cargoes delivery *in vivo*. However, in revealing the impact of mechanical properties on targeting delivery, it is an urgent issue to separate mechanical properties as a single variable with all other physicochemical properties. Moreover, the smart NPs with varied stiffness and soft deformation should be rationally designed in response to different stresses in versatile tissues. Additionally, in very recent work, Chan *et al.* [579] presented an important dose threshold principle for predictable and significant delivery. When the dose of NPs is higher than the threshold (1 trillion NPs in mice), it will lead to the overwhelmed Kupffer cell uptake rates, nonlinearly decreased liver clearance, prolonged circulation and increased tumor delivery. Thusly, the comprehensive factors of smart NPs, including surface conversion, size translation, adjustable softness, and does threshold, should be systematically considered in barriers overcoming and NPs delivery *in vivo*.

Thirdly, these smart NPs with stimuli-responsive charge conversion, size switching, soft deformation, and controllable release have been obtained, but individual biomarkers are rarely unique to specific lesion regions, resulting in suboptimal selectivity and undesirable accuracy. Moreover, many biomarkers (e.g., pH, enzyme, redox, or oxygen) dynamically change during disease progression, and also coexist in normal tissues, potentially hindering theranostics in specific diseases. Therefore, some more accurate biomarkers (e.g., mRNA) should be discovered to precisely and effectively trigger the characteristic change of smart NPs [580,581]. Excitingly, in recent years, the concept of logic gates (i.e., YES/OR/AND logic outputs) was proposed to impart the smart NPs with precise multiple responsiveness in biomedical fields [582,583]. The integration of multiple endogenous or/and exogenous-responsive groups within one NPs should be performed for the programmed trigger their controlled behaviors, which is a daunting challenge for single-stimulus responsive NPs.

Fourth, some studies [6,87] have evidenced that almost all NPs were transported into solid tumors by the active transportation of transcytosis rather than EPR effect in vasculature extravasation. Research on the stimuli-activated transendothelial transport is still in its infancy and faces many challenges. Currently, only the strategy of GGT-triggered charge reversal is developed for enhanced therapeutic efficacy by the transendothelial and transcellular transport. More strategies and various responsiveness should be explored to verify and promote the application of active transportation.

Finally, for bioinspired systems, the use of a single type of cell membranes as the coating may limit the diversity of functions. Development of novel type of cell or bacterial membranes, or mixing of multiple types of cell membranes should be employed as coating components in the future. By introducing comprehensive biological moieties and functions, such as antibodies, enzymes, and

DNA/RNA, the multifunctional biomimetic NPs will be designed for improving the synergistic performance in biomedical applications. Moreover, living cells or bacterial or phages as carriers for nanomedicine can bring extra benefits for NP transportation to the disease areas. In recent years, tumor immunotherapy, which triggers effective antitumor responses *via* the regulation or alteration of the immune system, has emerged as one novel powerful strategy to fight tumor and inhibit metastasis. The cancer vaccine for tumor immunotherapy, that can radically change the cancer therapy landscape, was developed. However, due to the endosomal trapping and low immunogenicity of tumor antigens, developing of highly efficient antitumor vaccines-especially personalized vaccines that can potently induce T cell priming in humans-is still a challenge. Through combining these strategies, the cancer vaccine is expected to further enhance immune response *in vivo*, improving anti-tumor immunity without substantial systemic toxicity. Once such issues are resolved, the revolutionary change in nanomedicine will appear to achieve efficient delivery to targeted region by overcoming a series of complicated biological barriers *in vivo*, which is expected to be extendable for highly effective disease theranostics in clinical translation in the near future.

Declaration of Competing Interest

The authors declare that they have no known competing financial interests or personal relationships that could have appeared to influence the work reported in this paper.

Data availability

No data was used for the research described in the article.

Acknowledgements

X. Li and Y. Gao contributed equally to this work. This work was financially supported by the Sino-German Center for Research Promotion (GZ1505), DFG (SFB 985, Functional Microgels and Microgel Systems), National Natural Science Foundation of China (81761148028), Natural Science Foundation of Zhejiang Province (LTGY23B040001), Science and Technology Commission of Shanghai Municipality (19XD1400100), and China Scholarship Council (for X. Li).

References

[1] Martin JD, Cabral H, Stylianopoulos T, Jain RK. Improving cancer immunotherapy using nanomedicines: progress, opportunities and challenges. Nat Rev Clin Oncol 2020;17:251–66.
[2] van der Meel R, Sulheim E, Shi Y, Kiessling F, Mulder WJM, Lammers T. Smart cancer nanomedicine. Nat Nanotechnol 2019;14:1007–17.
[3] Binderup T, Duivenvoorden R, Fay F, van Leent MMT, Malkus J, Baxter S, et al. Imaging-assisted nanoimmunotherapy for atherosclerosis in multiple species. Sci Transl Med 2019;11:eaaw7736.
[4] Hamadani CM, Goetz MJ, Mitragotri S, Tanner EEL. Protein-avoidant ionic liquid (PAIL)–coated nanoparticles to increase bloodstream circulation and drive biodistribution. Sci Adv 2020;6:eabd7563.
[5] Wilhelm S, Tavares AJ, Dai Q, Ohta S, Audet J, Dvorak HF, et al. Analysis of nanoparticle delivery to tumours. Nat Rev Mater 2016;1:16014.
[6] Pandit S, Dutta D, Nie S. Active transcytosis and new opportunities for cancer nanomedicine. Nat Mater 2020;19:478–80.
[7] Li X, Sun H, Li H, Hu C, Luo Y, Shi X, et al. Multi-responsive biodegradable cationic nanogels for highly efficient treatment of tumors. Adv Funct Mater 2021; 31:2100227.
[8] Xing L, Li X, Xing Z, Li F, Shen M, Wang H, et al. Silica/gold nanoplatform combined with a thermosensitive gel for imaging-guided interventional therapy in PDX of pancreatic cancer. Chem Eng J 2020;382:122949.
[9] Parodi A, Quattrocchi N, van de Ven AL, Chiappini C, Evangelopoulos M, Martinez JO, et al. Synthetic nanoparticles functionalized with biomimetic leukocyte membranes possess cell-like functions. Nat Nanotechnol 2013;8:61–8.
[10] Ben-Akiva E, Meyer RA, Yu H, Smith JT, Pardoll DM, Green JJ. Biomimetic anisotropic polymeric nanoparticles coated with red blood cell membranes for enhanced circulation and toxin removal. Sci Adv 2020;6:eaay9035.
[11] Xue X, Huang Y, Bo R, Jia B, Wu H, Yuan Y, et al. Trojan Horse nanotheranostics with dual transformability and multifunctionality for highly effective cancer treatment. Nat Commun 2018;9:3653.
[12] Locard-Paulet M, Lim L, Veluscek G, McMahon K, Sinclair J, van Weverwijk A, et al. Phosphoproteomic analysis of interacting tumor and endothelial cells identifies regulatory mechanisms of transendothelial migration. Sci Signal 2016;9:ra15.
[13] Zhou C, Long M, Qin Y, Sun X, Zheng J. Luminescent gold nanoparticles with efficient renal clearance. Angew Chem Int Ed 2011;50:3168–72.
[14] Gnach A, Lipinski T, Bednarkiewicz A, Rybka J, Capobianco JA. Upconverting nanoparticles: assessing the toxicity. Chem Soc Rev 2015;44:1561–84.
[15] Jang HL, Sengupta S. Transcellular transfer of nanomedicine. Nat Nanotechnol 2019;14:731–2.
[16] Rajora MA, Lou JWH, Zheng G. Advancing porphyrin's biomedical utility via supramolecular chemistry. Chem Soc Rev 2017;46:6433–69.
[17] Mitragotri S, Anderson DG, Chen X, Chow EK, Ho D, Kabanov AV, et al. Accelerating the translation of nanomaterials in biomedicine. ACS Nano 2015;9: 6644–54.
[18] Jin Q, Deng Y, Chen X, Ji J. Rational design of cancer nanomedicine for simultaneous stealth surface and enhanced cellular uptake. ACS Nano 2019;13:954–77.
[19] Luo Y, Huang L, Yang Y, Zhuang X, Hu S, Ju H, et al. A programmed nanoparticle with self-adapting for accurate cancer cell eradication and therapeutic self-reporting. Theranostics 2017;7:1245–56.
[20] Xiong H, Wang Z, Wang C, Yao J. Correction to "Transforming Complexity to Simplicity: Protein-Like Nanotransformer for Improving Tumor Drug Delivery Programmatically". Nano Lett 2020;20:4060.
[21] Dong Z, Hao Y, Li Q, Yang Z, Zhu Y, Liu Z, et al. Metal-polyphenol-network coated CaCO3 as pH-responsive nanocarriers to enable effective intratumoral penetration and reversal of multidrug resistance for augmented cancer treatments. Nano Res 2020;13:3057–67.
[22] Zhu H, Cao G, Fu Y, Fang C, Chu Q, Li X, et al. ATP-responsive hollow nanocapsules for DOX/GOx delivery to enable tumor inhibition with suppressed P-glycoprotein. Nano Res 2021;14:222–31.
[23] Fu X, Shi Y, Qi T, Qiu S, Huang Y, Zhao X, et al. Precise design strategies of nanomedicine for improving cancer therapeutic efficacy using subcellular targeting. Signal Transduct Target Ther 2020;5:262.
[24] Ding Y, Sun Z, Tong Z, Zhang S, Min J, Xu Q, et al. Tumor microenvironment-responsive multifunctional peptide coated ultrasmall gold nanoparticles and their application in cancer radiotherapy. Theranostics 2020;10:5195–208.

[25] Huo D, Jiang X, Hu Y. Recent advances in nanostrategies capable of overcoming biological barriers for tumor management. Adv Mater 2020;32:1904337.
[26] Li X, Xing L, Hu Y, Xiong Z, Wang R, Xu X, et al. An RGD-modified hollow silica@Au core/shell nanoplatform for tumor combination therapy. Acta Biomater 2017;62:273–83.
[27] Li H, Mergel O, Jain P, Li X, Peng H, Rahimi K, et al. Electroactive and degradable supramolecular microgels. Soft Matter 2019;15:8589–602.
[28] Li Z, Shan X, Chen Z, Gao N, Zeng W, Zeng X, et al. Applications of surface modification technologies in nanomedicine for deep tumor penetration. Adv Sci 2021;8:2002589.
[29] Tietjen GT, Hosgood SA, DiRito J, Cui J, Deep D, Song E, et al. Nanoparticle targeting to the endothelium during normothermic machine perfusion of human kidneys. Sci Transl Med 2017;9:eaam6764.
[30] Ryu JH, Yoon HY, Sun I-C, Kwon IC, Kim K. Tumor-targeting glycol chitosan nanoparticles for cancer heterogeneity. Adv Mater 2020;32:2002197.
[31] Jiang D, Rosenkrans ZT, Ni D, Lin J, Huang P, Cai W. Nanomedicines for renal management: from imaging to treatment. Acc Chem Res 2020;53:1869–80.
[32] Gao L, Feng L, Sauer DF, Wittwer M, Hu Y, Schiffels J, et al. Engineered living hydrogels for robust biocatalysis in pure organic solvents. Cell Rep Phys Sci 2022;3:101054.
[33] Li X, Ouyang Z, Li H, Hu C, Saha P, Xing L, et al. Dendrimer-decorated nanogels: efficient nanocarriers for biodistribution in vivo and chemotherapy of ovarian carcinoma. Bioact Mater 2021;6:3244–53.
[34] Li X, Xiong Z, Xu X, Luo Y, Peng C, Shen M, et al. Tc-99m-labeled multifunctional low-generation dendrimer-entrapped gold nanoparticles for targeted SPECT/CT dual-mode imaging of tumors. ACS Appl Mater Interfaces 2016;8:19883–91.
[35] Li X, Kong L, Hu W, Zhang C, Pich A, Shi X, et al. Safe and efficient 2D molybdenum disulfide platform for cooperative imaging-guided photothermal-selective chemotherapy: a preclinical study. J Adv Res 2022;37:255–66.
[36] Li W, Qiu J, Li X-L, Aday S, Zhang J, Conley G, et al. BBB pathophysiology-independent delivery of siRNA in traumatic brain injury. Sci Adv 2021;7:eabd6889.
[37] Furtado D, Bjornmalm M, Ayton S, Bush AI, Kempe K, Caruso F. Overcoming the blood-brain barrier: the role of nanomaterials in treating neurological diseases. Adv Mater 2018;30:1801362.
[38] Zhao Y, Tian S, Zhang J, Cheng X, Huang W, Cao G, et al. Regulation of neuroinflammation with GLP-1 receptor targeting nanostructures to alleviate Alzheimer's symptoms in the disease models. Nano Today 2022;44:101457.
[39] Sunil V, Mozhi A, Zhan W, Teoh JH, Ghode PB, Thakor VN, et al. In-situ vaccination using dual responsive organelle targeted nanoreactors. Biomaterials 2022;290:121843.
[40] Sun C-Y, Liu Y, Du J-Z, Cao Z-T, Xu C-F, Wang J. Facile generation of tumor-pH-labile linkage-bridged block copolymers for chemotherapeutic delivery. Angew Chem Int Ed 2016;55:1010–4.
[41] Blackman LD, Gunatillake PA, Cass P, Locock KES. An introduction to zwitterionic polymer behavior and applications in solution and at surfaces. Chem Soc Rev 2019;48:757–70.
[42] Cabral H, Matsumoto Y, Mizuno K, Chen Q, Murakami M, Kimura M, et al. Accumulation of sub-100 nm polymeric micelles in poorly permeable tumours depends on size. Nat Nanotechnol 2011;6:815–23.
[43] Zhang X, Chen X, Song J, Zhang J, Ren X, Zhao Y. Size-transformable nanostructures: from design to biomedical applications. Adv Mater 2020;32:2003752.
[44] Sun T, Zhang YS, Pang B, Hyun DC, Yang M, Xia Y. Engineered nanoparticles for drug delivery in cancer therapy. Angew Chem Int Ed 2014;53:12320–64.
[45] Li L, Xing H, Zhang J, Lu Y. Functional DNA molecules enable selective and stimuli-responsive nanoparticles for biomedical applications. Acc Chem Res 2019;52:2415–26.
[46] Chen H, Zhang W, Zhu G, Xie J, Chen X. Rethinking cancer nanotheranostics. Nat Rev Mater 2017;2:17024.
[47] Zhang Y-R, Lin R, Li H-J, He W-l, Du J-Z, Wang J. Strategies to improve tumor penetration of nanomedicines through nanoparticle design. WIREs Nanomed Nanobiotechnol 2019;11:e1519.
[48] Li X, Lu Y, Hu Y. A wireless and battery-free DNA hydrogel biosensor for wound infection monitoring. Matter 2022;5:2473–5.
[49] Cao X, Luo Q, Song F, Liu G, Chen S, Li Y, et al. Effects of oxidative torrefaction on the physicochemical properties and pyrolysis products of hemicellulose in bamboo processing residues. Ind Crop Prod 2023;191:115986.
[50] He C, Hu Y, Yin L, Tang C, Yin C. Effects of particle size and surface charge on cellular uptake and biodistribution of polymeric nanoparticles. Biomaterials 2010;31:3657–66.
[51] Wang H-X, Zuo Z-Q, Du J-Z, Wang Y-C, Sun R, Cao Z-T, et al. Surface charge critically affects tumor penetration and therapeutic efficacy of cancer nanomedicines. Nano Today 2016;11:133–44.
[52] Liang S, Yang X-Z, Du X-J, Wang H-X, Li H-J, Liu W-W, et al. Optimizing the size of micellar nanoparticles for efficient siRNA delivery. Adv Funct Mater 2015;25:4778–87.
[53] Chen J, Ding J, Wang Y, Cheng J, Ji S, Zhuang X, et al. Sequentially responsive shell-stacked nanoparticles for deep penetration into solid tumors. Adv Mater 2017;29:1701170.
[54] Gref R, Domb A, Quellec P, Blunk T, Müller RH, Verbavatz JM, et al. The controlled intravenous delivery of drugs using PEG-coated sterically stabilized nanospheres. Adv Drug Deliv Rev 2012;64:316–26.
[55] Zhou H, Fan Z, Li PY, Deng J, Arhontoulis DC, Li CY, et al. Dense and dynamic polyethylene glycol shells cloak nanoparticles from uptake by liver endothelial cells for long blood circulation. ACS Nano 2018;12:10130–41.
[56] Dufort S, Sancey L, Coll J-L. Physico-chemical parameters that govern nanoparticles fate also dictate rules for their molecular evolution. Adv Drug Deliv Rev 2012;64:179–89.
[57] Cong Z, Zhang L, Ma S-Q, Lam KS, Yang F-F, Liao Y-H. Size-transformable hyaluronan stacked self-assembling peptide nanoparticles for improved transcellular tumor penetration and photo-chemo combination therapy. ACS Nano 2020;14:1958–70.
[58] Nia HT, Munn LL, Jain RK. Physical traits of cancer. Science 2020;370:eaaz0868.
[59] Miao L, Lin CM, Huang L. Stromal barriers and strategies for the delivery of nanomedicine to desmoplastic tumors. J Control Release 2015;219:192–204.
[60] Fang T, Zhang J, Zuo T, Wu G, Xu Y, Yang Y, et al. Chemo-photothermal combination cancer therapy with ROS scavenging, extracellular matrix depletion, and tumor immune activation by telmisartan and diselenide-paclitaxel prodrug loaded nanoparticles. ACS Appl Mater Interfaces 2020;12:31292–308.
[61] Chen Y-Q, Kuo J-C, Wei M-T, Wu M-C, Yang M-H, Chiou A. Fibroblast promotes head and neck squamous cell carcinoma cell invasion through mechanical barriers in 3D collagen microenvironments. ACS Appl Bio Mater 2020;3:6419–29.
[62] Zhang B, Hu Y, Pang Z. Modulating the tumor microenvironment to enhance tumor nanomedicine delivery. Front Pharmacol 2017;8:952.
[63] Ho LWC, Liu Y, Han R, Bai Q, Choi CHJ. Nano-cell interactions of non-cationic bionanomaterials. Acc Chem Res 2019;52:1519–30.
[64] Kinnear C, Moore TL, Rodriguez-Lorenzo L, Rothen-Rutishauser B, Petri-Fink A. Form follows function: nanoparticle shape and its implications for nanomedicine. Chem Rev 2017;117:11476–521.
[65] Lu S, Li X, Zhang J, Peng C, Shen M, Shi X. Dendrimer-stabilized gold nanoflowers embedded with ultrasmall iron oxide nanoparticles for multimode imaging-guided combination therapy of tumors. Adv Sci 2018;5:1801612.
[66] Xu J, Wang X, Yin H, Cao X, Hu Q, Lv W, et al. Sequentially site-specific delivery of thrombolytics and neuroprotectant for enhanced treatment of ischemic stroke. ACS Nano 2019;13:8577–88.
[67] Zhang Y, Xu C, Yang X, Pu K. Photoactivatable protherapeutic nanomedicine for cancer. Adv Mater 2020;32:2002661.
[68] Cong TD, Wang Z, Hu M, Han Q, Xing B. Extraspecific manifestation of nanoheater's position effect on distinctive cellular photothermal responses. ACS Nano 2020;14:5836–44.
[69] Li Y, Ding J, Xu X, Shi R, Saw PE, Wang J, et al. Dual hypoxia-targeting rnai nanomedicine for precision cancer therapy. Nano Lett 2020;20:4857–63.
[70] Xiang H, Feng W, Chen Y. Single-atom catalysts in catalytic biomedicine. Adv Mater 2020;32:1905994.
[71] Li X, Sun H, Lu Y, Xing L. Radiotherapy-triggered prodrug activation: a new era in precise chemotherapy. Med 2022;3:600–2.
[72] Yoo J-W, Irvine DJ, Discher DE, Mitragotri S. Bio-inspired, bioengineered and biomimetic drug delivery carriers. Nat Rev Drug Discov 2011;10:521–35.

[73] Merkel TJ, Jones SW, Herlihy KP, Kersey FR, Shields AR, Napier M, et al. Using mechanobiological mimicry of red blood cells to extend circulation times of hydrogel microparticles. Proc Natl Acad Sci 2011;108:586–91.
[74] Li X, Lu Y, Kong L, Shi X, Pich A. Leukocyte-nanomedicine system for targeted delivery and precise theragnostics. Chem 2022;8:2591–3.
[75] Yu H, Yang Z, Li F, Xu L, Sun Y. Cell-mediated targeting drugs delivery systems. Drug Deliv 2020;27:1425–37.
[76] Zhang Z, Wang H, Tan T, Li J, Wang Z, Li Y. Rational design of nanoparticles with deep tumor penetration for effective treatment of tumor metastasis. Adv Funct Mater 2018;28:1801840.
[77] Zhang F, Zhuang J, Li Z, Gong H, de Avila B-E-F, Duan Y, et al. Nanoparticle-modified microrobots for in vivo antibiotic delivery to treat acute bacterial pneumonia. Nat Mater 2022;21:1324–32.
[78] Kreitz J, Friedrich MJJ, Guru A, Lash B, Saito M, Macrae RKK, et al. Programmable protein delivery with a bacterial contractile injection system. Nature 2023;616:357–64.
[79] Wang S, Huang P, Chen X. Hierarchical targeting strategy for enhanced tumor tissue accumulation/retention and cellular internalization. Adv Mater 2016;28:7340–64.
[80] Du J-Z, Li H-J, Wang J. Tumor-acidity-cleavable maleic acid amide (TACMAA): a powerful tool for designing smart nanoparticles to overcome delivery barriers in cancer nanomedicine. Acc Chem Res 2018;51:2848–56.
[81] Feng L, Dong Z, Tao D, Zhang Y, Liu Z. The acidic tumor microenvironment: a target for smart cancer nano-theranostics. Natl Sci Rev 2017;5:269–86.
[82] Lu Y, Gao Y, Yang H, Hu Y, Li X. Nanomedicine-boosting icaritin-based immunotherapy of advanced hepatocellular carcinoma. Mil Med Res 2022;9:69.
[83] Prabhakar U, Maeda H, Jain RK, Sevick-Muraca EM, Zamboni W, Farokhzad OC, et al. Challenges and key considerations of the enhanced permeability and retention effect for nanomedicine drug delivery in oncology. Cancer Res 2013;73:2412–7.
[84] Hubbell JA, Chilkoti A. Nanomaterials for drug delivery. Science 2012;337:303–5.
[85] Peng F, Setyawati MI, Tee JK, Ding X, Wang J, Nga ME, et al. Nanoparticles promote in vivo breast cancer cell intravasation and extravasation by inducing endothelial leakiness. Nat Nanotechnol 2019;14:279–86.
[86] Lu Y, Luo Q, Jia X, Tam JP, Yang H, Shen Y, et al. Multidisciplinary strategies to enhance therapeutic effects of flavonoids from Epimedii Folium: Integration of herbal medicine, enzyme engineering, and nanotechnology. J Pharm Anal 2023;13:239–54.
[87] Sindhwani S, Syed AM, Ngai J, Kingston BR, Maiorino L, Rothschild J, et al. The entry of nanoparticles into solid tumours. Nat Mater 2020;19:566–75.
[88] Zhou Q, Shao S, Wang J, Xu C, Xiang J, Piao Y, et al. Enzyme-activatable polymer–drug conjugate augments tumour penetration and treatment efficacy. Nat Nanotechnol 2019;14:799–809.
[89] Zhang W, Zhao Q, Yuan J. Porous polyelectrolytes: the interplay of charge and pores for new functionalities. Angew Chem Int Ed 2018;57:6754–73.
[90] Liu J, Wu Y, Fu C, Li B, Li L, Zhang R, et al. Charge reversion simultaneously enhances tumor accumulation and cell uptake of layered double hydroxide nanohybrids for effective imaging and therapy. Small 2020;16:2002115.
[91] Sivaram AJ, Wardiana A, Alcantara S, Sonderegger SE, Fletcher NL, Houston ZH, et al. Controlling the biological fate of micellar nanoparticles: balancing stealth and targeting. ACS Nano 2020;14:13739–53.
[92] Vu MN, Kelly HG, Wheatley AK, Peng S, Pilkington EH, Veldhuis NA, et al. Cellular interactions of liposomes and PISA nanoparticles during human blood flow in a microvascular network. Small 2020;16:2002861.
[93] Li H, Li X, Jain P, Peng H, Rahimi K, Singh S, et al. Dual-degradable biohybrid microgels by direct cross-linking of chitosan and dextran using azide-alkyne cycloaddition. Biomacromolecules 2020;21:4933–44.
[94] Yang Y, Xu L, Zhu W, Feng L, Liu J, Chen Q, et al. One-pot synthesis of pH-responsive charge-switchable PEGylated nanoscale coordination polymers for improved cancer therapy. Biomaterials 2018;156:121–33.
[95] Syvänen S, Edén D, Sehlin D. Cationization increases brain distribution of an amyloid-beta protofibril selective F(ab')2 fragment. Biochem Biophys Res Commun 2017;493:120–5.
[96] Miura S, Suzuki H, Bae YH. A multilayered cell culture model for transport study in solid tumors: evaluation of tissue penetration of polyethyleneimine based cationic micelles. Nano Today 2014;9:695–704.
[97] Yu H, Li J-M, Deng K, Zhou W, Wang C-X, Wang Q, et al. Tumor acidity activated triphenylphosphonium-based mitochondrial targeting nanocarriers for overcoming drug resistance of cancer therapy. Theranostics 2019;9:7033–50.
[98] Ke W, Yin W, Zha Z, Mukerabigwi JF, Chen W, Wang Y, et al. A robust strategy for preparation of sequential stimuli-responsive block copolymer prodrugs via thiolactone chemistry to overcome multiple anticancer drug delivery barriers. Biomaterials 2018;154:261–74.
[99] Li X, Hetjens L, Wolter N, Li H, Shi X, Pich A. Charge-reversible and biodegradable chitosan-based microgels for lysozyme-triggered release of vancomycin. J Adv Res 2023;43:87–96.
[100] Lee Y, Ishii T, Kim HJ, Nishiyama N, Hayakawa Y, Itaka K, et al. Efficient delivery of bioactive antibodies into the cytoplasm of living cells by charge-conversional polyion complex micelles. Angew Chem Int Ed 2010;49:2552–5.
[101] Zhang C, Yan L, Wang X, Zhu S, Chen C, Gu Z, et al. Progress, challenges, and future of nanomedicine. Nano Today 2020;35:101008.
[102] Du Y, Li Y, Li X, Jia C, Wang L, Wang Y, et al. Sequential enzyme activation of a "Pro-Staramine"-based nanomedicine to target tumor mitochondria. Adv Funct Mater 2020;30:1904697.
[103] Gu Z, Dang TT, Ma M, Tang BC, Cheng H, Jiang S, et al. Glucose-responsive microgels integrated with enzyme nanocapsules for closed-loop insulin delivery. ACS Nano 2013;7:6758–66.
[104] Dreaden EC, Morton SW, Shopsowitz KE, Choi J-H, Deng ZJ, Cho N-J, et al. Bimodal tumor-targeting from microenvironment responsive hyaluronan layer-by-layer (LbL) nanoparticles. ACS Nano 2014;8:8374–82.
[105] Hung C-C, Huang W-C, Lin Y-W, Yu T-W, Chen H-H, Lin S-C, et al. Active tumor permeation and uptake of surface charge-switchable theranostic nanoparticles for imaging-guided photothermal/chemo combinatorial therapy. Theranostics 2016;6:302–17.
[106] Danhier F, Feron O, Preat V. To exploit the tumor microenvironment: Passive and active tumor targeting of nanocarriers for anti-cancer drug delivery. J Control Release 2010;148:135–46.
[107] Wong PT, Choi SK. Mechanisms of drug release in nanotherapeutic delivery systems. Chem Rev 2015;115:3388–432.
[108] Du JZ, Lane LA, Nie SM. Stimuli-responsive nanoparticles for targeting the tumor microenvironment. J Control Release 2015;219:205–14.
[109] Li B, Gu Z, Kurniawan N, Chen WY, Xu ZP. Manganese-based layered double hydroxide nanoparticles as a T-1-MRI contrast agent with ultrasensitive pH response and high relaxivity. Adv Mater 2017;29.
[110] Guo Y, Wu Z, Shen S, Guo R, Wang J, Wang W, et al. Nanomedicines reveal how PBOV1 promotes hepatocellular carcinoma for effective gene therapy. Nat Commun 2018;9:3430.
[111] Keefe AJ, Jiang SY. Poly(zwitterionic)protein conjugates offer increased stability without sacrificing binding affinity or bioactivity. Nat Chem 2012;4:60–4.
[112] Amoozgar Z, Yeo Y. Recent advances in stealth coating of nanoparticle drug delivery systems. Wiley Interdiscip Rev Nanomed Nanobiotechnol 2012;4:219–33.
[113] Yuan YY, Mao CQ, Du XJ, Du JZ, Wang F, Wang J. Surface charge switchable nanoparticles based on zwitterionic polymer for enhanced drug delivery to tumor. Adv Mater 2012;24:5476–80.
[114] Du JZ, Mao CQ, Yuan YY, Yang XZ, Wang J. Tumor extracellular acidity-activated nanoparticles as drug delivery systems for enhanced cancer therapy. Biotechnol Adv 2014;32:789–803.
[115] Maier K, Wagner E. Acid-labile traceless click linker for protein transduction. J Am Chem Soc 2012;134:10169–73.
[116] Takemoto H, Miyata K, Hattori S, Ishii T, Suma T, Uchida S, et al. Acidic pH-responsive siRNA conjugate for reversible carrier stability and accelerated endosomal escape with reduced IFN alpha-associated immune response. Angew Chem-Int Ed 2013;52:6218–21.
[117] Murakami M, Cabral H, Matsumoto Y, Wu SR, Kano MR, Yamori T, et al. Improving drug potency and efficacy by nanocarrier-mediated subcellular targeting. Sci Transl Med 2011;3:64ra2.
[118] Ganta S, Devalapally H, Shahiwala A, Amiji M. A review of stimuli-responsive nanocarriers for drug and gene delivery. J Control Release 2008;126:187–204.
[119] Binauld S, Stenzel MH. Acid-degradable polymers for drug delivery: a decade of innovation. Chem Commun 2013;49:2082–102.

[120] Du JZ, Du XJ, Mao CQ, Wang J. Tailor-made dual pH-sensitive polymer-doxorubicin nanoparticles for efficient anticancer drug delivery. J Am Chem Soc 2011; 133:17560–3.
[121] Peng L, You M, Wu C, Han D, Öçsoy I, Chen T, et al. Reversible phase transfer of nanoparticles based on photoswitchable host-guest chemistry. ACS Nano 2014; 8:2555–61.
[122] Yuan W, Shen J, Guo W. Thermoresponse and light-induced reversible self-assembly/disassembly of supra-amphiphiles from azobenzene- and β-cyclodextrin-containing copolymers. Mater Lett 2014;134:259–62.
[123] Sánchez-Iglesias A, Grzelczak M, Altantzis T, Goris B, Pérez-Juste J, Bals S, et al. Hydrophobic interactions modulate self-assembly of nanoparticles. ACS Nano 2012;6:11059–65.
[124] Akagi T, Watanabe K, Kim H, Akashi M. Stabilization of polyion complex nanoparticles composed of poly(amino acid) using hydrophobic interactions. Langmuir 2010;26:2406–13.
[125] Dupont J, Scholten JD. On the structural and surface properties of transition-metal nanoparticles in ionic liquids. Chem Soc Rev 2010;39:1780–804.
[126] Altintas O, Barner-Kowollik C. Single chain folding of synthetic polymers by covalent and non-covalent interactions: current status and future perspectives. Macromol Rapid Commun 2012;33:958–71.
[127] He C, Liu D, Lin W. Nanomedicine applications of hybrid nanomaterials built from metal-ligand coordination bonds: nanoscale metal-organic frameworks and nanoscale coordination polymers. Chem Rev 2015;115:11079–108.
[128] Wang S, McGuirk CM, d'Aquino A, Mason JA, Mirkin CA. Metal-organic framework nanoparticles. Adv Mater 2018;30:1800202.
[129] Huang J, Fan J, Cao L, Xu C, Chen Y. A novel strategy to construct co-continuous PLA/NBR thermoplastic vulcanizates: Metal-ligand coordination-induced dynamic vulcanization, balanced stiffness-toughness and shape memory effect. Chem Eng J 2020;385:123828.
[130] Wang CR, Chen XF, Yao XM, Chen L, Chen XS. Dual acid-responsive supramolecular nanoparticles as new anticancer drug delivery systems. Biomater Sci 2016; 4:104–14.
[131] Hu DF, Deng YY, Jia F, Jin Q, Ji J. Surface charge switchable supramolecular nanocarriers for nitric oxide synergistic photodynamic eradication of biofilms. ACS Nano 2020;14:347–59.
[132] Sun CY, Shen S, Xu CF, Li HJ, Liu Y, Cao ZT, et al. Tumor acidity-sensitive polymeric vector for active targeted siRNA delivery. J Am Chem Soc 2015;137: 15217–24.
[133] Poon Z, Chang D, Zhao XY, Hammond PT. Layer-by-layer nanoparticles with a pH-sheddable layer for in vivo targeting of tumor hypoxia. ACS Nano 2011;5: 4284–92.
[134] Li M, Ning Y, Chen J, Duan X, Song N, Ding D, et al. Proline isomerization-regulated tumor microenvironment-adaptable self-assembly of peptides for enhanced therapeutic efficacy. Nano Lett 2019;19:7965–76.
[135] Zhang CY, Gao J, Wang Z. Bioresponsive nanoparticles targeted to infectious microenvironments for sepsis management. Adv Mater 2018;30:1803618.
[136] Wang X, Yao C, Zhang G, Liu S. Regulating vesicle bilayer permeability and selectivity via stimuli-triggered polymersome-to-PICsome transition. Nat Commun 2020;11:1524.
[137] Mable CJ, Canton I, Mykhaylyk OO, Ustbas Gul B, Chambon P, Themistou E, et al. Targeting triple-negative breast cancer cells using Dengue virus-mimicking pH-responsive framboidal triblock copolymer vesicles. Chem Sci 2019;10:4811–21.
[138] Aouameur D, Cheng H, Opoku-Damoah Y, Sun B, Dong Q, Han Y, et al. Stimuli-responsive gel-micelles with flexible modulation of drug release for maximized antitumor efficacy. Nano Res 2018;11:4245–64.
[139] He H, Ostwaldt J-E, Hirschhäuser C, Schmuck C, Niemeyer J. Dual pH-induced reversible self-assembly of gold nanoparticles by surface functionalization with zwitterionic ligands. Small 2020;16:2001044.
[140] Jana P, Ehlers M, Zellermann E, Samanta K, Schmuck C. pH-controlled formation of a stable β-sheet and amyloid-like fibers from an amphiphilic peptide: the importance of a tailor-made binding motif for secondary structure formation. Angew Chem Int Ed 2016;55:15287–91.
[141] Zhang Y, Clausmeyer J, Babakinejad B, López Córdoba A, Ali T, Shevchuk A, et al. Spearhead nanometric field-effect transistor sensors for single-cell analysis. ACS Nano 2016;10:3214–21.
[142] Baroni S, Stefania R, Broche LM, Senn N, Lurie DJ, Ross PJ, et al. A novel class of H-1-MRI contrast agents based on the relaxation enhancement induced on water protons by N-14-containing imidazole moieties. Angew Chem-Int Ed 60:4208–14.
[143] Li Y, Zhao P, Gong T, Wang H, Jiang X, Cheng H, et al. Redox dyshomeostasis strategy for hypoxic tumor therapy based on DNAzyme-loaded electrophilic ZIFs. Angew Chem Int Ed 2020;59:22537–43.
[144] Li Y, Zhang K, Liu P, Chen M, Zhong Y, Ye Q, et al. Encapsulation of plasmid DNA by nanoscale metal-organic frameworks for efficient gene transportation and expression. Adv Mater 2019;31:1901570.
[145] Liu J, Iqbal S, Du X-J, Yuan Y, Yang X, Li H-J, et al. Ultrafast charge-conversional nanocarrier for tumor-acidity-activated targeted drug elivery. Biomater Sci 2018;6:350–5.
[146] Zhu JZ, Xiao TT, Zhang JL, Che HL, Shi YX, Shi XY, et al. Surface-charge-switchable nanoclusters for magnetic resonance imaging-guided and glutathione depletion-enhanced photodynamic therapy. ACS Nano 2020;14:11225–37.
[147] Li X, Li H, Zhang C, Pich A, Xing L, Shi X. Intelligent nanogels with self-adaptive responsiveness for improved tumor drug delivery and augmented chemotherapy. Bioact Mater 2021;6:3473–84.
[148] Xu WJ, Rudov AA, Schroeder R, Portnov IV, Richtering W, Potemkin II, et al. Distribution of ionizable groups in polyampholyte microgels controls interactions with captured proteins: from blockade and "levitation" to accelerated release. Biomacromolecules 2019;20:1578–91.
[149] Mizuhara T, Saha K, Moyano DF, Kim CS, Yan B, Kim YK, et al. Acylsulfonamide-functionalized zwitterionic gold nanoparticles for enhanced cellular uptake at tumor pH. Angew Chem-Int Ed 2015;54:6567–70.
[150] Zhu JY, Zhao LZ, Yang JX, Chen L, Shi JH, Zhao JH, et al. Tc-99m-labeled polyethylenimine-entrapped gold nanoparticles with pH-responsive charge conversion property for enhanced dual mode SPECT/CT imaging of cancer cells. Langmuir 2019;35:13405–12.
[151] Gao A, Chen B, Gao J, Zhou F, Saeed M, Hou B, et al. Sheddable prodrug vesicles combating adaptive immune resistance for improved photodynamic immunotherapy of cancer. Nano Lett 2020;20:353–62.
[152] Zhang R, Liu R, Liu C, Pan L, Qi Y, Cheng J, et al. A pH/ROS dual-responsive and targeting nanotherapy for vascular inflammatory diseases. Biomaterials 2020; 230:119605.
[153] Wu J, Chen J, Feng Y, Zhang S, Lin L, Guo Z, et al. An immune cocktail therapy to realize multiple boosting of the cancer-immunity cycle by combination of drug/gene delivery nanoparticles. Sci Adv 2020;6:eabc7828.
[154] Wang Q, Liu F, Wang L, Xie C, Wu P, Du S, et al. Enhanced and prolonged antitumor effect of salinomycin-loaded gelatinase-responsive nanoparticles via targeted drug delivery and inhibition of cervical cancer stem cells. Int J Nanomed 2020;15:1283–95.
[155] Kinoh H, Quader S, Shibasaki H, Liu X, Maity A, Yamasoba T, et al. Translational nanomedicine boosts anti-PD1 therapy to eradicate orthotopic PTEN-negative glioblastoma. ACS Nano 2020;14:10127–40.
[156] Hongu T, Oskarsson T. Addicted to acidic microenvironment. Dev Cell 2020;55:381–2.
[157] Funato Y, Yoshida A, Hirata Y, Hashizume O, Yamazaki D, Miki H. The oncogenic PRL protein causes acid addiction of cells by stimulating lysosomal exocytosis. Dev Cell 2020;55:387–97.e8.
[158] Forsyth PA, Wong H, Laing TD, Rewcastle NB, Morris DG, Muzik H, et al. Gelatinase-A (MMP-2), gelatinase-B (MMP-9) and membrane type matrix metalloproteinase-1 (MT1-MMP) are involved in different aspects of the pathophysiology of malignant gliomas. Br J Cancer 1999;79:1828–35.
[159] Erster O, Thomas JM, Hamzah J, Jabaiah AM, Getz JA, Schoep TD, et al. Site-specific targeting of antibody activity in vivo mediated by disease-associated proteases. J Control Release 2012;161:804–12.
[160] Olson ES, Aguilera TA, Jiang T, Ellies LG, Nguyen QT, Wong EH, et al. In vivo characterization of activatable cell penetrating peptides for targeting protease activity in cancer. Integr Biol 2009;1:382–93.

[161] Xia HM, Gu GZ, Hu QY, Liu ZY, Jiang MY, Kang T, et al. Activatable cell penetrating peptide-conjugated nanoparticles with enhanced permeability for site-specific targeting delivery of anticancer drug. Bioconjug Chem 2013;24:419–30.
[162] Olson ES, Jiang T, Aguilera TA, Nguyen QT, Ellies LG, Scadeng M, et al. Activatable cell penetrating peptides linked to nanoparticles as dual probes for in vivo fluorescence and MR imaging of proteases. Proc Natl Acad Sci U S A. 2010;107:4311–6.
[163] Gao HL, Zhang S, Cao SJ, Yang Z, Pang ZQ, Jiang XG. Angiopep-2 and activatable cell-penetrating peptide dual-functionalized nanoparticles for systemic glioma-targeting delivery. Mol Pharm 2014;11:2755–63.
[164] Huang S, Shao K, Kuang Y, Liu Y, Li J, An S, et al. Tumor targeting and microenvironment-responsive nanoparticles for gene delivery. Biomaterials 2013;34:5294–302.
[165] Huang S, Shao K, Liu Y, Kuang Y, Li J, An S, et al. Tumor-targeting and microenvironment-responsive smart nanoparticles for combination therapy of antiangiogenesis and apoptosis. ACS Nano 2013;7:2860–71.
[166] Lee MY, Park SJ, Park K, Kim KS, Lee H, Hahn SK. Target-specific gene silencing of layer-by-layer assembled gold-cysteamine/siRNA/PEI/HA nanocomplex. ACS Nano 2011;5:6138–47.
[167] Tian HY, Lin L, Chen J, Chen XS, Park TG, Maruyama A. RGD targeting hyaluronic acid coating system for PEI-PBLG polycation gene carriers. J Control Release 2011;155:47–53.
[168] Yu W, Cheng Q, Ye J, Zhang M, Zhang C, Gao F, et al. Establishment of facile nanomedicine construction methodology to comprehensively overcome hurdles across tumor-specific nano-delivery. Adv Funct Mater 2020;30:2002239.
[169] Jiang TY, Zhang ZH, Zhang YL, Lv HX, Zhou JP, Li CC, et al. Dual-functional liposomes based on pH-responsive cell-penetrating peptide and hyaluronic acid for tumor-targeted anticancer drug delivery. Biomaterials 2012;33:9246–58.
[170] Ma BJ, Wang S, Liu F, Zhang S, Duan JZ, Li Z, et al. Self-assembled copper amino acid nanoparticles for in situ glutathione "AND" H2O2 sequentially triggered chemodynamic therapy. J Am Chem Soc 2019;141:849–57.
[171] Lu Y, Aimetti AA, Langer R, Gu Z. Bioresponsive materials. Nat Rev Mater 2017;2:16075.
[172] Szabo C, Coletta C, Chao C, Modis K, Szczesny B, Papapetropoulos A, et al. Tumor-derived hydrogen sulfide, produced by cystathionine-beta-synthase, stimulates bioenergetics, cell proliferation, and angiogenesis in colon cancer. Proc Natl Acad Sci U S A. 2013;110:12474–9.
[173] Weekley CM, Jeong G, Tierney ME, Hossain F, Maw AM, Shanu A, et al. Selenite-mediated production of superoxide radical anions in A549 cancer cells is accompanied by a selective increase in SOD1 concentration, enhanced apoptosis and Se-Cu bonding. J Biol Inorg Chem 2014;19:813–28.
[174] Chen WB, Balakrishnan K, Kuang YY, Han YY, Fu M, Gandhi V, et al. Reactive oxygen species (ROS) inducible DNA cross-linking agents and their effect on cancer cells and normal lymphocytes. J Med Chem 2014;57:4498–510.
[175] Xu J, Zhang Y, Yu H, Gao XD, Shao SJ. Mitochondria-targeted fluorescent probe for imaging hydrogen peroxide in living cells. Anal Chem 2016;88:1455–61.
[176] Kuang YY, Baakrishnan K, Gandhi V, Peng XH. Hydrogen peroxide inducible DNA cross-linking agents: targeted anticancer prodrugs. J Am Chem Soc 2011;133:19278–81.
[177] Maji SK, Sreejith S, Mandal AK, Ma X, Zhao YL. Immobilizing gold nanoparticles in mesoporous silica covered reduced graphene oxide: a hybrid material for cancer cell detection through hydrogen peroxide sensing. ACS Appl Mater Interfaces 2014;6:13648–56.
[178] Adarsh N, Krishnan MS, Ramaiah D. Sensitive naked eye detection of hydrogen sulfide and nitric oxide by Aza-BODIPY dyes in aqueous medium. Anal Chem 2014;86:9335–42.
[179] Bailey TS, Pluth MD. Chemiluminescent detection of enzymatically produced hydrogen sulfide: substrate hydrogen bonding influences selectivity for H2S over biological thiols. J Am Chem Soc 2013;135:16697–704.
[180] Montoya LA, Pluth MD. Selective turn-on fluorescent probes for imaging hydrogen sulfide in living cells. Chem Commun 2012;48:4767–9.
[181] Yu CM, Li XZ, Zeng F, Zheng FY, Wu SZ. Carbon-dot-based ratiometric fluorescent sensor for detecting hydrogen sulfide in aqueous media and inside live cells. Chem Commun 2013;49:403–5.
[182] Cadotte AJ, DeMarse TB. Poly-HEMA as a drug delivery device for in vitro neural networks on micro-electrode arrays. J Neural Eng 2005;2:114–22.
[183] Shi DT, Zhou D, Zang Y, Li J, Chen GR, James TD, et al. Selective fluorogenic imaging of hepatocellular H2S by a galactosyl azidonaphthalimide probe. Chem Commun 2015;51:3653–5.
[184] Zhang HT, Kong XQ, Tang YH, Lin WY. Hydrogen sulfide triggered charge-reversal micelles for cancer-targeted drug delivery and imaging. ACS Appl Mater Interfaces 2016;8:16227–39.
[185] Hayashi Y, Homma K, Ichijo H. SOD1 in neurotoxicity and its controversial roles in SOD1 mutation-negative ALS. Adv Biol Regul 2015;60:95–104.
[186] Emerit J, Edeas A, Bricaire F. Neurodegenerative diseases and oxidative stress. Biomed Pharmacother 2004;58:39–46.
[187] Rosen DR, Siddique T, Patterson D, Figlewicz DA, Sapp P, Hentati A, et al. Mutations in Cu/Zn superoxide-dismutase gene are associated with familial amyotrophic-lateral-sclerosis. Nature 1993;362:59–62.
[188] Di Matteo V, Esposito E. Biochemical and therapeutic effects of antioxidants in the treatment of Alzheimer's disease, Parkinson's disease, and amyotrophic lateral sclerosis. CNS & Neurol Disorders-Drug Targets 2003;2:95–107.
[189] Lin VS, Dickinson BC, Chang CJ. Boronate-based fluorescent probes: imaging hydrogen peroxide in living systems. In: Cadenas E, Packer L, editors. Hydrogen peroxide and cell signaling, Pt A2013. p. 19–43.
[190] Lippert AR, De Bittner GCV, Chang CJ. Boronate oxidation as a bioorthogonal reaction approach for studying the chemistry of hydrogen peroxide in living systems. Acc Chem Res 2011;44:793–804.
[191] Peng X, Gandhi V. ROS-activated anticancer prodrugs: a new strategy for tumor-specific damage. Ther Deliv 2012;3:823–33.
[192] Hoang TT, Smith TP, Raines RT. A boronic acid conjugate of angiogenin that shows ROS-responsive neuroprotective activity. Angew Chem-Int Ed 2017;56:2619–22.
[193] Fan WP, Yung B, Huang P, Chen XY. Nanotechnology for multimodal synergistic cancer therapy. Chem Rev 2017;117:13566–638.
[194] Gilkes DM, Semenza GL, Wirtz D. Hypoxia and the extracellular matrix: drivers of tumour metastasis. Nat Rev Cancer 2014;14:430–9.
[195] Liu JN, Bu WB, Shi JL. Chemical design and synthesis of functionalized probes for imaging and treating tumor hypoxia. Chem Rev 2017;117:6160–224.
[196] Wilson WR, Hay MP. Targeting hypoxia in cancer therapy. Nat Rev Cancer 2011;11:393–410.
[197] Fan Y, Tu WZ, Shen MW, Chen XM, Ning YS, Li JJ, et al. Targeted tumor hypoxia dual-mode CT/MR imaging and enhanced radiation therapy using dendrimer-based nanosensitizers. Adv Funct Mater 2020;30:1909285.
[198] Thambi T, Park JH, Lee DS. Hypoxia-responsive nanocarriers for cancer imaging and therapy: recent approaches and future perspectives. Chem Commun 2016;52:8492–500.
[199] Qian CG, Yu JC, Chen YL, Hu QY, Xiao XZ, Sun WJ, et al. Light-activated hypoxia-responsive nanocarriers for enhanced anticancer therapy. Adv Mater 2016;28:3313–20.
[200] Lin QN, Bao CY, Yang YL, Liang QN, Zhang DS, Cheng SY, et al. Highly discriminating photorelease of anticancer drugs based on hypoxia activatable phototrigger conjugated chitosan nanoparticles. Adv Mater 2013;25:1981–6.
[201] Kizaka-Kondoh S, Konse-Nagasawa H. Significance of nitroimidazole compounds and hypoxia-inducible factor-1 for imaging tumor hypoxia. Cancer Sci 2009;100:1366–73.
[202] Li YH, Sun Y, Li JC, Su QQ, Yuan W, Dai Y, et al. Ultrasensitive near-infrared fluorescence-enhanced probe for in vivo nitroreductase imaging. J Am Chem Soc 2015;137:6407–16.
[203] Liu W, Liu HT, Peng XR, Zhou GQ, Liu DD, Li SH, et al. Hypoxia-activated anticancer prodrug for bioimaging, tracking drug release, and anticancer application. Bioconjug Chem 2018;29:3332–43.
[204] Brown JM, William WR. Exploiting tumour hypoxia in cancer treatment. Nat Rev Cancer 2004;4:437–47.
[205] Piao W, Tsuda S, Tanaka Y, Maeda S, Liu FY, Takahashi S, et al. Development of azo-based fluorescent probes to detect different levels of hypoxia. Angew Chem-Int Ed 2013;52:13028–32.

[206] Wang WL, Lin L, Ma XJ, Wang B, Liu SR, Yan XX, et al. Light-induced hypoxia-triggered living nanocarriers for synergistic cancer therapy. ACS Appl Mater Interfaces 2018;10:19398–407.
[207] Kiyose K, Hanaoka K, Oushiki D, Nakamura T, Kajimura M, Suematsu M, et al. Hypoxia-sensitive fluorescent probes for in vivo real-time fluorescence imaging of acute ischemia. J Am Chem Soc 2010;132:15846–8.
[208] Zhen JR, Tian S, Liu Q, Zheng CX, Zhang ZZ, Ding YX, et al. Nanocarriers responsive to a hypoxia gradient facilitate enhanced tumor penetration and improved anti-tumor efficacy. Biomater Sci 2019;7:2986–95.
[209] Perche F, Biswas S, Wang T, Zhu L, Torchilin VP. Hypoxia-targeted siRNA delivery. Angew Chem-Int Ed 2014;53:3362–6.
[210] Wu Y, Zheng J, Zeng Q, Zhang T, Xing D. Light-responsive charge-reversal nanovector for high-efficiency in vivo CRISPR/Cas9 gene editing with controllable location and time. Nano Res 2020;13:2399–406.
[211] Paris JL, Manzano M, Cabañas MV, Vallet-Regí M. Mesoporous silica nanoparticles engineered for ultrasound-induced uptake by cancer cells. Nanoscale 2018; 10:6402–8.
[212] Richardson JJ, Tardy BL, Ejima H, Guo J, Cui J, Liang K, et al. Thermally induced charge reversal of layer-by-layer assembled single-component polymer films. ACS Appl Mater Interfaces 2016;8:7449–55.
[213] Mosquera J, Henriksen-Lacey M, Garcia I, Martinez-Calvo M, Rodriguez J, Mascarenas JL, et al. Cellular uptake of gold nanoparticles triggered by host-guest interactions. J Am Chem Soc 2018;140:4469–72.
[214] Wang S, Zhang F, Yu G, Wang Z, Jacobson O, Ma Y, et al. Zwitterionic-to-cationic charge conversion polyprodrug nanomedicine for enhanced drug delivery. Theranostics 2020;10:6629–37.
[215] Klan P, Solomek T, Bochet CG, Blanc A, Givens R, Rubina M, et al. Photoremovable protecting groups in chemistry and biology: reaction mechanisms and efficacy. Chem Rev 2013;113:119–91.
[216] Han G, You CC, Kim BJ, Turingan RS, Forbes NS, Martin CT, et al. Light-regulated release of DNA and its delivery to nuclei by means of photolabile gold nanoparticles. Angew Chem-Int Ed 2006;45:3165–9.
[217] Vivero-Escoto JL, Slowing II, Wu CW, Lin VSY. Photoinduced intracellular controlled release drug delivery in human cells by gold-capped mesoporous silica nanosphere. J Am Chem Soc 2009;131:3462–3.
[218] Hu LC, Yonamine Y, Lee SH, van der Veer WE, Shea KJ. Light-triggered charge reversal of organic-silica hybrid nanoparticles. J Am Chem Soc 2012;134: 11072–5.
[219] Arias-Alpizar G, Kong L, Vlieg RC, Rabe A, Papadopoulou P, Meijer MS, et al. Light-triggered switching of liposome surface charge directs delivery of membrane impermeable payloads in vivo. Nat Commun 2020;11:3638.
[220] Vahrmeijer AL, Hutteman M, van der Vorst JR, van de Velde CJH, Frangioni JV. Image-guided cancer surgery using near-infrared fluorescence. Nat Rev Clin Oncol 2013;10:507–18.
[221] Yang K, Feng LZ, Shi XZ, Liu Z. Nano-graphene in biomedicine: theranostic applications. Chem Soc Rev 2013;42:530–47.
[222] Zhang J, Chen HY, Xu L, Gu YQ. The targeted behavior of thermally responsive nanohydrogel evaluated by NIR system in mouse model. J Control Release 2008;131:34–40.
[223] Melancon MP, Elliott AM, Shetty A, Huang Q, Stafford RJ, Li C. Near-infrared light modulated photothermal effect increases vascular perfusion and enhances polymeric drug delivery. J Control Release 2011;156:265–72.
[224] Zhao JY, Zhong D, Zhou SB. NIR-I-to-NIR-II fluorescent nanomaterials for biomedical imaging and cancer therapy. J Mater Chem B 2018;6:349–65.
[225] Qiu M, Ren WX, Jeong T, Won M, Park GY, Sang DK, et al. Omnipotent phosphorene: a next-generation, two-dimensional nanoplatform for multidisciplinary biomedical applications. Chem Soc Rev 2018;47:5588–601.
[226] Fang Y, Shang JZ, Liu DK, Shi W, Li XH, Ma HM. Design, synthesis, and application of a small molecular NIR-II fluorophore with maximal emission beyond 1200 nm. J Am Chem Soc 2020;142:15271–5.
[227] Shen YZ, Shuhendler AJ, Ye DJ, Xu JJ, Chen HY. Two-photon excitation nanoparticles for photodynamic therapyt. Chem Soc Rev 2016;45:6725–41.
[228] Kantevari S, Hoang CJ, Ogrodnik J, Egger M, Niggli E, Ellis-Davies GCR. Synthesis and two-photon photolysis of 6-(ortho-nitroveratryl)-caged IP3 in living cells. Chembiochem 2006;7:174–80.
[229] Neveu P, Aujard I, Benbrahim C, Le Saux T, Allemand JF, Vriz S, et al. A caged retinoic acid for one- and two-photon excitation in zebrafish embryos. Angew Chem-Int Ed 2008;47:3744–6.
[230] Zhao J, Gover TD, Muralidharan S, Auston DA, Weinreich D, Kao JPY. Caged vanilloid ligands for activation of TRPV1 receptors by 1-and 2-photon excitation. Biochemistry 2006;45:4915–26.
[231] Shigenaga A, Yamamoto J, Sumikawa Y, Furuta T, Otaka A. Development and photo-responsive peptide bond cleavage reaction of two-photon near-infrared excitation-responsive peptide. Tetrahedron Lett 2010;51:2868–71.
[232] Yang Y, Xie XY, Yang YF, Li ZP, Yu FL, Gong W, et al. Polymer nanoparticles modified with photo- and pH-dual-responsive polypeptides for enhanced and targeted cancer therapy. Mol Pharm 2016;13:1508–19.
[233] Ksiazkiewicz AN, Bering L, Jung F, Wolter NA, Viell J, Mitsos A, et al. Closing the 1–5 μm size gap: temperature-programmed, fed-batch synthesis of μm-sized microgels. Chem Eng J 2020;379:122293.
[234] Nöth M, Hussmann L, Belthle T, El-Awaad I, Davari MD, Jakob F, et al. MicroGelzymes: pH-independent immobilization of cytochrome P450 BM3 in microgels. Biomacromolecules 2020;21:5128–38.
[235] Saha P, Santi M, Frenken M, Palanisamy AR, Ganguly R, Singha NK, et al. Dual-temperature-responsive microgels from a zwitterionic functional graft copolymer with superior protein repelling property. ACS Macro Lett 2020;9:895–901.
[236] Gau E, Flecken F, Ksiazkiewicz AN, Pich A. Enzymatic synthesis of temperature-responsive poly(N-vinylcaprolactam) microgels with glucose oxidase. Green Chem 2018;20:431–9.
[237] Mutharani B, Ranganathan P, Chen S-M, Chen T-W, Eldesoky GE, Ajmal Ali M, et al. Temperature-enabled reversible "On/Off" switch-like hazardous herbicide picloram voltammetric sensor in agricultural and environmental samples based on thermo-responsive PVCL-tethered MWCNT@Au catalyst. J Hazard Mater 2021;402:123672.
[238] Jiang T, Olson ES, Nguyen QT, Roy M, Jennings PA, Tsien RY. Tumor imaging by means of proteolytic activation of cell-penetrating peptides. Proc Natl Acad Sci U S A. 2004;101:17867–72.
[239] Penas C, Sanchez MI, Guerra-Varela J, Sanchez L, Vazquez ME, Mascarenas JL. Light-controlled cellular internalization and cytotoxicity of nucleic acid-binding agents: studies in vitro and in zebrafish embryos. Chembiochem 2016;17:37–41.
[240] Jimenez-Balsa A, Pazos E, Martinez-Albardonedo B, Mascarenas JL, Vazquez ME. Temporary electrostatic impairment of DNA recognition: light-driven DNA binding of peptide dimers. Angew Chem-Int Ed 2012;51:8825–9.
[241] Busschaert N, Caltagirone C, Van Rossom W, Gale PA. Applications of supramolecular anion recognition. Chem Rev 2015;115:8038–155.
[242] Langton MJ, Serpell CJ, Beer PD. Anion recognition in water: recent advances from a supramolecular and macromolecular perspective. Angew Chem-Int Ed 2016;55:1974–87.
[243] Mosquera J, Zarra S, Nitschke JR. Aqueous anion receptors through reduction of subcomponent self-assembled structures. Angew Chem-Int Ed 2014;53: 1556–9.
[244] Rodriguez J, Mosquera J, Couceiro JR, Nitschke JR, Vazquez ME, Mascarenas JL. Anion recognition as a supramolecular switch of cell internalization. J Am Chem Soc 2017;139:55–8.
[245] Hobbs SK, Monsky WL, Yuan F, Roberts WG, Griffith L, Torchilin VP, et al. Regulation of transport pathways in tumor vessels: role of tumor type and microenvironment. Proc Natl Acad Sci U S A. 1998;95:4607–12.
[246] Shi JJ, Kantoff PW, Wooster R, Farokhzad OC. Cancer nanomedicine: progress, challenges and opportunities. Nat Rev Cancer 2017;17:20–37.
[247] Danhier F. To exploit the tumor microenvironment: since the EPR effect fails in the clinic, what is the future of nanomedicine? J Control Release 2016;244: 108–21.

[248] Chan WCW. Nanomedicine 2.0. Acc Chem Res 2017;50:627–32.
[249] Nakamura H, Jun F, Maeda H. Development of next-generation macromolecular drugs based on the EPR effect: challenges and pitfalls. Expert Opin Drug Deliv 2015;12:53–64.
[250] Nakamura Y, Mochida A, Choyke PL, Kobayashi H. Nanodrug delivery: is the enhanced permeability and retention effect sufficient for curing cancer? Bioconjug Chem 2016;27:2225–38.
[251] Chen S, Zhong Y, Fan W, Xiang J, Wang G, Zhou Q, et al. Enhanced tumour penetration and prolonged circulation in blood of polyzwitterion-drug conjugates with cell-membrane affinity. Nat Biomed Eng 2021;5:1019–37.
[252] Xiang J, Shen Y, Zhang Y, Liu X, Zhou Q, Zhou Z, et al. Multipotent poly(tertiary amine-oxide) micelles for efficient cancer drug delivery. Adv Sci 2022;9:2200173.
[253] Wang GW, Zhou ZX, Zhao ZH, Li QY, Wu YL, Yan S, et al. Enzyme-triggered transcytosis of dendrimer-drug conjugate for deep penetration into pancreatic tumors. ACS Nano 2020;14:4890–904.
[254] Chauhan VP, Jain RK. Strategies for advancing cancer nanomedicine. Nat Mater 2013;12:958–62.
[255] Wang XB, Jia YL, Wang P, Liu QH, Zheng HR. Current status and future perspectives of sonodynamic therapy in glioma treatment. Ultrason Sonochem 2017;37:592–9.
[256] Cao W, He Y, Zhu R, He Y, Hao Z, Zhao Q, et al. NIR light triggered size variable “remote-controlled cluster bomb” for deep penetration and tumor therapy. Chem Eng J 2019;375:122080.
[257] Jiang X, Fan X, Zhang R, Xu W, Wu H, Zhao F, et al. In situ tumor-triggered subcellular precise delivery of multi-drugs for enhanced chemo-photothermal-starvation combination antitumor therapy. Theranostics 2020;10:12158–73.
[258] Liu JF, Lan Z, Ferrari C, Stein JM, Higbee-Dempsey E, Yan L, et al. Use of oppositely polarized external magnets to improve the accumulation and penetration of magnetic nanocarriers into solid tumors. ACS Nano 2020;14:142–52.
[259] Sun Y, Wang HP, Wang P, Zhang K, Geng XR, Liu QH, et al. Tumor targeting DVDMS-nanoliposomes for an enhanced sonodynamic therapy of gliomas. Biomater Sci 2019;7:985–94.
[260] Chen W-H, Luo G-F, Qiu W-X, Lei Q, Liu L-H, Zheng D-W, et al. Tumor-triggered drug release with tumor-targeted accumulation and elevated drug retention to overcome multidrug resistance. Chem Mater 2016;28:6742–52.
[261] Pan L, Liu J, Shi J. Cancer cell nucleus-targeting nanocomposites for advanced tumor therapeutics. Chem Soc Rev 2018;47:6930–46.
[262] Xu F, Zhu JZ, Lin LZ, Zhang CC, Sun WJ, Fan Y, et al. Multifunctional PVCL nanogels with redox-responsiveness enable enhanced MR imaging and ultrasound-promoted tumor chemotherapy. Theranostics 2020;10:4349–58.
[263] Zhu Y-X, Jia H-R, Pan G-Y, Ulrich NW, Chen Z, Wu F-G. Development of a light-controlled nanoplatform for direct nuclear delivery of molecular and nanoscale materials. J Am Chem Soc 2018;140:4062–70.
[264] Kunjachan S, Rychlik B, Storm G, Kiessling F, Lammers T. Multidrug resistance: physiological principles and nanomedical solutions. Adv Drug Deliv Rev 2013;65:1852–65.
[265] Rosenblum D, Joshi N, Tao W, Karp JM, Peer D. Progress and challenges towards targeted delivery of cancer therapeutics. Nat Commun 2018;9:1410.
[266] Huang J, Wang L, Zhong X, Li Y, Yang L, Mao H. Facile non-hydrothermal synthesis of oligosaccharide coated sub-5 nm magnetic iron oxide nanoparticles with dual MRI contrast enhancement effects. J Mater Chem B 2014;2:5344–51.
[267] Choi HS, Liu W, Misra P, Tanaka E, Zimmer JP, Itty Ipe B, et al. Renal clearance of quantum dots. Nat Biotechnol 2007;25:1165–70.
[268] Larsen EKU, Nielsen T, Wittenborn T, Birkedal H, Vorup-Jensen T, Jakobsen MH, et al. Size-dependent accumulation of PEGylated silane-coated magnetic iron oxide nanoparticles in murine tumors. ACS Nano 2009;3:1947–51.
[269] Pan L, He Q, Liu J, Chen Y, Ma M, Zhang L, et al. Nuclear-targeted drug delivery of TAT peptide-conjugated monodisperse mesoporous silica nanoparticles. J Am Chem Soc 2012;134:5722–5.
[270] Wang L, Huang J, Chen H, Wu H, Xu Y, Li Y, et al. Exerting enhanced permeability and retention effect driven delivery by ultrafine iron oxide nanoparticles with T1–T2 switchable magnetic resonance imaging contrast. ACS Nano 2017;11:4582–92.
[271] Cho EC, Zhang Q, Xia YN. The effect of sedimentation and diffusion on cellular uptake of gold nanoparticles. Nat Nanotechnol 2011;6:385–91.
[272] Albanese A, Chan WCW. Effect of gold nanoparticle aggregation on cell uptake and toxicity. ACS Nano 2011;5:5478–89.
[273] Nam J, Won N, Jin H, Chung H, Kim S. pH-induced aggregation of gold nanoparticles for photothermal cancer therapy. J Am Chem Soc 2009;131:13639–45.
[274] Shim JY, Gupta VK. Reversible aggregation of gold nanoparticles induced by pH dependent conformational transitions of a self-assembled polypeptide. J Colloid Interface Sci 2007;316:977–83.
[275] Wu W, Zhang QJ, Wang JT, Chen M, Li S, Lin ZF, et al. Tumor-targeted aggregation of pH-sensitive nanocarriers for enhanced retention and rapid intracellular drug release. Polym Chem 2014;5:5668–79.
[276] Pillai PP, Huda S, Kowalczyk B, Grzybowski BA. Controlled pH stability and adjustable cellular uptake of mixed-charge nanoparticles. J Am Chem Soc 2013;135:6392–5.
[277] Liu XS, Huang HY, Jin Q, Ji J. Mixed charged zwitterionic self-assembled monolayers as a facile way to stabilize large gold nanoparticles. Langmuir 2011;27:5242–51.
[278] Li H, Liu XS, Huang N, Ren KF, Jin Q, Ji J. “Mixed-charge Self-Assembled Monolayers” as a facile method to design ph-induced aggregation of large gold nanoparticles for near-infrared photothermal cancer therapy. ACS Appl Mater Interfaces 2014;6:18930–7.
[279] Liu XS, Chen YJ, Li H, Huang N, Jin Q, Ren KF, et al. Enhanced retention and cellular uptake of nanoparticles in tumors by controlling their aggregation behavior. ACS Nano 2013;7:6244–57.
[280] Liu Q, Fang H, Gai Y, Lan X. pH-triggered assembly of natural melanin nanoparticles for enhanced PET imaging. Front Chem 2020;8:755.
[281] Han K, Zhang W-Y, Ma Z-Y, Wang S-B, Xu L-M, Liu J, et al. Acidity-triggered tumor retention/internalization of chimeric peptide for enhanced photodynamic therapy and real-time monitoring of therapeutic effects. ACS Appl Mater Interfaces 2017;9:16043–53.
[282] Zhang BY, Wan SY, Peng XY, Zhao MY, Li S, Pu YJ, et al. Human serum albumin-based doxorubicin prodrug nanoparticles with tumor pH-responsive aggregation-enhanced retention and reduced cardiotoxicity. J Mater Chem B 2020;8:3939–48.
[283] Wang Y, Du JW, Wang YX, Jin Q, Ji J. Pillar 5 arene based supramolecular prodrug micelles with pH induced aggregate behavior for intracellular drug delivery. Chem Commun 2015;51:2999–3002.
[284] Geng Y, Dalhaimer P, Cai SS, Tsai R, Tewari M, Minko T, et al. Shape effects of filaments versus spherical particles in flow and drug delivery. Nat Nanotechnol 2007;2:249–55.
[285] Ye DJ, Shuhendler AJ, Cui LN, Tong L, Tee SS, Tikhomirov G, et al. Bioorthogonal cyclization-mediated in situ self-assembly of small-molecule probes for imaging caspase activity in vivo. Nat Chem 2014;6:519–26.
[286] Powell DR, Huttenlocher A. Neutrophils in the tumor microenvironment. Trends Immunol 2016;37:41–52.
[287] Dumitru CA, Lang S, Brandau S. Modulation of neutrophil granulocytes in the tumor microenvironment: Mechanisms and consequences for tumor progression. Semin Cancer Biol 2013;23:141–8.
[288] Kraman M, Bambrough PJ, Arnold JN, Roberts EW, Magiera L, Jones JO, et al. Suppression of antitumor immunity by stromal cells expressing fibroblast activation protein–α. Science 2010;330:827–30.
[289] Bear AS, Vonderheide RH, O'Hara MH. Challenges and opportunities for pancreatic cancer immunotherapy. Cancer Cell 2020;38:788–802.
[290] Ho WJ, Jaffee EM, Zheng L. The tumour microenvironment in pancreatic cancer — clinical challenges and opportunities. Nat Rev Clin Oncol 2020;17:527–40.
[291] Maman S, Witz IP. A history of exploring cancer in context. Nat Rev Cancer 2018;18:359–76.
[292] Sharma MD, Shinde R, McGaha TL, Huang L, Holmgaard RB, Wolchok JD, et al. The PTEN pathway in T_{regs} is a critical driver of the suppressive tumor microenvironment. Sci Adv 2015;1:e1500845.
[293] Vidimar V, Gius D, Chakravarti D, Bulun SE, Wei J-J, Kim JJ. Dysfunctional MnSOD leads to redox dysregulation and activation of prosurvival AKT signaling in uterine leiomyomas. Sci Adv 2016;2:e1601132.

[294] Heidegger S, Wintges A, Stritzke F, Bek S, Steiger K, Koenig P-A, et al. RIG-I activation is critical for responsiveness to checkpoint blockade. Sci Immunol 2019;4:eaau8943.
[295] Furuta S, Jeng Y-M, Zhou L, Huang L, Kuhn I, Bissell MJ, et al. IL-25 causes apoptosis of IL-25R–expressing breast cancer cells without toxicity to nonmalignant cells. Sci Transl Med 2011;3:78ra31.
[296] Ruan S, Xie R, Qin L, Yu M, Xiao W, Hu C, et al. Aggregable nanoparticles-enabled chemotherapy and autophagy inhibition combined with anti-PD-L1 antibody for improved glioma treatment. Nano Lett 2019;19:8318–32.
[297] Liu Z, Xiong M, Gong J, Zhang Y, Bai N, Luo Y, et al. Legumain protease-activated TAT-liposome cargo for targeting tumours and their microenvironment. Nat Commun 2014;5:4280.
[298] Zhang D, Qi GB, Zhao YX, Qiao SL, Yang C, Wang H. In situ formation of nanofibers from purpurin18-peptide conjugates and the assembly induced retention effect in tumor sites. Adv Mater 2015;27:6125–30.
[299] Zhao XX, Li LL, Zhao Y, An HW, Cai Q, Lang JY, et al. In situ self-assembled nanofibers precisely target cancer-associated fibroblasts for improved tumor imaging. Angew Chem-Int Ed 2019;58:15287–94.
[300] Ji TJ, Zhao Y, Ding YP, Wang J, Zhao RF, Lang JY, et al. Transformable peptide nanocarriers for expeditious drug release and effective cancer therapy via cancer-associated fibroblast activation. Angew Chem-Int Ed 2016;55:1050–5.
[301] O'Brien P, O'Connor BF. Seprase: an overview of an important matrix serine protease. Biochim Biophys Acta Proteins Proteom BBA-Proteins Proteom 2008;1784:1130–45.
[302] Riek R, Eisenberg DS. The activities of amyloids from a structural perspective. Nature 2016;539:227–35.
[303] Xing RR, Yuan CQ, Li SK, Song JW, Li JB, Yan XH. Charge-induced secondary structure transformation of amyloid-derived dipeptide assemblies from beta-sheet to alpha-helix. Angew Chem-Int Ed 2018;57:1537–42.
[304] Jain S, Bates FS. On the origins of morphological complexity in block copolymer surfactants. Science 2003;300:460–4.
[305] Chien MP, Thompson MP, Lin EC, Gianneschi NC. Fluorogenic enzyme-responsive micellar nanoparticles. Chem Sci 2012;3:2690–4.
[306] Chien M-P, Thompson MP, Barback CV, Ku T-H, Hall DJ, Gianneschi NC. Enzyme-directed assembly of a nanoparticle probe in tumor tissue. Adv Mater 2013;25:3599–604.
[307] Chien M-P, Carlini AS, Hu D, Barback CV, Rush AM, Hall DJ, et al. Enzyme-directed assembly of nanoparticles in tumors monitored by in vivo whole animal imaging and ex vivo super-resolution fluorescence imaging. J Am Chem Soc 2013;135:18710–3.
[308] Nguyen MM, Carlini AS, Chien MP, Sonnenberg S, Luo CL, Braden RL, et al. Enzyme-responsive nanoparticles for targeted accumulation and prolonged retention in heart tissue after myocardial infarction. Adv Mater 2015;27:5547–52.
[309] Gao Y, Shi JF, Yuan D, Xu B. Imaging enzyme-triggered self-assembly of small molecules inside live cells. Nat Commun 2012;3:1033.
[310] Liang GL, Ren HJ, Rao JH. A biocompatible condensation reaction for controlled assembly of nanostructures in living cells. Nat Chem 2010;2:54–60.
[311] Huang P, Gao Y, Lin J, Hu H, Liao H-S, Yan X, et al. Tumor-specific formation of enzyme-instructed supramolecular self-assemblies as cancer theranostics. ACS Nano 2015;9:9517–27.
[312] Yang SY, Yao DF, Wang YS, Yang WT, Zhang BB, Wang DB. Enzyme-triggered self-assembly of gold nanoparticles for enhanced retention effects and photothermal therapy of prostate cancer. Chem Commun 2018;54:9841–4.
[313] An HW, Li LL, Wang Y, Wang ZQ, Hou DY, Lin YX, et al. A tumour-selective cascade activatable self-detained system for drug delivery and cancer imaging. Nat Commun 2019;10:4861.
[314] Nykypanchuk D, Maye MM, van der Lelie D, Gang O. DNA-guided crystallization of colloidal nanoparticles. Nature 2008;451:549–52.
[315] Rouge JL, Sita TL, Hao LL, Kouri FM, Briley WE, Stegh AH, et al. Ribozyme-spherical nucleic acids. J Am Chem Soc 2015;137:10528–31.
[316] Maye MM, Nykypanchuk D, Cuisinier M, van der Lelie D, Gang O. Stepwise surface encoding for high-throughput assembly of nanoclusters. Nat Mater 2009;8:388–91.
[317] Skakuj K, Wang SY, Qin L, Lee A, Zhang B, Mirkin CA. Conjugation chemistry-dependent T-cell activation with spherical nucleic acids. J Am Chem Soc 2018;140:1227–30.
[318] Park SY, Lytton-Jean AKR, Lee B, Weigand S, Schatz GC, Mirkin CA. DNA-programmable nanoparticle crystallization. Nature 2008;451:553–6.
[319] Li T, Famulok M. I-motif-programmed functionalization of DNA nanocircles. J Am Chem Soc 2013;135:1593–9.
[320] Lu YJ, Hu DP, Deng Q, Wang ZY, Huang BH, Fang YX, et al. Sensitive and selective detection of uracil-DNA glycosylase activity with a new pyridinium luminescent switch-on molecular probe. Analyst 2015;140:5998–6004.
[321] Day HA, Pavlou P, Waller ZAE. i-Motif DNA: structure, stability and targeting with ligands. Bioorg Med Chem 2014;22:4407–18.
[322] Chao ZC, Lu HW, Xiao F, Shao C, Wei ZX, Yu JT, et al. Robust and tumor-environment-activated DNA cross-linker driving nanoparticle accumulation for enhanced therapeutics. CCS Chem. 2020;2:349–61.
[323] Rozhkova EA. Nanoscale materials for tackling brain cancer: recent progress and outlook. Adv Mater 2011;23:H136–50.
[324] Chen Y, Liu LH. Modern methods for delivery of drugs across the blood-brain barrier. Adv Drug Deliv Rev 2012;64:640–65.
[325] Qiao RR, Jia QJ, Huwel S, Xia R, Liu T, Gao FB, et al. Receptor-mediated delivery of magnetic nanoparticles across the blood-brain barrier. ACS Nano 2012;6:3304–10.
[326] Rapoport SI. Advances in osmotic opening of the blood-brain barrier to enhance CNS chemotherapy. Expert Opin Invest Drugs 2001;10:1809–18.
[327] Ruan SB, Hu C, Tang X, Cun XL, Xiao W, Shi KR, et al. Increased gold nanoparticle retention in brain tumors by in situ enzyme-induced aggregation. ACS Nano 2016;10:10086–98.
[328] Xu XY, Han MS, Mirkin CA. A gold-nanoparticle-based real-time colorimetric screening method for endonuclease activity and inhibition. Angew Chem-Int Ed 2007;46:3468–70.
[329] Cheng XJ, Sun R, Yin L, Chai ZF, Shi HB, Gao MY. Light-triggered assembly of gold nanoparticles for photothermal therapy and photoacoustic imaging of tumors in vivo. Adv Mater 2017;29:1604894.
[330] Massich MD, Giljohann DA, Seferos DS, Ludlow LE, Horvath CM, Mirkin CA. Regulating immune response using polyvalent nucleic acid-gold nanoparticle conjugates. Mol Pharm 2009;6:1934–40.
[331] Deng KR, Li CX, Huang SS, Xing BG, Jin DY, Zeng QG, et al. Recent progress in near infrared light triggered photodynamic therapy. Small 2017;13:1702299.
[332] Zhang PC, Hu CH, Ran W, Meng J, Yin Q, Li YP. Recent progress in light-triggered nanotheranostics for cancer treatment. Theranostics 2016;6:948–68.
[333] del Rosal B, Jia BH, Jaque D. Beyond phototherapy: recent advances in multifunctional fluorescent nanoparticles for light-triggered tumor theranostics. Adv Funct Mater 2018;28:1803733.
[334] Goncalves ASC, Rodrigues CF, Moreira AF, Correia IJ. Strategies to improve the photothermal capacity of gold-based nanomedicines. Acta Biomater 2020;116:105–37.
[335] He HB, Feng M, Chen QD, Zhang XQ, Zhan HB. Light-induced reversible self-assembly of gold nanoparticles surface-immobilized with coumarin ligands. Angew Chem-Int Ed 2016;55:936–40.
[336] Zhang Q, Qu DH, Wang QC, Tian H. Dual-mode controlled self-assembly of TiO2 nanoparticles through a cucurbit 8 uril-enhanced radical cation dimerization interaction. Angew Chem-Int Ed 2015;54:15789–93.
[337] Bian T, Shang L, Yu HJ, Perez MT, Wu LZ, Tung CH, et al. Spontaneous organization of inorganic nanoparticles into nanovesicles triggered by UV light. Adv Mater 2014;26:5613–8.
[338] Kundu PK, Samanta D, Leizrowice R, Margulis B, Zhao H, Borner M, et al. Light-controlled self-assembly of non-photoresponsive nanoparticles. Nat Chem 2015;7:646–52.
[339] Liu DB, Chen WW, Sun K, Deng K, Zhang W, Wang Z, et al. Resettable, multi-readout logic gates based on controllably reversible aggregation of gold nanoparticles. Angew Chem-Int Ed 2011;50:4103–7.
[340] Shiraishi Y, Shirakawa E, Tanaka K, Sakamoto H, Ichikawa S, Hirai T. Spiropyran-modified gold nanoparticles: reversible size control of aggregates by UV and visible light irradiations. ACS Appl Mater Interfaces 2014;6:7554–62.

[341] Klajn R, Wesson PJ, Bishop KJM, Grzybowski BA. Writing self-erasing images using metastable nanoparticle "Inks". Angew Chem-Int Ed 2009;48:7035–9.
[342] Zhang JJ, Zou Q, Tian H. Photochromic materials: more than meets the eye. Adv Mater 2013;25:378–99.
[343] Li X, Lu SY, Xiong ZG, Hu Y, Ma D, Lou WQ, et al. Light-addressable nanoclusters of ultrasmall iron oxide nanoparticles for enhanced and dynamic magnetic resonance imaging of arthritis. Adv Sci 2019;6:1901800.
[344] Zhou LY, Lv FT, Liu LB, Shen GZ, Yan XH, Bazan GC, et al. Cross-linking of thiolated paclitaxel-oligo(p-phenylene vinylene) conjugates aggregates inside tumor cells leads to "Chemical Locks" that increase drug efficacy. Adv Mater 2018;30:1704888.
[345] Tay CY, Yuan L, Leong DT. Nature-inspired DNA nanosensor for real-time in situ detection of mRNA in living cells. ACS Nano 2015;9:5609–17.
[346] Yang YJ, Huang J, Yang XH, Quan K, Wang H, Ying L, et al. FRET nanoflares for intracellular mRNA detection: avoiding false positive signals and minimizing effects of system fluctuations. J Am Chem Soc 2015;137:8340–3.
[347] Yang ZM, Xu KM, Guo ZF, Guo ZH, Xu B. Intracellular enzymatic formation of nanofibers results in hydrogelation and regulated cell death. Adv Mater 2007;19:3152–6.
[348] Yu HJ, Cui ZR, Yu PC, Guo CY, Feng B, Jiang TY, et al. pH- and NIR light-responsive micelles with hyperthermia-triggered tumor penetration and cytoplasm drug release to reverse doxorubicin resistance in breast cancer. Adv Funct Mater 2015;25:2489–500.
[349] Yameen B, Choi WI, Vilos C, Swami A, Shi JJ, Farokhzad OC. Insight into nanoparticle cellular uptake and intracellular targeting. J Control Release 2014;190:485–99.
[350] Kanapathipillai M, Brock A, Ingber DE. Nanoparticle targeting of anti-cancer drugs that alter intracellular signaling or influence the tumor microenvironment. Adv Drug Deliv Rev 2014;79–80:107–18.
[351] Neri D, Supuran CT. Interfering with pH regulation in tumours as a therapeutic strategy. Nat Rev Drug Discov 2011;10:767–77.
[352] Tanaka A, Fukuoka Y, Morimoto Y, Honjo T, Koda D, Goto M, et al. Cancer cell death induced by the intracellular self-assembly of an enzyme-responsive supramolecular gelator. J Am Chem Soc 2015;137:770–5.
[353] Hsu PP, Sabatini DM. Cancer cell metabolism: Warburg and beyond. Cell 2008;134:703–7.
[354] Kuang Y, Xu B. Disruption of the dynamics of microtubules and selective inhibition of glioblastoma cells by nanofibers of small hydrophobic molecules. Angew Chem-Int Ed 2013;52:6944–8.
[355] Wang Y, Li H, Jin Q, Ji J. Intracellular host-guest assembly of gold nanoparticles triggered by glutathione. Chem Commun 2016;52:582–5.
[356] Yang ZM, Liang GL, Wang L, Xu B. Using a kinase/phosphatase switch to regulate a supramolecular hydrogel and forming the supramoleclar hydrogel in vivo. J Am Chem Soc 2006;128:3038–43.
[357] Ku TH, Chien MP, Thompson MP, Sinkovits RS, Olson NH, Baker TS, et al. Controlling and switching the morphology of micellar nanoparticles with enzymes. J Am Chem Soc 2011;133:8392–5.
[358] Feng ZQQ, Wang HM, Zhou R, Li J, Xu B. Enzyme-Instructed assembly and disassembly processes for targeting downregulation in cancer cells. J Am Chem Soc 2017;139:3950–3.
[359] Zheng Z, Chen PY, Xie ML, Wu CF, Luo YF, Wang WT, et al. Cell environment-differentiated self-assembly of nanofibers. J Am Chem Soc 2016;138:11128–31.
[360] Gong NQ, Zhang YX, Teng XC, Wang YC, Huo SD, Qing GC, et al. Proton-driven transformable nanovaccine for cancer immunotherapy. Nat Nanotechnol 2020;15:1053–64.
[361] Polette M, Nawrocki-Raby B, Gilles C, Clavel C, Birembaut P. Tumour invasion and matrix metalloproteinases. Crit Rev Oncol Hematol 2004;49:179–86.
[362] Noctor G, Foyer CH. Ascorbate and glutathione: Keeping active oxygen under control. Annu Rev Plant Physiol Plant Mol Biol 1998;49:249–79.
[363] Calin GA, Croce CM. MicroRNA signatures in human cancers. Nat Rev Cancer 2006;6:857–66.
[364] He L, Hannon GJ. Micrornas: small RNAs with a big role in gene regulation. Nat Rev Genet 2004;5:522–31.
[365] Altieri DC. Validating survivin as a cancer therapeutic target. Nat Rev Cancer 2003;3:46–54.
[366] Qian RC, Lv J, Long YT. Controllable aggregation-induced exocytosis inhibition (CAIEI) of plasmonic nanoparticles in cancer cells regulated by microRNA. Mol Pharm 2018;15:4031–7.
[367] Ye WY, Li H, Li X, Fan XL, Jin Q, Ji J. mRNA guided intracellular self-assembly of DNA-gold nanoparticle conjugates as a precise trigger to up-regulate cell apoptosis and activate photothermal therapy. Bioconjug Chem 2019;30:1763–72.
[368] Zhou LY, Lv FT, Liu LB, Wang S. In situ-induced multivalent anticancer drug clusters in cancer cells for enhancing drug efficacy. CCS Chem. 2019;1:97–105.
[369] Ma JJ, Li PJ, Wang WW, Wang SH, Pan XT, Zhang FR, et al. Biodegradable poly(amino acid)-gold-magnetic complex with efficient endocytosis for multimodal imaging-guided chemo-photothermal therapy. ACS Nano 2018;12:9022–32.
[370] Zhang J, Cui YX, Feng XN, Cheng M, Tang AN, Kong DM. pH-Controlled intracellular in situ reversible assembly of a photothermal agent for smart chemo-photothermal synergetic therapy and ATP imaging. ACS Appl Mater Interfaces 2019;11:39624–32.
[371] Ju CY, Mo R, Xue JW, Zhang L, Zhao ZK, Xue LJ, et al. Sequential intra-intercellular nanoparticle delivery system for deep tumor penetration. Angew Chem-Int Ed 2014;53:6253–8.
[372] Guo X, Wei X, Jing YT, Zhou SB. Size changeable nanocarriers with nuclear targeting for effectively overcoming multidrug resistance in cancer therapy. Adv Mater 2015;27:6450–6.
[373] Niu YM, Zhu JH, Li Y, Shi HH, Gong YX, Li R, et al. Size shrinkable drug delivery nanosystems and priming the tumor microenvironment for deep intratumoral penetration of nanoparticles. J Control Release 2018;277:35–47.
[374] McKee TD, Grandi P, Mok W, Alexandrakis G, Insin N, Zimmer JP, et al. Degradation of fibrillar collagen in a human melanoma xenograft improves the efficacy of an oncolytic herpes simplex virus vector. Cancer Res 2006;66:2509–13.
[375] Chen L, Zhuang WH, Hu C, Yu T, Su X, Liang Z, et al. pH and singlet oxygen dual-responsive GEM prodrug micelles for efficient combination therapy of chemotherapy and photodynamic therapy. J Mater Chem B 2020;8:5645–54.
[376] Peng H, Huang XB, Melle A, Karperien M, Pich A. Redox-responsive degradable prodrug nanogels for intracellular drug delivery by crosslinking of amine-functionalized poly(N-vinylpyrrolidone) copolymers. J Colloid Interface Sci 2019;540:612–22.
[377] Hu C, Xu W, Conrads CM, Wu J, Pich A. Visible light and temperature dual-responsive microgels by crosslinking of spiropyran modified prepolymers. J Colloid Interface Sci 2020;582:1075–84.
[378] Peng H, Huang XB, Oppermann A, Melle A, Weger L, Karperien M, et al. A facile approach for thermal and reduction dual-responsive prodrug nanogels for intracellular doxorubicin delivery. J Mater Chem B 2016;4:7572–83.
[379] Tong R, Hemmati HD, Langer R, Kohane DS. Photoswitchable nanoparticles for triggered tissue penetration and drug delivery. J Am Chem Soc 2012;134:8848–55.
[380] Tong R, Chiang HH, Kohane DS. Photoswitchable nanoparticles for in vivo cancer chemotherapy. Proc Natl Acad Sci U S A. 2013;110:19048–53.
[381] Zhu MQ, Zhang GF, Li C, Aldred MP, Chang E, Drezek RA, et al. Reversible two-photon photoswitching and two-photon imaging of immunofunctionalized nanoparticles targeted to cancer cells. J Am Chem Soc 2011;133:365–72.
[382] Chen ZJ, Liu Y, Wagner W, Stepanenko V, Ren XK, Ogi S, et al. Near-IR absorbing J-aggregate of an amphiphilic BF2-azadipyrromethene dye by kinetic cooperative self-assembly. Angew Chem-Int Ed 2017;56:5729–33.
[383] Liu Y, Zhang YJ, Fennel F, Wagner W, Wurthner F, Chen YF, et al. Coupled cooperative supramolecular polymerization: a new model applied to the competing aggregation pathways of an amphiphilic aza-BODIPY dye into spherical and rod-like aggregates. Chem-Eur J 2018;24:16388–94.
[384] Chen YF, Zhang XH, Cheng DB, Zhang YJ, Liu Y, Ji L, et al. Near-infrared laser-triggered in situ dimorphic transformation of BF2-azadipyrromethene nanoaggregates for enhanced solid tumor penetration. ACS Nano 2020;14:3640–50.
[385] Bae J, Lawrence J, Miesch C, Ribbe A, Li WK, Emrick T, et al. Multifunctional nanoparticle-loaded spherical and wormlike micelles formed by interfacial instabilities. Adv Mater 2012;24:2735–41.
[386] Toft DJ, Moyer TJ, Standley SM, Ruff Y, Ugolkov A, Stupp SI, et al. Coassembled cytotoxic and pegylated peptide amphiphiles form filamentous nanostructures with potent antitumor activity in models of breast cancer. ACS Nano 2012;6:7956–65.

[387] Zhang L, Tian B, Li Y, Lei T, Meng J, Yang L, et al. A copper-mediated disulfiram-loaded pH-triggered PEG-shedding TAT peptide-modified lipid nanocapsules for use in tumor therapy. ACS Appl Mater Interfaces 2015;7:25147–61.
[388] Xiong Z, Wang Y, Zhu W, Ouyang Z, Zhu Y, Shen M, et al. A dual-responsive platform based on antifouling dendrimer-CuS nanohybrids for enhanced tumor delivery and combination therapy. Small Methods 2021;5:2100204.
[389] Poon Z, Lee JB, Morton SW, Hammond PT. Controlling in vivo stability and biodistribution in electrostatically assembled nanoparticles for systemic delivery. Nano Lett 2011;11:2096–103.
[390] Kurosaki T, Kitahara T, Kawakami S, Higuchi Y, Yamaguchi A, Nakagawa H, et al. gamma-Polyglutamic acid-coated vectors for effective and safe gene therapy. J Control Release 2010;142:404–10.
[391] Trubetskoy VS, Wong SC, Subbotin V, Budker VG, Loomis A, Hagstrom JE, et al. Recharging cationic DNA complexes with highly charged polyanions for in vitro and in vivo gene delivery. Gene Ther 2003;10:261–71.
[392] Shutava TG, Balkundi SS, Vangala P, Steffan JJ, Bigelow RL, Cardelli JA, et al. Layer-by-layer-coated gelatin nanoparticles as a vehicle for delivery of natural polyphenols. ACS Nano 2009;3:1877–85.
[393] Wang LN, Su WJ, Liu Z, Zhou MQ, Chen S, Chen YA, et al. CD44 antibody-targeted liposomal nanoparticles for molecular imaging and therapy of hepatocellular carcinoma. Biomaterials 2012;33:5107–14.
[394] Li J, Huo MR, Wang J, Zhou JP, Mohammad JM, Zhang YL, et al. Redox-sensitive micelles self-assembled from amphiphilic hyaluronic acid-deoxycholic acid conjugates for targeted intracellular delivery of paclitaxel. Biomaterials 2012;33:2310–20.
[395] Yoon HY, Koo H, Choi KY, Lee SJ, Kim K, Kwon IC, et al. Tumor-targeting hyaluronic acid nanoparticles for photodynamic imaging and therapy. Biomaterials 2012;33:3980–9.
[396] Stern R. Hyaluronidases in cancer biology. Semin Cancer Biol 2008;18:275–80.
[397] Girish KS, Kemparaju K, Nagaraju S, Vishwanath BS. Hyaluronidase inhibitors: a biological and therapeutic perspective. Curr Med Chem 2009;16:2261–88.
[398] Hu C, Cun XL, Ruan SB, Liu R, Xiao W, Yang XT, et al. Enzyme-triggered size shrink and laser-enhanced NO release nanoparticles for deep tumor penetration and combination therapy. Biomaterials 2018;168:64–75.
[399] Shuvaev VV, Khoshnejad M, Pulsipher KW, Kiseleva RY, Arguiri E, Cheung-Lau JC, et al. Spatially controlled assembly of affinity ligand and enzyme cargo enables targeting ferritin nanocarriers to caveolae. Biomaterials 2018;185:348–59.
[400] Wong AC, Wright DW. Size-dependent cellular uptake of DNA functionalized gold nanoparticles. Small 2016;12:5592–600.
[401] Jiang Y, Huo S, Mizuhara T, Das R, Lee Y-W, Hou S, et al. The interplay of size and surface functionality on the cellular uptake of sub-10 nm gold nanoparticles. ACS Nano 2015;9:9986–93.
[402] Song C, Shen MW, Rodrigues J, Mignani S, Majoral JP, Shi XY. Superstructured poly(amidoamine) dendrimer-based nanoconstructs as platforms for cancer nanomedicine: a concise review. Coord Chem Rev 2020;421:213463.
[403] Wang JJ, Wang XY, Lu SY, Hu J, Zhang W, Xu LE, et al. Integration of cascade delivery and tumor hypoxia modulating capacities in core-releasable satellite nanovehicles to enhance tumor chemotherapy. Biomaterials 2019;223:119465.
[404] Cun XL, Li M, Wang SY, Wang YF, Wang JL, Lu ZZ, et al. A size switchable nanoplatform for targeting the tumor microenvironment and deep tumor penetration. Nanoscale 2018;10:9935–48.
[405] Li HJ, Du JZ, Du XJ, Xu CF, Sun CY, Wang HX, et al. Stimuli-responsive clustered nanoparticles for improved tumor penetration and therapeutic efficacy. Proc Natl Acad Sci U S A. 2016;113:4164–9.
[406] Liu J, Li HJ, Luo YL, Xu CF, Du XJ, Du JZ, et al. Enhanced primary tumor penetration facilitates nanoparticle draining into lymph nodes after systemic injection for tumor metastasis inhibition. ACS Nano 2019;13:8648–58.
[407] Wang K, Tu Y, Yao W, Zong Q, Xiao X, Yang R-M, et al. Size-switchable nanoparticles with self-destructive and tumor penetration characteristics for site-specific phototherapy of cancer. ACS Appl Mater Interfaces 2020;12:6933–43.
[408] Wong C, Stylianopoulos T, Cui JA, Martin J, Chauhan VP, Jiang W, et al. Multistage nanoparticle delivery system for deep penetration into tumor tissue. Proc Natl Acad Sci U S A. 2011;108:2426–31.
[409] Ruan SB, He Q, Gao HL. Matrix metalloproteinase triggered size-shrinkable gelatin-gold fabricated nanoparticles for tumor microenvironment sensitive penetration and diagnosis of glioma. Nanoscale 2015;7:9487–96.
[410] Hu GL, Chun XL, Wang Y, He Q, Gao HL. Peptide mediated active targeting and intelligent particle size reduction-mediated enhanced penetrating of fabricated nanoparticles for triple-negative breast cancer treatment. Oncotarget 2015;6:41258–74.
[411] Ruan SB, Cao X, Cun XL, Hu GL, Zhou Y, Zhang YJ, et al. Matrix metalloproteinase-sensitive size-shrinkable nanoparticles for deep tumor penetration and pH triggered doxorubicin release. Biomaterials 2015;60:100–10.
[412] Bort G, Lux F, Dufort S, Crémillieux Y, Verry C, Tillement O. EPR-mediated tumor targeting using ultrasmall-hybrid nanoparticles: from animal to human with theranostic AGuIX nanoparticles. Theranostics 2020;10:1319–31.
[413] Raghupathi K, Li LY, Ventura J, Jennings M, Thayumanavan S. pH responsive soft nanoclusters with size and charge variation features. Polym Chem 2014;5:1737–42.
[414] Ma D, Shi MH, Li X, Zhang JL, Fan Y, Sun K, et al. Redox-sensitive clustered ultrasmall iron oxide nanoparticles for switchable T-2/T-1-weighted magnetic resonance imaging applications. Bioconjug Chem 2020;31:352–9.
[415] Li FY, Liang ZY, Liu JN, Sun JH, Hu X, Zhao M, et al. Dynamically reversible iron oxide nanoparticle assemblies for targeted amplification of T1-weighted magnetic resonance imaging of tumors. Nano Lett 2019;19:4213–20.
[416] Tian ZQ, Yang CL, Wang W, Yuan Z. Shieldable tumor targeting based on pH responsive self-assembly/disassembly of gold nanoparticles. ACS Appl Mater Interfaces 2014;6:17865–76.
[417] Chen LJ, Yang HB. Construction of stimuli-responsive functional materials via hierarchical self-assembly involving coordination interactions. Acc Chem Res 2018;51:2699–710.
[418] Cai LL, Liu S, Guo JW, Jia YG. Polypeptide-based self-healing hydrogels: Design and biomedical applications. Acta Biomater 2020;113:84–100.
[419] Wankar J, Kotla NG, Gera S, Rasala S, Pandit A, Rochev YA. Recent advances in host-guest self-assembled cyclodextrin carriers: implications for responsive drug delivery and biomedical engineering. Adv Funct Mater 30:1909049.
[420] Liao WC, Willner I. Synthesis and applications of stimuli-responsive DNA-based nano- and micro-sized capsules. Adv Funct Mater 2017;27:1702732.
[421] Kahn JS, Hu YW, Willner I. Stimuli-responsive DNA-based hydrogels: from basic principles to applications. Acc Chem Res 2017;50:680–90.
[422] Kim J, Lee YM, Kang Y, Kim WJ. Tumor-homing, size-tunable clustered nanoparticles for anticancer therapeutics. ACS Nano 2014;8:9358–67.
[423] Hu YW, Cecconello A, Idili A, Ricci F, Willner I. Triplex DNA nanostructures: from basic properties to applications. Angew Chem-Int Ed 2017;56:15210–33.
[424] Ye WY, Chen XH, Li X, Liu YM, Jia F, Jin Q, et al. Structure-switchable DNA programmed disassembly of nanoparticles for smart size tunability and cancer-specific drug release. ACS Appl Mater Interfaces 2020;12:22560–71.
[425] Lu JX, Sun JH, Li FY, Wang J, Liu JN, Kim D, et al. Highly sensitive diagnosis of small hepatocellular carcinoma using ph-responsive iron oxide nanocluster assemblies. J Am Chem Soc 2018;140:10071–4.
[426] Yuan P, Ruan Z, Li T, Tian Y, Cheng Q, Yan L. Sharp pH-responsive mannose prodrug polypeptide nanoparticles encapsulating a photosensitizer for enhanced near infrared imaging-guided photodynamic therapy. J Mater Chem B 2019;7:6770–7.
[427] Li Y, Gao GH, Lee DS. pH-sensitive polymeric micelles based on amphiphilic polypeptide as smart drug carriers. J Polym Sci A Polym Chem 2013;51:4175–82.
[428] Fu L, Yuan P, Ruan Z, Liu L, Li T, Yan L. Ultra-pH-sensitive polypeptide micelles with large fluorescence off/on ratio in near infrared range. Polym Chem 2017;8:1028–38.
[429] Wang YG, Zhou KJ, Huang G, Hensley C, Huang XN, Ma XP, et al. A nanoparticle-based strategy for the imaging of a broad range of tumours by nonlinear amplification of microenvironment signals. Nat Mater 2014;13:204–12.
[430] Chen B, Yan Y, Yang Y, Cao G, Wang X, Wang Y, et al. A pyroptosis nanotuner for cancer therapy. Nat Nanotechnol 2022;17:788–98.

[431] Li HJ, Du JZ, Liu J, Du XJ, Shen S, Zhu YH, et al. Smart superstructures with ultrahigh pH-sensitivity for targeting acidic tumor microenvironment: instantaneous size switching and improved tumor penetration. ACS Nano 2016;10:6753–61.
[432] Shen S, Li HJ, Chen KG, Wang YC, Yang XZ, Lian ZX, et al. Spatial targeting of tumor-associated macrophages and tumor cells with a pH-sensitive cluster nanocarrier for cancer chemoimmunotherapy. Nano Lett 2017;17:3822–9.
[433] Wang L, Jiang W, Xiao L, Li HJ, Chen ZQ, Liu Y, et al. Self-reporting and splitting nanopomegranates potentiate deep tissue cancer radiotherapy via elevated diffusion and transcytosis. ACS Nano 2020;14:8459–72.
[434] Wang XY, Xuan ZL, Zhu XF, Sun HT, Li JC, Xie ZY. Near-infrared photoresponsive drug delivery nanosystems for cancer photo-chemotherapy. J Nanobiotechnol 2020;18:108.
[435] Xiong X, Xu Z, Huang HB, Wang Y, Zhao JY, Guo X, et al. A NIR light triggered disintegratable nanoplatform for enhanced penetration and chemotherapy in deep tumor tissues. Biomaterials 2020;245:119840.
[436] Chen R, Chen Q, Qin H, Xing D. A photoacoustic shockwave triggers the size shrinkage of nanoparticles to obviously improve tumor penetration and therapeutic efficacy. Nanoscale 2019;11:1423–36.
[437] Fox ME, Szoka FC, Frechet JMJ. Soluble polymer carriers for the treatment of cancer: the importance of molecular architecture. Acc Chem Res 2009;42:1141–51.
[438] Chen HB, Gu ZJ, An HW, Chen CY, Chen J, Cui R, et al. Precise nanomedicine for intelligent therapy of cancer. Sci China-Chem 2018;61:1503–52.
[439] Li Z, Xiao C, Yong T, Li Z, Gan L, Yang X. Influence of nanomedicine mechanical properties on tumor targeting delivery. Chem Soc Rev 2020;49:2273–229.
[440] Anselmo AC, Zhang MW, Kumar S, Vogus DR, Menegatti S, Helgeson ME, et al. Elasticity of nanopartides influences their blood circulation, phagocytosis, endocytosis, and targeting. ACS Nano 2015;9:3169–77.
[441] Teng ZG, Wang CY, Tang YX, Li W, Bao L, Zhang XH, et al. Deformable hollow periodic mesoporous organosilica nanocapsules for significantly improved cellular uptake. J Am Chem Soc 2018;140:1385–93.
[442] Peng X, Chen K, Liu WH, Cao XF, Wang MR, Tao J, et al. Soft mesoporous organosilica nanoplatforms improve blood circulation, tumor accumulation/penetration, and photodynamic efficacy. Nano-Micro Lett 2020;12:137.
[443] Liang QL, Bie NN, Yong TY, Tang K, Shi XL, Wei ZH, et al. The softness of tumour-cell-derived microparticles regulates their drug-delivery efficiency. Nat Biomed Eng 2019;3:729–40.
[444] Wu HY, Yu MR, Miao YQ, He SF, Dai Z, Song WY, et al. Cholesterol-tuned liposomal membrane rigidity directs tumor penetration and anti-tumor effect. Acta Pharm Sin B 2019;9:858–70.
[445] Nie D, Dai Z, Li JL, Yang YW, Xi ZY, Wang J, et al. Cancer-cell-membrane-coated nanoparticles with a yolk-shell structure augment cancer chemotherapy. Nano Lett 2020;20:936–46.
[446] Dai Z, Yu M, Yi X, Wu Z, Tian F, Miao Y, et al. Chain-length- and saturation-tuned mechanics of fluid nanovesicles direct tumor delivery. ACS Nano 2019;13:7676–89.
[447] Peng H, Rubsam K, Hu C, Jakob F, Schwaneberg U, Pich A. Stimuli-responsive poly(N-vinyllactams) with glycidyl side groups: synthesis, characterization, and conjugation with enzymes. Biomacromolecules 2019;20:992–1006.
[448] Lopez CM, Pich A. Supramolecular stimuli-responsive microgels crosslinked by tannic acid. Macromol Rapid Commun 2018;39:1700808.
[449] Hendrickson GR, Lyon LA. Microgel translocation through pores under confinement. Angew Chem-Int Ed 2010;49:2193–7.
[450] Cui JW, Bjornmalm M, Liang K, Xu CL, Best JP, Zhang XH, et al. Super-soft hydrogel particles with tunable elasticity in a microfluidic blood capillary model. Adv Mater 2014;26:7295–9.
[451] Sun WJ, Thies S, Zhang JL, Peng C, Tang GY, Shen MW, et al. Gadolinium-loaded poly(N-vinylcaprolactam) nanogels: synthesis, characterization, and application for enhanced tumor MR imaging. ACS Appl Mater Interfaces 2017;9:3411–8.
[452] Sun WJ, Yang J, Zhu JZ, Zhou YW, Li JC, Zhu XY, et al. Immobilization of iron oxide nanoparticles within alginate nanogels for enhanced MR imaging applications. Biomater Sci 2016;4:1422–30.
[453] Zhu JZ, Peng C, Sun WJ, Yu ZB, Zhou BQ, Li D, et al. Formation of iron oxide nanoparticle-loaded gamma-polyglutamic acid nanogels for MR imaging of tumors. J Mater Chem B 2015;3:8684–93.
[454] Zhou YW, Hu Y, Sun WJ, Lu SY, Cai C, Peng C, et al. Radiotherapy-sensitized tumor photothermal ablation using gamma-polyglutamic acid nanogels loaded with polypyrrole. Biomacromolecules 2018;19:2034–42.
[455] Zhu JZ, Sun WJ, Zhang JL, Zhou YW, Shen MW, Peng C, et al. Facile formation of gold-nanoparticle-loaded gamma-polyglutamic acid nanogels for tumor computed tomography imaging. Bioconjug Chem 2017;28:2692–7.
[456] Zou Y, Li D, Shen MW, Shi XY. Polyethylenimine-based nanogels for biomedical applications. Macromol Biosci 2019;19:1900272.
[457] Anselmo AC, Mitragotri S. Impact of particle elasticity on particle-based drug delivery systems. Adv Drug Deliv Rev 2017;108:51–67.
[458] Zhang L, Feng Q, Wang J, Zhang S, Ding B, Wei Y, et al. Microfluidic synthesis of hybrid nanoparticles with controlled lipid layers: understanding flexibility-regulated cell-nanoparticle interaction. ACS Nano 2015;9:9912–21.
[459] Alexander JF, Kozlovskaya V, Chen J, Kuncewicz T, Kharlampieva E, Godin B. Cubical shape enhances the interaction of layer-by-layer polymeric particles with breast cancer cells. Adv Healthc Mater 2015;4:2657–66.
[460] Yu MR, Xu L, Tian FL, Su Q, Zheng N, Yang YW, et al. Rapid transport of deformation-tuned nanoparticles across biological hydrogels and cellular barriers. Nat Commun 2018;9:2607.
[461] Bartneck M, Keul HA, Zwadlo-Klarwasser G, Groll J. Phagocytosis independent extracellular nanoparticle clearance by human immune cells. Nano Lett 2010;10:59–63.
[462] Malam Y, Loizidou M, Seifalian AM. Liposomes and nanoparticles: nanosized vehicles for drug delivery in cancer. Trends Pharmacol Sci 2009;30:592–9.
[463] Zeng ZL, Pu KY. Improving cancer immunotherapy by cell membrane-camouflaged nanoparticles. Adv Funct Mater 2020;30:2004397.
[464] Chen HY, Deng J, Wang Y, Wu CQ, Li X, Dai HW. Hybrid cell membrane-coated nanoparticles: a multifunctional biomimetic platform for cancer diagnosis and therapy. Acta Biomater 2020;112:1–13.
[465] Chen ZW, Wang ZJ, Gu Z. Bioinspired and biomimetic nanomedicines. Acc Chem Res 2019;52:1255–64.
[466] Mine Y, Munir H, Nakanishi Y, Sugiyama D. Biomimetic peptides for the treatment of cancer. Anticancer Res 2016;36:3565–70.
[467] Xu XH, Jian YT, Li YK, Zhang X, Tu ZX, Gu ZW. Bio-inspired supramolecular hybrid dendrimers self-assembled from low-generation peptide dendrons for highly efficient gene delivery and biological tracking. ACS Nano 2014;8:9255–64.
[468] Hedegaard CL, Redondo-Gomez C, Tan BY, Ng KW, Loessner D, Mata A. Peptide-protein coassembling matrices as a biomimetic 3D model of ovarian cancer. Sci Adv 2020;6:eabb3298.
[469] Liao YY, Zhang YF, Blum NT, Lin J, Huang P. Biomimetic hybrid membrane-based nanoplatforms: synthesis, properties and biomedical applications. Nanoscale Horiz 2020;5:1293–302.
[470] Li RX, He YW, Zhang SY, Qin J, Wang JX. Cell membrane-based nanoparticles: a new biomimetic platform for tumor diagnosis and treatment. Acta Pharm Sin B 2018;8:14–22.
[471] Kong LD, Yuan F, Huang PP, Yan L, Cai ZZ, Lawson T, et al. A metal-polymer hybrid biomimetic system for use in the chemodynamic-enhanced photothermal therapy of cancers. Small 2020;16:2004161.
[472] Sevenson S, Tomalia DA. Dendrimers in biomedical applications-reflections on the field. Adv Drug Deliv Rev 2012;64:102–15.
[473] Percec V, Wilson DA, Leowanawat P, Wilson CJ, Hughes AD, Kaucher MS, et al. Self-Assembly of Janus dendrimers into uniform dendrimersomes and other complex architectures. Science 2010;328:1009–14.
[474] Akbarzadeh A, Khalilov R, Mostafavi E, Annabi N, Abasi E, Kafshdooz T, et al. Role of dendrimers in advanced drug delivery and biomedical applications: a review. Exp Oncol 2018;40:178–83.
[475] Zhang X, Zhang ZJ, Xu XH, Li YK, Li YC, Jian YT, et al. Bioinspired therapeutic dendrimers as efficient peptide drugs based on supramolecular interactions for tumor inhibition. Angew Chem-Int Ed 2015;54:4289–94.

[476] Xu XH, Yuan H, Chang J, He B, Gu ZW. Cooperative hierarchical self-assembly of peptide dendrimers and linear polypeptides into nanoarchitectures mimicking viral capsids. Angew Chem-Int Ed 2012;51:3130–3.
[477] Xu XH, Li YK, Li HP, Liu R, Sheng MM, He B, et al. Smart nanovehicles based on pH-triggered disassembly of supramolecular peptide-amphiphiles for efficient intracellular drug delivery. Small 2014;10:1133–40.
[478] Zhang ZJ, Zhang X, Xu XH, Li YK, Li YC, Zhong D, et al. Virus-inspired mimics based on dendritic lipopeptides for efficient tumor-specific infection and systemic drug delivery. Adv Funct Mater 2015;25:5250–60.
[479] Stephan MT, Irvine DJ. Enhancing cell therapies from the outside in: cell surface engineering using synthetic nanomaterials. Nano Today. 2011;6:309–25.
[480] Kroll AV, Fang RH, Zhang LF. Biointerfacing and applications of cell membrane-coated nanoparticles. Bioconjug Chem 2017;28:23–32.
[481] Wang C, Ye YQ, Sun WJ, Yu JC, Wang JQ, Lawrence DS, et al. Red blood cells for glucose-responsive insulin delivery. Adv Mater 2017;29:1606617.
[482] Tan SW, Wu TT, Zhang D, Zhang ZP. Cell or cell membrane-based drug delivery systems. Theranostics 2015;5:863–81.
[483] Dehaini D, Fang RH, Zhang LF. Biomimetic strategies for targeted nanoparticle delivery. Bioeng Transl Med 2016;1:30–46.
[484] Fang RH, Kroll AV, Gao WW, Zhang LF. Cell membrane coating nanotechnology. Adv Mater 2018;30:1706759.
[485] Hu CMJ, Fang RH, Zhang LF. Erythrocyte-inspired delivery systems. Adv Healthc Mater 2012;1:537–47.
[486] Allen TM, Cullis PR. Liposomal drug delivery systems: from concept to clinical applications. Adv Drug Deliv Rev 2013;65:36–48.
[487] Singh S, Sharma A, Robertson GP. Realizing the clinical potential of cancer nanotechnology by minimizing toxicologic and targeted delivery concerns. Cancer Res 2012;72:5663–8.
[488] Pearce TR, Shroff K, Kokkoli E. Peptide targeted lipid nanoparticles for anticancer drug delivery. Adv Mater 2012;24:3803–22.
[489] Hu CMJ, Zhang L, Aryal S, Cheung C, Fang RH, Zhang LF. Erythrocyte membrane-camouflaged polymeric nanoparticles as a biomimetic delivery platform. Proc Natl Acad Sci U S A. 2011;108:10980–5.
[490] Zhang LF, Chan JM, Gu FX, Rhee JW, Wang AZ, Radovic-Moreno AF, et al. Self-assembled lipid-polymer hybrid nanoparticles: a robust drug delivery platform. ACS Nano 2008;2:1696–702.
[491] Sun QH, Sun XR, Ma XP, Zhou ZX, Jin EL, Zhang B, et al. Integration of nanoassembly functions for an effective delivery cascade for cancer drugs. Adv Mater 2014;26:7615–21.
[492] Kiessling LL, Grim JC. Glycopolymer probes of signal transduction. Chem Soc Rev 2013;42:4476–91.
[493] Godula K, Rabuka D, Nam KT, Bertozzi CR. Synthesis and microcontact printing of dual end-functionalized mucin-like glycopolymers for microarray applications. Angew Chem-Int Ed 2009;48:4973–6.
[494] Zhang Q, Haddleton DM. Synthetic glycopolymers: some recent developments. In: Percec V, editor. Hierarchical macromolecular structures: 60 years after the Staudinger Nobel prize Ii2013. p. 39–59.
[495] Lee CC, MacKay JA, Frechet JMJ, Szoka FC. Designing dendrimers for biological applications. Nat Biotechnol 2005;23:1517–26.
[496] Munoz EM, Correa J, Riguera R, Fernandez-Megia E. Real-time evaluation of binding mechanisms in multivalent interactions: a surface plasmon resonance kinetic approach. J Am Chem Soc 2013;135:5966–9.
[497] Chabre YM, Roy R. Multivalent glycoconjugate syntheses and applications using aromatic scaffolds. Chem Soc Rev 2013;42:4657–708.
[498] Percec V, Leowanawat P, Sun HJ, Kulikov O, Nusbaum CD, Tran TM, et al. Modular synthesis of amphiphilic Janus glycodendrimers and their self-assembly into glycodendrimersomes and other complex architectures with bioactivity to biomedically relevant lectins. J Am Chem Soc 2013;135:9055–77.
[499] Zhang SD, Sun HJ, Hughes AD, Draghici B, Lejnieks J, Leowanawat P, et al. "Single-Single" amphiphilic janus dendrimers self-assemble into uniform dendrimersomes with predictable size. ACS Nano 2014;8:1554–65.
[500] Peterca M, Percec V, Leowanawat P, Bertin A. Predicting the size and properties of dendrimersomes from the lamellar structure of their amphiphilic Janus dendrimers. J Am Chem Soc 2011;133:20507–20.
[501] Anish C, Schumann B, Pereira CL, Seeberger PH. Chemical biology approaches to designing defined carbohydrate vaccines. Chem Biol 2014;21:38–50.
[502] Farokhzad OC, Langer R. Impact of nanotechnology on drug delivery. ACS Nano 2009;3:16–20.
[503] Xuan MJ, Shao JX, Li JB. Cell membrane-covered nanoparticles as biomaterials. Natl Sci Rev 2019;6:551–61.
[504] Hu QY, Qian CG, Sun WJ, Wang JQ, Chen ZW, Bomba HN, et al. Engineered nanoplatelets for enhanced treatment of multiple myeloma and thrombus. Adv Mater 2016;28:9573–80.
[505] Wei XL, Ying M, Dehaini D, Su YY, Kroll AV, Zhou JR, et al. Nanoparticle functionalization with platelet membrane enables multifactored biological targeting and detection of atherosclerosis. ACS Nano 2018;12:109–16.
[506] Rao L, Bu LL, Ma L, Wang WB, Liu HQ, Wan D, et al. Platelet-facilitated photothermal therapy of head and neck squamous cell carcinoma. Angew Chem-Int Ed 2018;57:986–91.
[507] Gao J, Chu DF, Wang ZJ. Cell membrane-formed nanovesicles for disease-targeted delivery. J Control Release 2016;224:208–16.
[508] Xuan MJ, Shao JX, Dai LR, Li JB, He Q. Macrophage cell membrane camouflaged Au nanoshells for in vivo prolonged circulation life and enhanced cancer photothermal therapy. ACS Appl Mater Interfaces 2016;8:9610–8.
[509] Oldenborg PA, Zheleznyak A, Fang YF, Lagenaur CF, Gresham HD, Lindberg FP. Role of CD47 as a marker of self on red blood cells. Science 2000;288:2051–4.
[510] Hu CMJ, Fang RH, Luk BT, Chen KNH, Carpenter C, Gao WW, et al. 'Marker-of-self' functionalization of nanoscale particles through a top-down cellular membrane coating approach. Nanoscale 2013;5:2664–8.
[511] Hanahan D, Weinberg RA. Hallmarks of cancer: the next generation. Cell 2011;144:646–74.
[512] Rao L, Bu LL, Cai B, Xu JH, Li A, Zhang WF, et al. Cancer cell membrane-coated upconversion nanoprobes for highly specific tumor imaging. Adv Mater 2016;28:3460–6.
[513] Fang RH, Hu CMJ, Luk BT, Gao WW, Copp JA, Tai YY, et al. Cancer cell membrane-coated nanoparticles for anticancer vaccination and drug delivery. Nano Lett 2014;14:2181–8.
[514] Sun HP, Su JH, Meng QS, Yin Q, Chen LL, Gu WW, et al. Cancer-cell-biomimetic nanoparticles for targeted therapy of homotypic tumors. Adv Mater 2016;28:9581–8.
[515] Cheng H, Zhu JY, Li SY, Zeng JY, Lei Q, Chen KW, et al. An O-2 self-sufficient biomimetic nanoplatform for highly specific and efficient photodynamic therapy. Adv Funct Mater 2016;26:7847–60.
[516] Xie W, Deng WW, Zan MH, Rao L, Yu GT, Zhu DM, et al. Cancer cell membrane camouflaged nanoparticles to realize starvation therapy together with checkpoint blockades for enhancing cancer therapy. ACS Nano 2019;13:2849–57.
[517] Jia L, Li X, Liu H, Xia JD, Shi XY, Shen MW. Ultrasound-enhanced precision tumor theranostics using cell membrane-coated and pH-responsive nanoclusters assembled from ultrasmall iron oxide nanoparticles. Nano Today 2021;36:101022.
[518] Hosseinidoust Z, Mostaghaci B, Yasa O, Park BW, Singh AV, Sitti M. Bioengineered and biohybrid bacteria-based systems for drug delivery. Adv Drug Deliv Rev 2016;106:27–44.
[519] Luo CH, Huang CT, Su CH, Yeh CS. Bacteria-mediated hypoxia-specific delivery of nanoparticles for tumors imaging and therapy. Nano Lett 2016;16:3493–9.
[520] Chen WF, Wang Y, Qin M, Zhang XD, Zhang ZR, Sun X, et al. Bacteria-driven hypoxia targeting for combined biotherapy and photothermal therapy. ACS Nano 2018;12:5995–6005.
[521] Paukner S, Stiedl T, Kudela P, Bizik J, Al Laham F, Lubitz W. Bacterial ghosts as a novel advanced targeting system for drug and DNA delivery. Expert Opin Drug Deliv 2006;3:11–22.
[522] Shao JX, Xuan MJ, Zhang HY, Lin XK, Wu ZG, He Q. Chemotaxis-guided hybrid neutrophil micromotors for targeted drug transport. Angew Chem-Int Ed 2017;56:12935–9.
[523] Poetsch A, Wdlters D. Bacterial membrane proteomics. Proteomics 2008;8:4100–22.
[524] Kuehn MJ, Kesty NC. Bacterial outer membrane vesicles and the host-pathogen interaction. Genes Dev 2005;19:2645–55.
[525] Lee EY, Bang JY, Park GW, Choi DS, Kang JS, Kim HJ, et al. Global proteomic profiling of native outer membrane vesicles derived from *Escherichia coli*. Proteomics 2007;7:3143–53.

[526] Luk BT, Hu CMJ, Fang RNH, Dehaini D, Carpenter C, Gao WW, et al. Interfacial interactions between natural RBC membranes and synthetic polymeric nanoparticles. Nanoscale 2014;6:2730–7.
[527] Gao WW, Fang RH, Thamphiwatana S, Luk BT, Li JM, Angsantikul P, et al. Modulating antibacterial immunity via bacterial membrane-coated nanoparticles. Nano Lett 2015;15:1403–9.
[528] Wang H, Alarcón CN, Liu B, Watson F, Searles S, Lee CK, et al. Genetically engineered and enucleated human mesenchymal stromal cells for the targeted delivery of therapeutics to diseased tissue. Nat Biomed Eng 2021;6:882–97.
[529] Muzykantov VR. Drug delivery by red blood cells: vascular carriers designed by mother nature. Expert Opin Drug Deliv 2010;7:403–27.
[530] Jensen FB. The dual roles of red blood cells in tissue oxygen delivery: oxygen carriers and regulators of local blood flow. J Exp Biol 2009;212:3387–93.
[531] Ahn S, Jung SY, Seo E, Lee SJ. Gold nanoparticle-incorporated human red blood cells (RBCs) for X-ray dynamic imaging. Biomaterials 2011;32:7191–9.
[532] He H, Ye J, Wang Y, Liu Q, Chung HS, Kwon YM, et al. Cell-penetrating peptides meditated encapsulation of protein therapeutics into intact red blood cells and its application. J Control Release 2014;176:123–32.
[533] Tang W, Zhen Z, Wang M, Wang H, Chuang Y-J, Zhang W, et al. Red blood cell-facilitated photodynamic therapy for cancer treatment. Adv Funct Mater 2016;26:1757–68.
[534] Singh A, Talekar M, Raikar A, Amiji M. Macrophage-targeted delivery systems for nucleic acid therapy of inflammatory diseases. J Control Release 2014;190:515–30.
[535] Yi L, Xiao H, Xu M, Ye X, Hu J, Li F, et al. Glioma-initiating cells: a predominant role in microglia/macrophages tropism to glioma. J Neuroimmunol 2011;232:75–82.
[536] Beduneau A, Ma Z, Grotepas CB, Kabanov A, Rabinow BE, Gong N, et al. Facilitated monocyte-macrophage uptake and tissue distribution of superparmagnetic iron-oxide nanoparticles. PLoS One 2009;4:e4343.
[537] Zhang W, Wang M, Tang W, Wen R, Zhou S, Lee C, et al. Nanoparticle-laden macrophages for tumor-tropic drug delivery. Adv Mater 2018;30:1805557.
[538] Xiao T, Hu W, Fan Y, Shen M, Shi X. Macrophage-mediated tumor homing of hyaluronic acid nanogels loaded with polypyrrole and anticancer drug for targeted combinational photothermo-chemotherapy. Theranostics 2021;11:7057–71.
[539] Zheng LY, Hu XX, Wu H, Mo LT, Xie ST, Li J, et al. In vivo monocyte/macrophage-hitchhiked intratumoral accumulation of nanomedicines for enhanced tumor therapy. J Am Chem Soc 2020;142:382–91.
[540] Mantovani A, Allavena P, Marchesi F, Garlanda C. Macrophages as tools and targets in cancer therapy. Nat Rev Drug Discov 2022;21:799–820.
[541] Yin F, Fan Y, Xu L, Yin F, He M, Xiao T, et al. Macrophages loaded with dendrimer-entrapped gold nanoparticles as a theranostic platform for CT imaging-guided combinational therapy of orthotopic osteosarcoma. Chem Eng J 2021;417:129273.
[542] Xue JW, Zhao ZK, Zhang L, Xue LJ, Shen SY, Wen YJ, et al. Neutrophil-mediated anticancer drug delivery for suppression of postoperative malignant glioma recurrence. Nat Nanotechnol 2017;12:692–700.
[543] Shen J, Hao J, Chen Y, Liu H, Wu J, Hu B, et al. Neutrophil-mediated clinical nanodrug for treatment of residual tumor after focused ultrasound ablation. J Nanobiotechnology. 2021;19:345.
[544] Chu D, Zhao Q, Yu J, Zhang F, Zhang H, Wang Z. Nanoparticle targeting of neutrophils for improved cancer immunotherapy. Adv Healthc Mater 2016;5:1088–93.
[545] Myerson JW, Patel PN, Rubey KM, Zamora ME, Zaleski MH, Habibi N, et al. Supramolecular arrangement of protein in nanoparticle structures predicts nanoparticle tropism for neutrophils in acute lung inflammation. Nat Nanotechnol 2022;17:86–97.
[546] Huang BN, Abraham WD, Zheng YR, Lopez SCB, Luo SS, Irvine DJ. Active targeting of chemotherapy to disseminated tumors using nanoparticle-carrying T cells. Sci Transl Med 2015;7:291ra94.
[547] Kennedy LC, Bear AS, Young JK, Lewinski NA, Kim J, Foster AE, et al. T cells enhance gold nanoparticle delivery to tumors in vivo. Nanoscale Res Lett 2011;6:283.
[548] Steinfeld U, Pauli C, Kaltz N, Bergemann C, Lee H-H. T lymphocytes as potential therapeutic drug carrier for cancer treatment. Int J Pharm 2006;311:229–36.
[549] Meir R, Shamalov K, Betzer O, Motiei M, Horovitz-Fried M, Yehuda R, et al. Nanomedicine for cancer immunotherapy: tracking cancer-specific T-cells in vivo with gold nanoparticles and CT imaging. ACS Nano 2015;9:6363–72.
[550] Stephan MT, Moon JJ, Um SH, Bershteyn A, Irvine DJ. Therapeutic cell engineering with surface-conjugated synthetic nanoparticles. Nat Med 2010;16:1035–41.
[551] Roger M, Clavreul A, Venier-Julienne M-C, Passirani C, Sindji L, Schiller P, et al. Mesenchymal stem cells as cellular vehicles for delivery of nanoparticles to brain tumors. Biomaterials 2010;31:8393–401.
[552] Mooney R, Roma L, Zhao D, Van Haute D, Garcia E, Kim SU, et al. Neural stem cell-mediated intratumoral delivery of gold nanorods improves photothermal therapy. ACS Nano 2014;8:12450–60.
[553] Hao XX, Xu B, Chen H, Wang XM, Zhang JL, Guo R, et al. Stem cell-mediated delivery of nanogels loaded with ultrasmall iron oxide nanoparticles for enhanced tumor MR imaging. Nanoscale 2019;11:4904–10.
[554] Li L, Guan Y, Liu H, Hao N, Liu T, Meng X, et al. Silica nanorattle–doxorubicin-anchored mesenchymal stem cells for tumor-tropic therapy. ACS Nano 2011;5:7462–70.
[555] Hao M, Xia H, Duan J, Zhou H, Zhang G, Li D, et al. A living material constructed from stem cells for tumor-tropic oncotherapy with real-time imaging. Adv Funct Mater 2022;32:2201013.
[556] Zhou Y, Han Y. Engineered bacteria as drug delivery vehicles: principles and prospects. Eng Microbiol 2022;2:100034.
[557] Zhou S. SYNTHETIC BIOLOGY bacteria synchronized for drug delivery. Nature 2016;536:34–5.
[558] Thomas SC, Madaan T, Kamble NS, Siddiqui NA, Pauletti GM, Kotagiri N. Engineered bacteria enhance immunotherapy and targeted therapy through stromal remodeling of tumors. Adv Healthc Mater 2022;11:2101487.
[559] Dougan M, Dougan SK. Programmable bacteria as cancer therapy. Nat Med 2019;25:1030–1.
[560] Chowdhury S, Castro S, Coker C, Hinchliffe TE, Arpaia N, Danino T. Programmable bacteria induce durable tumor regression and systemic antitumor immunity. Nat Med 2019;25:1057–63.
[561] Zhou S, Gravekamp C, Bermudes D, Liu K. Tumour-targeting bacteria engineered to fight cancer. Nat Rev Cancer 2018;18:727–43.
[562] Fan J-X, Li Z-H, Liu X-H, Zheng D-W, Chen Y, Zhang X-Z. Bacteria-mediated tumor therapy utilizing photothermally-controlled TNF-alpha expression via oral administration. Nano Lett 2018;18:2373–80.
[563] Wang L, Cao Z, Zhang M, Lin S, Liu J. Spatiotemporally controllable distribution of combination therapeutics in solid tumors by dually modified bacteria. Adv Mater 2022;34:2106669.
[564] St Jean AT, Swofford CA, Panteli JT, Brentzel ZJ, Forbes NS. Bacterial delivery of *Staphylococcus aureus* alpha-hemolysin causes regression and necrosis in murine tumors. Mol Ther 2014;22:1266–74.
[565] Pizarro-Cerda J, Cossart P. Bacterial adhesion and entry into host cells. Cell 2006;124:715–27.
[566] Ganai S, Arenas RB, Sauer JP, Bentley B, Forbes NS. In tumors Salmonella migrate away from vasculature toward the transition zone and induce apoptosis. Cancer Gene Ther 2011;18:457–66.
[567] Zheng JH, Nguyen VH, Jiang S-N, Park S-H, Tan W, Hong SH, et al. Two-step enhanced cancer immunotherapy with engineered Salmonella typhimurium secreting heterologous flagellin. Sci Transl Med 2017;9:eaak9537.
[568] Raman V, Van Dessel N, Hall CL, Wetherby VE, Whitney SA, Kolewe EL, et al. Intracellular delivery of protein drugs with an autonomously lysing bacterial system reduces tumor growth and metastases. Nat Commun 2021;12:6116.
[569] Servick K. DRUG DEVELOPMENT Beleaguered phage therapy trial presses on. Science 2016;352:1506.
[570] Cho I, Blaser MJ. APPLICATIONS OF NEXT-GENERATION SEQUENCING The human microbiome: at the interface of health and disease. Nat Rev Genet 2012;13:260–70.
[571] Citorik RJ, Mimee M, Lu TK. Sequence-specific antimicrobials using efficiently delivered RNA-guided nucleases. Nat Biotechnol 2014;32:1141–5.

[572] Agarwal R, Johnson CT, Imhoff BR, Donlan RM, McCarty NA, Garcia AJ. Inhaled bacteriophage-loaded polymeric microparticles ameliorate acute lung infections. Nat Biomed Eng 2018;2:841–9.
[573] Schroeder B, Backhed F. Signals from the gut microbiota to distant organs in physiology and disease. Nat Med 2016;22:1079–89.
[574] Tremaroli V, Backhed F. Functional interactions between the gut microbiota and host metabolism. Nature 2012;489:242–9.
[575] Yu T, Guo F, Yu Y, Sun T, Ma D, Han J, et al. Fusobacterium nucleatum promotes chemoresistance to colorectal cancer by modulating autophagy. Cell 2017;170:548–63.
[576] Cani PD, Jordan BF. Gut microbiota-mediated inflammation in obesity: a link with gastrointestinal cancer. Nat Rev Gastroenterol Hepatol 2018;15:671–82.
[577] Zheng D-W, Dong X, Pan P, Chen K-W, Fan J-X, Cheng S-X, et al. Phage-guided modulation of the gut microbiota of mouse models of colorectal cancer augments their responses to chemotherapy. Nat Biomed Eng 2019;3:717–28.
[578] Poon W, Kingston BR, Ouyang B, Ngo W, Chan WCW. A framework for designing delivery systems. Nat Nanotechnol 2020;15:819–29.
[579] Ouyang B, Poon W, Zhang Y-N, Lin ZP, Kingston BR, Tavares AJ, et al. The dose threshold for nanoparticle tumour delivery. Nat Mater 2020;19:1362–71.
[580] Bakshi SF, Guz N, Zakharchenko A, Deng H, Tumanov AV, Woodworth CD, et al. Magnetic field-activated sensing of mRNA in Living Cells. J Am Chem Soc 2017;139:12117–20.
[581] Tang Y, Li Y, Hu X, Zhao H, Ji Y, Chen L, et al. "Dual Lock-and-Key"-controlled nanoprobes for ultrahigh specific fluorescence imaging in the second near-infrared window. Adv Mater 2018;30:1801140.
[582] Zhang P, Gao D, An K, Shen Q, Wang C, Zhang Y, et al. A programmable polymer library that enables the construction of stimuli-responsive nanocarriers containing logic gates. Nat Chem 2020;12:381–90.
[583] Badeau BA, Comerford MP, Arakawa CK, Shadish JA, DeForest CA. Engineered modular biomaterial logic gates for environmentally triggered therapeutic delivery. Nat Chem 2018;10:251–8.